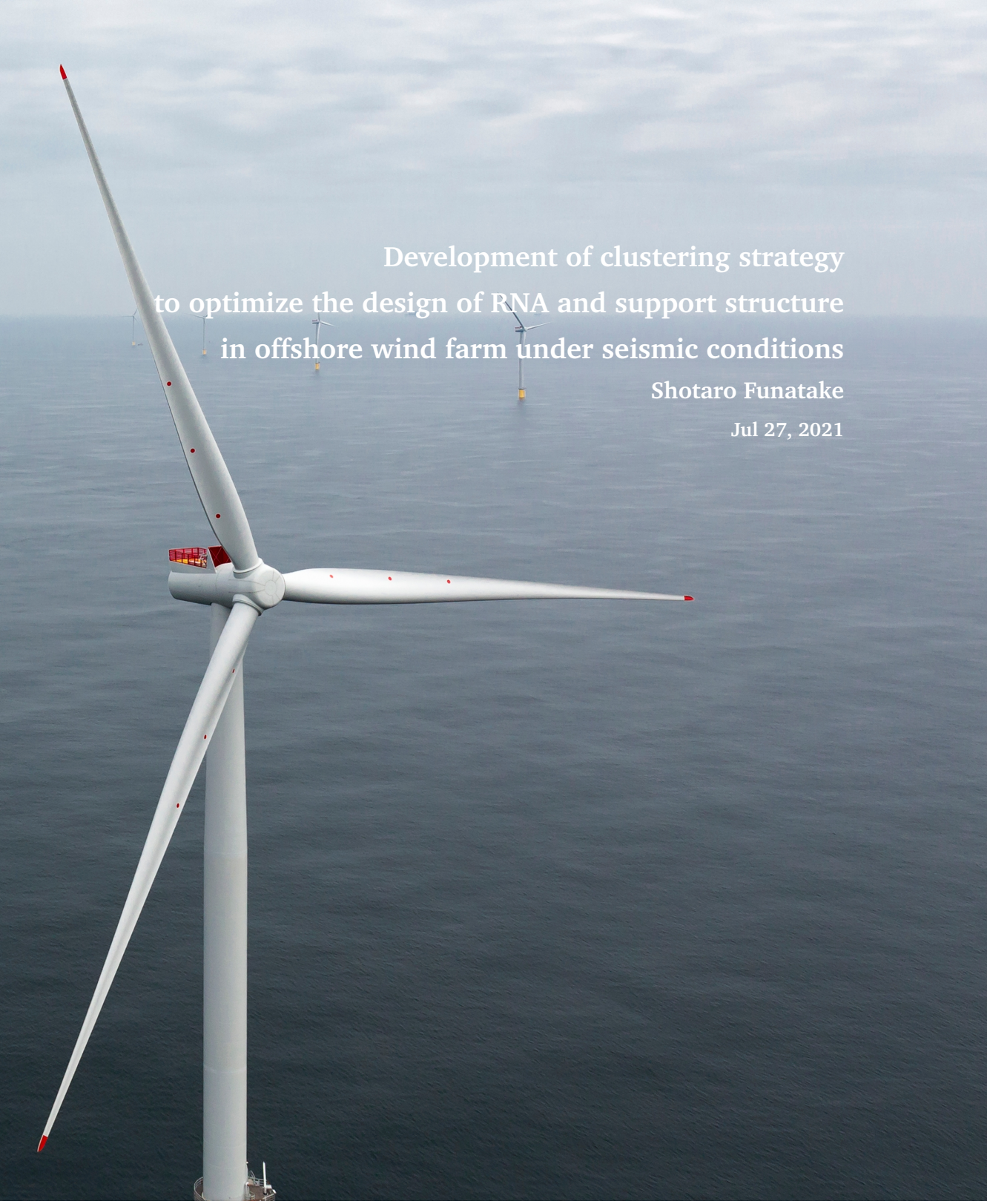

Development of clustering strategy to optimize the design of RNA and support structure in offshore wind farm under seismic conditions

Shotaro Funatake

Jul 27, 2021

TU Delft Delft University of Technology

SIEMENS Gamesa RENEWABLE ENERGY

Development of clustering strategy to optimize the design of RNA and support structure in offshore wind farm under seismic conditions

Master of Science Thesis

Version for TU Delft repository (Some outputs are excluded and normalized)

Author:	Shotaro Funatake	
Committee:	Dr. ir. Apostolos.Tsouvalas	TU Delft - Chairman
	Dr. ir. Karel van Dalen	TU Delft
	Ir. Timo Molenkamp	TU Delft
	Ir. Matteo Ravasio	Siemens Gamesa
	Ir. Corine de Winter	Siemens Gamesa

JUL 27, 2021

- CONFIDENTIAL -

TU Delft Delft University of Technology

SIEMENS Gamesa RENEWABLE ENERGY

Summary

Offshore wind energy is one of the emerging renewable technologies toward a zero-carbon emission society. Historically, offshore wind farms have been developed in the North Sea, but nowadays wind farms are expanded to other regions such as North America and Asia, which are seismic prone.

In the design of Rotor-Nacelle-Assembly (RNA) and support structure for offshore wind farms, the number of design positions is reduced by using representative design positions (i.e. clustering). The number of designs is directly related to the efficiency of the design work, so it is worthwhile to minimize it by wisely selecting the representative position. However, such a clustering methodology has not been systematically developed in seismic design due to the limited number of projects and researches in seismic regions.

As for seismic analysis, there are several challenges to develop an efficient clustering strategy. First, higher (and multiple) vibration modes are excited in the system consisting of the wind turbine itself in interaction with the soil. Second, blade vibration (and blade-tower coupling effect) has a significant role in the output forces. Third, energy intake from the seismic ground motion is dependent on the position due to soil amplification. Considering the problem statement above, this research develops a clustering strategy for seismic analysis to optimize the design process on RNA and support structure for offshore wind farms.

To achieve this goal, as a first step, a simplified calculation model is created to efficiently carry out the sensitivity studies. A combination of point masses with Euler-Bernoulli beam is used for RNA model while lumped mass at the tower top is conventionally used in past researches, which allows to properly represent the blade-tower coupling effect contrary to most of past researches. Considering modal participation mass, higher vibration modes are truncated, and principle vibration modes are detected, which improves the computational efficiency. Both the frequency domain method and the response spectrum method are developed and compared with

proven software, BhawC, to verify their accuracy.

Then, a sensitivity study is carried out by using the developed model. Through the sensitivity study, the system property is approximately quantified as a form of "scaling factor". Combining the scaling factor with acceleration response spectrum, the maximum bending moment for an arbitrary position (i.e. arbitrary water depth, soil condition and bedrock depth) can be quickly estimated. Subsequently, the positions in a wind farm are sorted into groups with similar load trends based on the estimated bending moment; this is the basis of the clustering strategy proposed in this thesis.

Finally, the strategy is applied to virtual wind farms and its applicability is verified. Although it shows some errors in the estimation of the maximum bending moment itself, the accuracy is considered satisfactory to detect the most loaded position (i.e. design representative position) and categorize the positions which have similar load trend, which are one of the main requirements for a reliable clustering methodology. Also, the strategy is applied to more realistic soil condition, such as inhomogeneous soil and its applicability and limitation are investigated.

Preface

Shotaro Funatake
Delft, July 2021

Thanks to Dr. Apostolos, my thesis chairman. His interest on this project, guidance on the process, patience and critical advice, which definitely, were fundamental to achieve the goal.

Thanks to Timo, my university daily supervisor. Whenever I was stuck to the thesis, he gave me a lot of useful advice. Especially as for model verification part, he joined many meetings to investigate the errors and provided clever tips to solve them, which helped me to finalize it at the end.

Thanks to Matteo and Corine, my supervisors from SGRE. They were always open to ask questions (even if it was not directly related to the thesis), and encouraged a lot when I was struggling to difficulties. I was very fortunate to meet them and develop a great teamwork.

Thanks to the whole Siemens Gamesa Renewable Energy team. When I joined, all of them gave me warm welcome, which allowed me to be easily accustomed to the company. I could learn a lot of things from them, which is not only engineering matters but also business manner in a global company. I'm looking forward to meeting them again in a real offshore wind project.

Thanks to Naoko, my wife. Living in the Netherlands was a quite big adventure for our family (since it was the first time for us to leave Japan), but she always enjoyed it very much with positive emotion, which provided a lot of smiles and happiness in our house. Let's enjoy the next adventure after returning back to Japan.

Thanks to Ryota, my son, for being an infinite source of love and motivation. Looking at his growing up every day is the most beautiful gift I received in my life.

Contents

Nomenclature

Latin symbols

$\mathbf{M}$	Mass matrix	
$\mathbf{C}$	Damping matrix	
$\mathbf{K}$	Stiffness matrix	
$\mathbf{r}$	Influence vector	
$\ddot{u_g}$	Seismic acceleration	ms^{-2}
$\tilde{u_g}$	u_g transformed with Fourier transform	
t	Time	s
u	Seismic displacement	m
$\tilde{U}$	u transformed with Fourier transform	
A_0	Amplitude of seismic acceleration	ms^{-2}
S_a	Acceleration response spectrum	ms^{-2}
$\boldsymbol{F}$	Maximum force vector	N
$\boldsymbol{Q}$	Maximum vending moment vector	Nm
$\boldsymbol{l}$	Lever arm vector	m
G	Shear modulus	Nm^{-2}
E_{eq}	Equivalent Elastic modulus	Nm^2

Greek symbols

ω	Circular frequency	$rads^{-1}$
$\mathbf{\Phi}$	Eigen vector	

Abbreviations

BDWF	Beam-on-Dynamic-Winkler-Foundation
BM	Bending moment
CV	Coefficient of variation
DLC	Design Load Case
FE	Finite Element
RNA	Rotor Nacelle Assembly
SGRE	Siemens Gamesa Renewable Energy
SH	Shear horizontally polarized
SF	Scaling factor
GW	Giga Watt
OWT	Offshore Wind Turbines
ODE	Ordinary Differential Equation
WT	Wall thickness
OD	Outside Diameter
LP	Length of pile penetration

Chapter 1

Introduction

1.1 Energy demand and offshore wind energy

Offshore wind energy is one of the emerging renewable technologies toward a zero-carbon emission society. IRENA [1] estimated that the cumulative capacity of offshore wind energy will be rapidly increased from 23GW in 2018 to 1000GW in 2050 in the report. Historically, offshore wind farms have been developed in the North Sea, but nowadays wind farms are expanded to other regions such as North America and Asia. De Risi [2] superposed three maps to visualize the correlation between seismic regions and potential offshore energy locations: first identified the countries which are investing in offshore wind energy, then the areas where subduction activity is relevant, and finally, the regions where the seismic hazard is important as shown in figure 1.1. It clearly shows that the development of offshore wind farms is expanded to seismic-prone regions, such as the USA, India, Korea, Japan, etc..

1.2 Problem statement

1.2.1 Clustering

Loads acting on offshore wind turbines (OWT) vary in large wind farms due to variation of site characteristics and environmental conditions. The most ideal way is to carry out full load calculation in each position, but it is computationally demanding and does not fit the project timeline. Hence, in practice, loads are evaluated for a

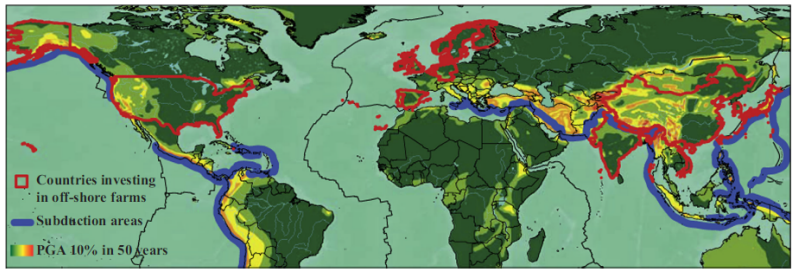

Figure 1.1: Countries investing in offshore wind energy (red), subduction zones (blue) and seismic hazard [2].

limited number of design positions within the wind farm (as explained in [3] and [4]).

The process with which positions with similar properties are grouped is called ”clustering”. In each cluster, one (or two) position is selected as a representative to perform the analysis. The number of design positions is directly related to the efficiency of the design work, so it is worthwhile to minimize it by clever strategy.

No regulations or design codes specify anything about clustering, but in practice, most projects adopt clustering for RNA and support structures to minimize the number of analyses as mentioned in [5].

As for wind-wave conditions, the clustering procedure has been sophisticated since there are a number of experiences. In the case of Siemens Gamesa Renewable Energy (SGRE), for example, they have a procedure to select clusters based on the first mode shape in each position (that means eigen analysis to be used for clustering). Also, there is some literature about clustering in the non-seismic region although the number is limited. Ziegler [5] studied fatigue damage on OWT with a probabilistic approach, and developed an efficient way to do clustering with reasonable accuracy. Seidel [6] also showed a sensitivity study on monopile considering wave-induced fatigue damage. This literature revealed a sensitivity of OWT to each design parameter to some extent. Meanwhile, the clustering strategy for seismic loads is still ambiguous because the sensitivity of each design parameter is not understood very well. Of course, some researchers carried out sensitivity studies on seismic design. For example, Maria [7] and De Risi [2] studied the seismic design of monopile in non-linear time-domain simulation. They provided useful insight, but they covered limited range of site conditions.

1.2.2 Challenges on seismic analysis

As expanding the development of OWT in seismic regions, the number of studies for seismic design has been increased nowadays.

Seismic loads cover a relatively higher frequency range compared to wind and wave loads. Figure 1.2 shows the normalized spectrum for wind, wave and seismic spectrum together with typical natural frequencies for offshore wind turbines. In the case of wind and wave conditions, only 1st structure mode is excited. In the case of seismic excitation, however, not only 1st structure mode but also higher modes are excited as well. This is one of the challenges to deal with seismic analysis.

Another important factor for seismic analysis is RNA model. Many researchers create a model which represents RNA as a single lumped mass at the tower top. However, recent studies show that RNA mode (i.e. blade vibration) can be excited by seismic input (as shown in the figure 1.2) and largely affects the structural dynamic property, so called blade-tower coupling effect. For example, Ali [8] mentioned that flexible foundation and discrete mass contribution of the slender tower, nacelle, hub, and blades that tend to induce rotary inertia in the tower, could result in the lengthening of natural periods.

There are a lot of software which has a function to capture the effect by using non-linear time-domain analysis, and some researchers studied it by using them, such as BHawC and FAST ([7] and [9]). But, their computational demand is quite high, and also the accessibility is limited.

In order to overcome this challenge, some researchers have developed a simplified calculation model which deals with the blade-tower coupling effect. Kang [10] represented blade and monopile as Euler-Bernoulli beam with constant cross-section property, and applied modal analysis to capture the dynamic property. Liu [11] created a similar model, but it contained more complexity such as several environmental loads, variation of cross-section on monopile. Furthermore, Iida [12] created a model which represents blades as multiple lumped masses distributed on blade section, and compared the result with a single lumped mass method. They provided insight to properly capture the blade-tower coupling effect.

The third important aspect of the seismic analysis is the effect of soil amplification. Seismic signals can be amplified during the propagation in shallow sub-surface due to the resonance of the soil column. Firat [13] studied its effect and mentioned that regional geology and subsoil conditions can significantly change the characteristics of ground motion. The effect shall be properly incorporated to make an efficient clustering strategy.

To sum up, a simplified analysis model with consideration of higher vibration mode, the blade-tower coupling effect and soil amplification is necessary to do

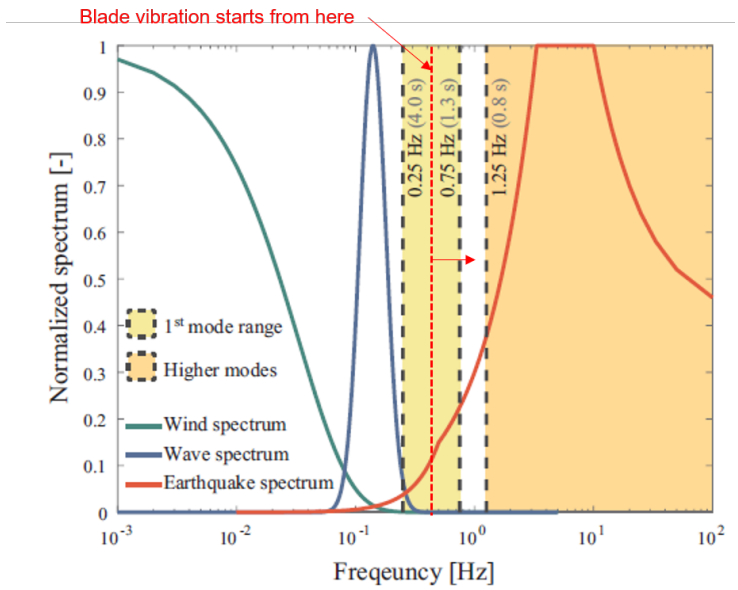

Figure 1.2: Typical frequency ranges of OWT and environmental loads [2]

proper sensitivity studies and develop a clustering strategy for the seismic analysis.

1.3 Goals and approaches of the thesis

Based on the problem statement above, the main goal of this thesis is set as below;

- **Development of clustering strategy to optimize the design of RNA and support structure in offshore wind farm under seismic conditions**

To achieve this goal, and based on the problem definition, three intermediate objectives need to be accomplished:

- Create a simple (but reasonable) calculation model which can properly include higher vibration modes and blade-tower coupling effect
- Check the relationship between input (i.e. site conditions) and output (i.e cross-section force) for structural analysis with the simple calculation model

- Develop a clustering strategy that can sort similar design cases and determine the representative case

1.4 Thesis outline

The structure of the thesis is as follows;

Chapter 1 explains the problem statement, goals and approaches of this thesis.

Chapter 2 introduces the development of a simplified calculation model. Theoretical background and assumptions to formulate the calculation model are explained.

Chapter 3 verifies the simplified calculation model in comparison with proven software, BHawC.

Chapter 4 explains the development of the clustering strategy.

Chapter 5 verifies the applicability of the new clustering strategy by applying it to virtual wind farms.

Chapter 6 verifies the applicability of the new clustering strategy especially for the inhomogeneous soil condition.

Chapter 7 summarizes the conclusions and recommendations of this study.

Chapter 2

Formulation of model for seismic analysis

This chapter explains background theory and assumptions for simplified calculatiom model.

2.1 Analysis method

There are several analysis methods for seismic design. The main options are reviewed in this section and the suitable one for this research is discussed. The section is mainly inspired by the lecture note used in Structural response to earthquake in TU Delft [14].

2.1.1 Time-history analysis method

One of the most common approaches is the time-history analysis method. Time-history of the seismic load is applied to the turbine and calculate the response of the system time by time.

The main advantage of this method is its accuracy because it can completely deal with the non-linearity of the system (such as material and soil non-linearity), the transient effect of seismic load and RNA mode, soil amplification, etc. Meanwhile, the computational demand is high in general.

2.1.2 Response spectrum method

Another common method is response spectrum analysis. The response of the system is evaluated with a maximum response spectrum for each vibration mode. Responses to seismic loads are strongly dependent on the natural frequencies of each structural vibration mode. For a particular earthquake, the response spectrum defines the maximum response (displacement, velocity or acceleration) of a single-degree-of-freedom system as a function of the natural period of the system, which can be used for calculating maximum forces and stresses at each section.

The main advantage of this method is its small computational demand because it requires modal analysis only. As a trade-off, it contains some errors due to its approximation. For example, it does not consider the material non-linearity and compromise it by scaling the response like ductility factor (q-factor in Eurocode) to some extent. Also, it does not consider other non-linearity (e.g. soil non-linearity).

For example, it can consider the material non-linearity by using ductility factor (q-factor in Eurocode) to some extent, but it cannot consider other non-linearity (e.g. soil non-linearity). Also, it cannot directly input the local damping (e.g. aerodynamic damping) because it needs to set the damping ratio for each vibration mode. Furthermore, it has a limitation for considering the effect of soil amplification since this method is not able to set different seismic signals at each embedded depth. In practice, an amplification factor is applied to represent the effect, but it has to contain some approximations.

2.1.3 Frequency domain method

The third approach is the frequency domain method. In this method, the response of the system is evaluated in the frequency domain. After creating a governing equation of motion in the time-domain, the equation is converted to the frequency domain by Fourier transform, then the response in the frequency domain can be solved. After that, it can be converted again to the time-domain by using inverse Fourier transform.

The advantage of this method is its small computational demand as well. Also, it can accurately deal with local damping. In the case of time history analysis, modal decomposition will yield a coupled system of ordinary differential equations (ODEs) for the non-proportional damping and complicated convolution integrals to account for the local damping, and therefore the benefit in using modal decomposition vanishes altogether. In the frequency domain method, however, modal decomposition will yield algebraic equations which for non-proportional damping will simply be coupled. However, solving coupled algebraic equations is as fast as solving uncou-

pled ones and thus there are no extra computational costs. That means that low computation demand can be achieved even if considering local damping in detail. Furthermore, the method is able to properly consider soil amplification.

The disadvantage of this method is the limitation of its applicability. First, it can be applied only to the linear system. Second, it can be applied only for the problem with damping and zero initial conditions. The formulas for this method are summarized below.

First, the equation of motion is written in time domain.

$$\mathbf{M}\ddot{\mathbf{x}}(t) + \mathbf{C}\dot{\mathbf{x}}(t) + \mathbf{K}\mathbf{x}(t) = -\mathbf{M}\mathbf{r}\ddot{u_g}(t) \tag{2.1}$$

Then, it is converted to frequency domain by applying the integral transform.

$$(-\omega^2\mathbf{M} + i\omega\mathbf{C} + \mathbf{K})\tilde{\mathbf{x}}(\omega) = -\mathbf{M}\mathbf{r}\tilde{u_g}(\omega) \tag{2.2}$$

$$\tilde{\mathbf{x}}(\omega) = (-\omega^2\mathbf{M} + i\omega\mathbf{C} + \mathbf{K})^-1(-\mathbf{M}\mathbf{r}\tilde{u_g}(\omega)) \tag{2.3}$$

Lastly, the response in frequency domain can be converted to time domain.

$$\mathbf{x}(t) = \frac{1}{2\pi}\int_{\infty}^{-\infty} \tilde{\mathbf{x}}(\omega)\exp(i\omega t)d\omega \tag{2.4}$$

2.1.4 Summary of analysis method and selection in this thesis

The features of these three analysis methods are summarized in the table 2.1.

Response spectrum method and frequency domain method are selected for this study because of the following two reasons;

First, we focus on the linear problem to develop a clustering strategy. The important thing for creating a clustering strategy is to grasp the general tendency and sensitivity of the system against each design parameter. Although the non-linearity of the system affects the details of the structural design, it is a reasonable assumption in this stage to concentrate on the linear problem only.

The second reason is the balance between accuracy and computational demand. In order to grasp the general tendency and sensitivity of the system against each design parameter, a lot of parametric studies are required. These two methods provide reasonably accurate results with quite low computational demand, which is suitable for doing a lot of parametric studies.

Through the model verification part, the accuracy and computational demand for these two methods are evaluated. Then, the suitable one is used for developing the clustering strategy.

Analysis method	Time domain Method	Response Spectrum Analysis Method	Frequency domain method
Soil non-linearity	considered	NOT considered	NOT considered
Structural non-linearity	considered	partially considered	NOT considered
Consideration of damping	considered	partially considered	considered
Soil amplification	considered	partially considered	considered
Computational demand	High	Low	Low

Table 2.1: Comparison of analysis methods

2.1.5 Introduction of BHawC

In order to verify the model's accuracy, the simplified model to be created in this study is compared with proven software, such as BHawC.

BHawC is a software for aeroelastic time-domain analysis of wind turbines developed and used by SGRE. BHawC is used for the dynamic time-domain analysis to retrieve loads on all relevant turbine components, including support structure, and has been tailored for and validated on all SGRE wind turbines. With this extensive track record, BHawC is a well-established and known in-house software of SGRE.

BHawC performs time-domain analysis under different environmental conditions (i.e. wind, wave, current and seismic excitation) with batch simulations. As discussed in 2.1.1, time-history analysis is able to capture the non-linear effect, and also RNA is modeled with complex structural elements in detail. Hence, BHawC shows a quite accurate results.

As a trade-off, the computational demand for BHawC is relatively high. On average, it takes around 30 minutes for one calculation in seismic analysis (of course, it depends on the mesh size and the duration of seismic signals, etc.).

This study tries to create a simplified calculation model which is accurate enough and less computational demanding by adopting some approximations.

2.2 Soil model

In accordance with Tsouvalas [14]. there are the following four types of analytical approaches for soil models especially on pile foundations.

1. Beam-on-Dynamic-Winkler-Foundation (BDWF) or Kelvin – Voigt model;
2. Analytical (or semi analytical) models.
3. Finite elements or Finite Elements/Boundary Elements formulations.
4. Analytical or semi-analytical for dynamic impedance matrix at the level of the pile-head.

Method-1 and method-4 are commonly used in engineering practice. Method-1 represents the soil reaction as springs or springs-dashpots, respectively, acting locally at the various points along with the pile-soil interface. Method-4 focuses on the dynamic impedance matrix at the level of the pile-head alone, which allows making the problem simple.

Method-1, BDWF, is selected as a soil-foundation model for this study because it is widely accepted in engineering practice and it shows reasonable accuracy. Soil spring is defined as a p-y curve, which represents the soil resistance (p, soil resistance per unit length of the pile) to the pile deflection (y) for the piles under lateral loading. This study limits the system response within the linear regime, so the soil stiffness is linearly increased as a function of the displacement.

The p-y curve is defined in several design standards. In the model verification part, the p-y curve used in the real project is directly applied. In the clustering strategy part, on the other hand, the p-y curve is calculated in accordance with DNVGL-ST-0126 [15].

2.3 Structure model (Monopile)

There are several types of foundations for offshore wind turbines. The most common system around the world is Monopile foundation since it has been proved to be economical at shallow water depth. In accordance with Wind Europe 2019 [16], the market share is more than 80%. In order to assure wide applicability, this study focuses on Monopile as its foundation type.

There are several options to model Monopile, such as Euler-Bernoulli beam, Timoshenko beam and rigid body. Gupta [17] studied the applicability of these three elements on monopile foundation. It found that Timoshenko beam has wide applicability both on structural geometries (i.e. diameter and wall thickness) and soil conditions. This research deals with a wide range of design parameters to develop a general strategy for clustering, so Timoshenko beam is selected. Panzer [18] summarized the procedure to create an FE model on Timoshenko by Matlab, so this thesis follows the procedure.

2.4 RNA model

Kang [10] tried to model the blade-tower coupling effect with a simple approach. It assumed Euler-Bernoulli beams both for monopile and blade sections, and applied force-equilibrium condition to connect two equations of motions as shown in figure

2.1. Moreover, centrifugal force due to blade rotation is included in the equation of motion as an axial force. Then, governing equations were analytically solved. Liu [11] also tried to model blade-tower coupling effect with a similar method, but it conducted not only modal analysis but also forced vibration analysis due to environmental loading and also it considered soil-structure interaction to some extent while Kang [10] assumed fixed boundary condition at mudline. These models didn't consider seismic loading, but provided useful knowledge to represent the blade-tower coupling effect.

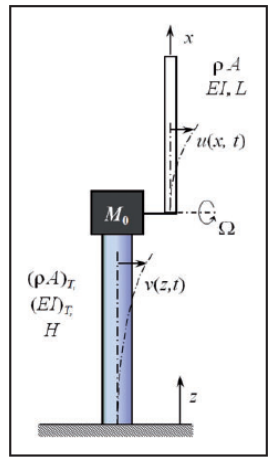

Figure 2.1: simplified model which represents blade-tower coupling effect [10]

RNA model and model overview in this thesis are summarized in the figure 2.2. The blade is modeled as Euler-Bernoulli beam because of its slender shape (Technically, Timoshenko model is used because of standardization with structure section, but shear stiffness is set to zero, which represents Euler-Bernoulli beam). Nacelle and Hub are modeled as point masses. Nacelle and Hub are connected by a rigid beam. In order to accurately model them, proper offset and tilt angle of the rotor is taken into account. Ali [8] compared the results with and without blade twist, which revealed the difference between these twos is not so large. Hence, blade twist is ignored in this study.

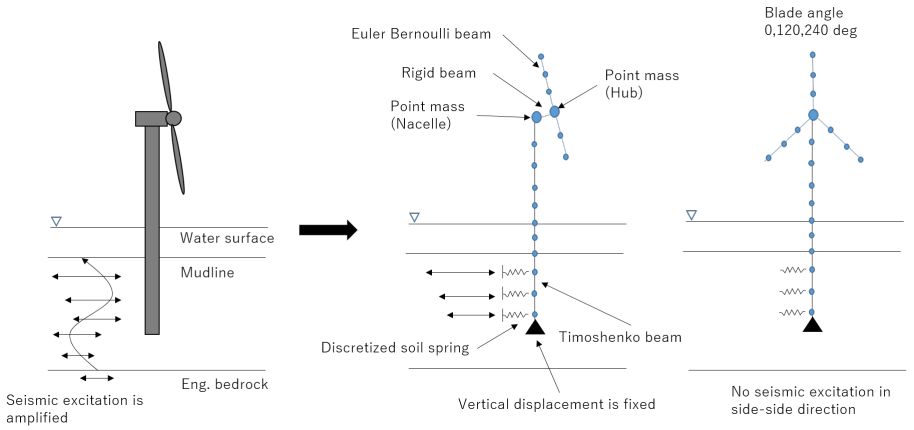

Figure 2.2: Model overview

2.5 Load application

2.5.1 Load combination and direction

DNVGL-ST-0437 [19] defines the combination of several environmental loads for seismic analysis, which corresponds to DLC 11.1 to 11.3 in the figure 2.3. DLC 11.3 tends to be a critical case based on SGRE's past experiences, so parked condition is selected as turbine operating status. Although DLC 11.3 requests a combination of several environmental loads, the only seismic load is considered in this study because the effect from wind, current and wave loads are much smaller than the one from seismic load based on SGRE's past experiences.

The Japanese design standard on wind turbine [20] mentioned that two horizontal and one vertical direction shall be considered for seismic design and also horizontal direction can be a design driver in most cases. Furthermore, it allows evaluating the effect from each direction independently when the effects of eccentricity are small. Hence, this study limits the direction of the seismic load to a single fore-aft direction since fore-aft direction tends to be a design driver in SGRE's past projects.

To sum up, following load conditions are considered in this study.

- Operating status: Parked condition
- Wind load: N/A

- Wave/current load: N/A
- Seismic load: single direction (only fore-aft direction) is considered

Table 4-4 Extended design load cases (Continued)

Design Situation	DLC	Wind Condition	Marine Condition				Other Conditions:	Type of Analysis		Partial safety factor
			Waves	Wind and wave directionality	Sea Currents	Water Level		Onshore	Offshore	
Temperature effects (parked, standing still or idling)	10.2	NWP $V_{hub} = V_1$	$H=H_S(V)$	COD, UNI	NCM	MSL	Temperature effects	U	U	N
Earthquake (power production)	11.1	NTM $V_{in} \le V_{hub} \le V_{out}$	$H=H_S(V)$	COD, UNI	NCM	NWLR	Earthquake	U	U	See [4.3.4]
Earthquake plus grid loss (power production)	11.2	NWP $V_{in} \le V_{hub} \le V_{out}$	$H=H_S(V)$	COD, UNI	NCM	NWLR	Earthquake plus grid loss	U	U	See [4.3.4]
Earthquake plus grid loss (parked, standing still or idling)	11.3	NWP $V_{hub} = V_1$	$H=H_S(V)$	COD, UNI	NCM	NWLR	Earthquake plus grid loss	U	U	See [4.3.4]
Wind farm influence (power production)	12.1	NTM $V_{in} \le V_{hub} \le V_{out}$	$H=H_S(V)$	COD, UNI	NCM	NWLR	Wind farm influence	F/U	F/U	F/N

Figure 2.3: Design load cases related to seismic load in [19]

2.5.2 Seismic loads

2.5.2.1 Source of seismic loads

As for the model verification part, seismic inputs are uniformly applied from pile tip to mudline for simplicity. It means that seismic inputs at mudline from the real Japanese project are extracted and uniformly applied to all the depth. Meanwhile, more realistic seismic input is used for the development of the clustering strategy. Seismic input at engineering bedrock is prepared in accordance with [20] by spectral matching approach, then the signal is amplified from the engineering bedrock to the surface in accordance with the method introduced in the section 2.5.2.2.

2.5.2.2 Wave propagation from the bedrock

Seismic excitation is amplified when propagating from the bedrock to the mudline (we call it ”soil amplification”), which means that seismic input is different at each position in the embedded pile section. There are several approaches to capture the soil amplification, such as 1D to 3D model as shown in [21]. This study uses a one-dimensional shear wave propagation model due to its reasonable accuracy and simplicity to implement in the finite element code. This is the same model as the

one used in the software SHAKE91 and STRATA which are popular to calculate wave propagation for seismic analysis. The main assumption of the one-dimensional shear wave propagation model is below;

- The response of the soil deposit is predominantly caused by SH waves (shear waves polarized in the horizontal plane) propagating vertically from the underlying bedrock.
- The boundaries between the different layers of the soil, the bedrock and the surface are horizontal.
- The soil behaves in a linear way.
- The soil material allows dissipation of energy (material damping).

Figure 2.4 represents wave propagation from bedrock to free surface in the homogeneous soil layer. Assuming the homogeneous soil conditions, the seismic excitation at each depth can be represented with the following equations.

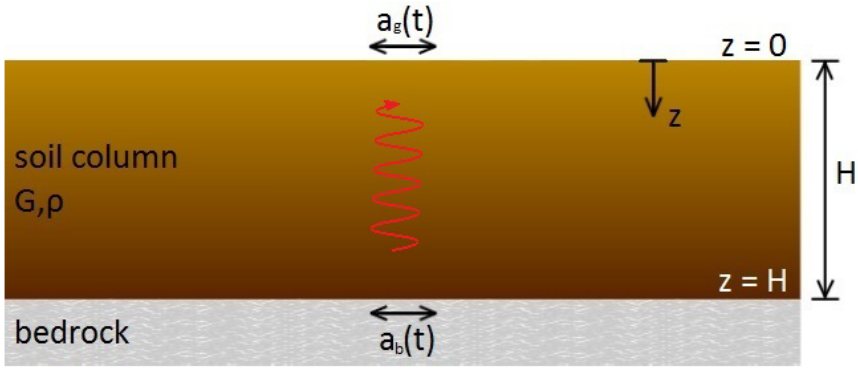

Figure 2.4: Schematic figure for wave propagation in single soil layer [14]

$$u(z,t) = \tilde{U}(z,\omega)\exp(i\omega t) \tag{2.5}$$

$$\tilde{U}(z,\omega) = -\frac{\cos(\frac{\omega}{c_s^*}z)}{\omega^2\cos(\frac{\omega H}{c_s^*})}A_0 \tag{2.6}$$

where $c_s^{*2} = \frac{G+i\omega\eta}{\rho}$, η represents material dissipation and A_0 represents acceleration at bedrock. $\tilde{U}(z,\omega)$ is used for seismic wave at each depth for the calculation model. 5% of material dissipation is assumed for this study (for all the soil condition).

In the case of real soil conditions, multiple soil layers exist and simultaneous equations shall be solved. In this study, however, a homogeneous soil layer is assumed for simplicity.

2.6 Damping

2.6.1 Damping in this study

As explained in Chen [22], there are four damping sources in offshore wind turbines, such as structural damping, soil damping, hydrodynamic damping and aerodynamic damping.

In this study, the effect of structural damping and soil damping are combined to the stiffness proportional damping, which is the same concept as BHawC. Hydrodynamic damping is neglected due to its small contribution. Aerodynamic damping is also neglected since idling condition is assumed.

Stiffness proportional damping is applied both for the blade and structure part, but a different damping ratio is applied for each part to represent realistic system property, which is the same concept with BHawC.

The damping ratio for the blade section is extracted from the SGRE's data sheet. 1st edgewise bending mode and 2nd edgewise bending mode are selected as representative cases for calculating the stiffness proportional damping. The damping ratio for the structure section is based on the SGRE's past project which uses similar turbines and foundations. The data is summarized in the table 2.2.

As for the response spectrum method, it is not possible to explicitly apply the damping ratio for each element. Hence, depending on the type of vibration modes, a suitable damping ratio is selected. For example, the damping ratio for blade mode is used in the case that blade vibration is dominant.

2.6.2 Frequency dependent soil damping

Some literature (e.g. Tsouvalas [14]) mentions the impact of the frequency dependency of soil damping. In order to check if the effect is important for this study or not, a sensitivity study is carried out.

	Structure		Blade	
	Damping ratio	Natural frequency	Damping ratio	Natural frequency
1st mode	0.4% (2.6% LogDec)	Natural frequency for the 1st structural mode	0.3% (1.6% LogDec)	0.76Hz
2nd mode	1.1% (8.3% LogDec)	Natural frequency for the 2nd structural mode	0.7% (4.4% LogDec)	2.05Hz

Table 2.2: Summary of damping ratio

The system responses (i.e. bending moment) with frequency-dependent and independent damping are compared with each other for various soil conditions (i.e. from soft to hard soil) and seismic inputs. The results show that the difference of the maximum bending moment at the tower top and mudline is less than 3.0%, which is not so impactive on the general trend for clustering. The range of dominant vibration modes is relatively small (i.e. from 0.2Hz to 1.0Hz) for the system studied in this research. If the range is much wider (e.g. seismic input with a large variety of frequency components, modal participation masses are widely distributed on a large number of modes etc.), the frequency-dependent soil damping could have an impact on the output.

In this study, however, frequency dependency on soil damping is neglected for simplicity since its impact is limited.

This is not the main topic in this study, so the content is summarized in the Appendix B as an additional study.

Chapter 3

Verification of the simplified calculation model

This chapter explains the process to verify the simplified calculation model is suitable for making the clustering strategy.

3.1 Procedure to verify the calculation model

This section explains the procedure to verify the simplified calculation model by comparing it with the results of a proven software (i.e. BHawC).

First, input parameters to be used for the verification are selected. In order to represent the realistic situation, most parameters are extracted from the project which SGRE carried out in seismic regions. The details are explained in the next section.

Second, two calculation models are prepared, such as the frequency domain method and response spectrum method, to compare the applicability of these methods. Then, the responses of the system are calculated. The maximum bending moment at the tower top and mudline are especially focused on because they are generally the dominant output for the structural design of RNA and support structure.

Then, the responses calculated by the simplified model is compared with the ones from proven software, such as BHawC, and the applicability of each method is discussed.

Additionally, the effect of the modeling approach on RNA is checked by comparing the model with a single lumped mass model. As discussed in the previous chapter, the modeling approach on RNA may provide a considerable difference in the structural analysis. Hence, the model, which uses discretized masses at the blade section, is compared with a single lumped mass model and checked if it properly represents the effect.

3.2 Input parameters

This section introduces the input parameters for the model verification.

3.2.1 Wind turbine

According to WindEurope Annual Offshore Statistics 2019 [16], the average turbine rating in 2019 is 7.8MW. Hence, SG-8.0-167-DD, which is a SGRE's turbine model with 8MW power capacity, is selected for the model to assure the wide applicability of this study.

The geometries of RNA and tower are extracted from the SGRE's data sheet for SG-8.0-167-DD. Idling condition is assumed as operating condition, so blade pitch angles are set to 90 degrees and any additional loads from the turbine's operation are neglected. The rotation of the rotor is fully restricted.

Figure 3.1 shows the overview of SG-8.0-167-DD from its brochure.

3.2.2 Geometry of foundation

The geometry of the foundation is extracted from the real project for SG-8.0-167-DD in the seismic region. Figure 3.2 shows the schematic figure for the whole structure and figure 3.3 shows the details about its geometry (i.e. outside diameter and wall thickness for each section).

The main parameters are summarized in the table 3.1.

3.2.3 Soil condition

As discussed in the section 2.2, soil stiffness is defined by py-curve, which defines the relationship between displacement and soil reaction at each depth. This study limits the system response within the linear regime, so the soil stiffness is linearly increased as a function of the displacement. The soil stiffness is also extracted from the real project for SG-8.0-167-DD in the seismic region as shown in the figure 3.4.

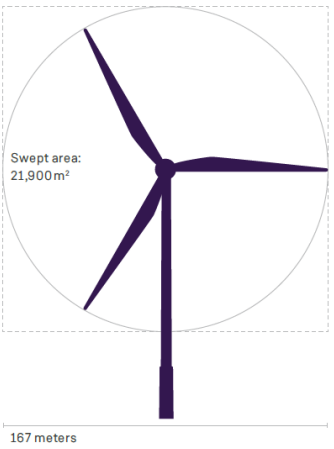

SG 8.0-167 DD	
IEC class	S (1B)
Nominal power	8,000 kW
Rotor diameter	167 m
Blade length	81.4 m
Swept area	21,900 m²
Hub height	Site specific
Power regulation	Pitch-regulated, variable speed

Figure 3.1: Overview of SG-8.0-167-DD in [23]

3.2.4 Truncation of higher vibration modes

In order to speed up the calculation, higher vibration modes are truncated with the modal decomposition technique. According to Wiley [24], 80% to 90% of modal participation mass can be considered sufficient to capture the dominant dynamic response of the structure. Kitahara [25] and Zhao [26] mentioned that 1st to 3rd structural modes are dominant for structural analysis on wind turbines (mainly 1st and 2nd modes).

Based on these findings, the modes from 1 to 30 are included in the calculation and the modes more than 31 are truncated. The range covers 1st, 2nd and 3rd structural modes. Also, the summation of the modal participation mass from mode-1 to mode-30 becomes around 80%, which corresponds to the requirement in [24].

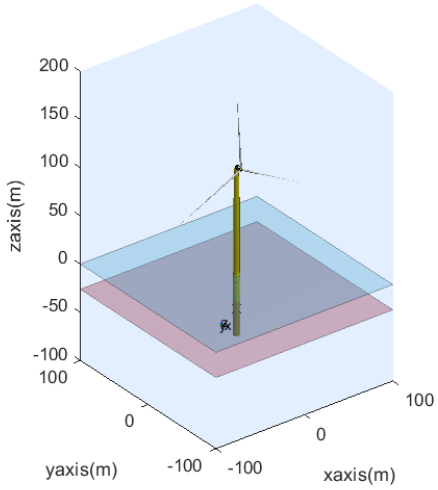

Figure 3.2: Schematic figure for turbine, tower and foundation

Excluded due to confidential reason

Figure 3.3: Geometry of tower and foundation

Hub height	110.33m
Interface level	21.51m
Water depth	-26.18m
Pile penetration depth	-62.18m (i.e. 40m is embedded)
Nacelle mass	253 ton
Hub mass	97 ton

Table 3.1: Main parameters

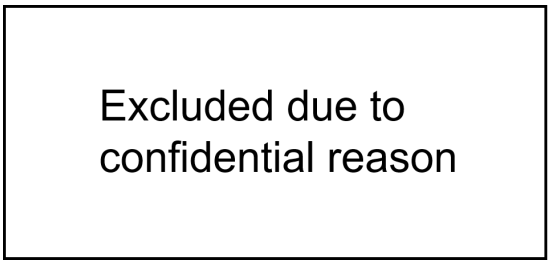

Figure 3.4: Soil stiffness

3.2.5 Seismic input

Seismic inputs for the model verification are extracted from the real project for SG-8.0-167-DD in the seismic region. In order to simplify the problem and focus on the verification of the calculation model itself, soil amplification is not included in the model verification. That means uniform seismic excitation is assumed from the pile tip to mudline.

The seismic inputs to be used for the model verification are summarized in the figure 3.5. Different 5 seismic signals are applied to check the wide applicability of the calculation model.

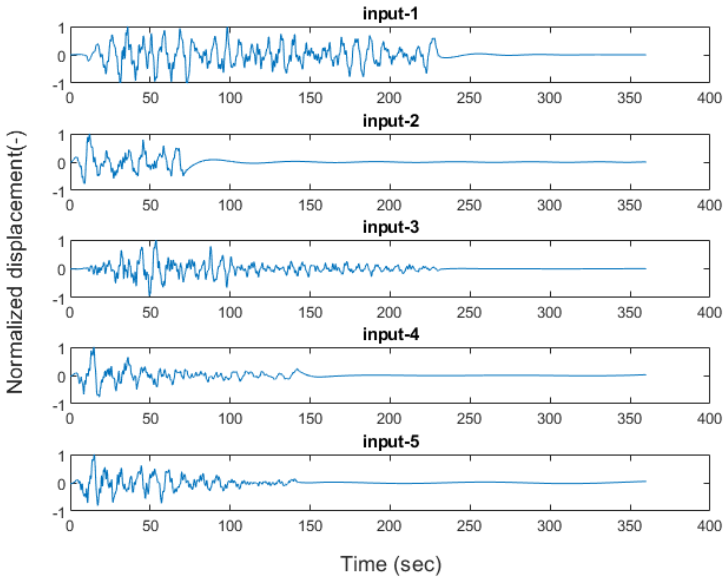

Figure 3.5: Time history of seismic inputs

3.3 Evaluation of the result

This section shows the output from the calculation models and discusses their applicability for further studies in comparison with the outputs from BHawC.

3.3.1 Eigen analysis

Dynamic property (i.e. natural frequencies and mode shapes) of the system is verified with eigen analysis in this section.

3.3.1.1 Eigen analysis on single blade

Natural frequencies and mode shapes for the single blade are calculated and compared with the ones from BHawC. As shown in table 3.2, the natural frequencies show small errors up to mode-4 (i.e. less than 4%) which corresponds to 2nd edgewise mode while they show relatively large deviation for 3rd and 4th flapwise modes. The same trend can be seen for the mode shapes as well (See figure 3.6). The error comes from the imperfection of the blade model. The created model used a simple Euler-Bernoulli beam and does not include the effect of blade twist and eccentricities while BHawC completely includes these effects. Although larger errors can be found in higher vibration modes, their contribution to the structural analysis is relatively small since the dominant vibration modes for seismic analysis are 1st and 2nd flapwise/edgewise modes. Hence, the blade model is accepted for further studies.

Mode		Natural frequency (Hz)		
No	**Description**	**BHawC**	**Model**	**Error**
1	1st flapwise	0.478	0.481	1%
2	1st edgewise	0.757	0.768	1%
3	2nd flapwise	1.285	1.296	1%
4	2nd edgewise	2.025	2.099	4%
5	3rd flapwise	2.516	2.214	12%
6	4th flapwise	3.945	3.002	24%

Table 3.2: Comparison of the natural frequency for single blade

3.3.1.2 Detect the dominant vibration modes

Modal participation mass represents the effective mass excited in each mode. It can be derived from mass matrix, eigen vector and participation factor for each degree

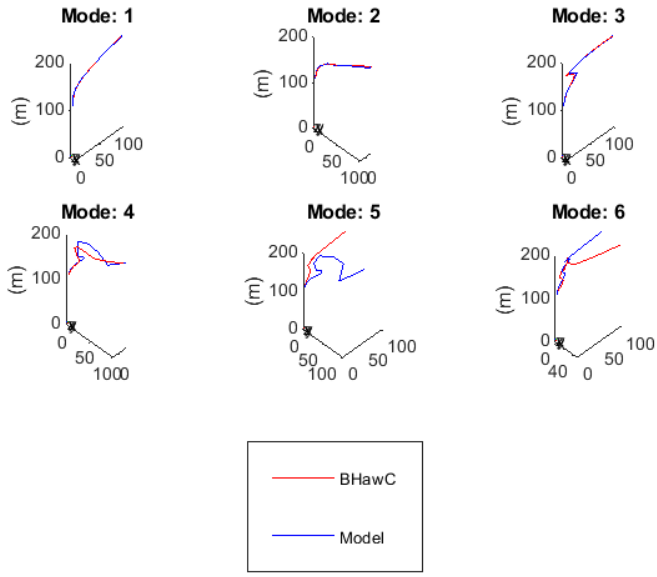

Figure 3.6: Comparison of mode shapes on single blade

of freedom system.

Modal participation mass for each mode is checked to figure out which mode has an impact on the structural analysis. The ratio of modal participation mass to the total mass is summarized in the figure 3.7. It clearly shows the top two largest values are mode-2 and mode10., which correspond to 1st and 2nd structural vibration mode for for-after direction respectively. The third-largest value is mode-21 which corresponds to 3rd structural vibration mode, but the value is much smaller than the top two (i.e. less than the half value). Also, small peaks (i.e. around 3%) can be found at mode-7, mode-15 and mode-26. These modes show large eigen values not at the structure part but at the blade part, so they are named 1st/2nd/3rd RNA modes respectively in this thesis.

The summation of modal participation mass up to mode-30 is around 78%, which corresponds to the requirement in [24] as discussed in the previous section.

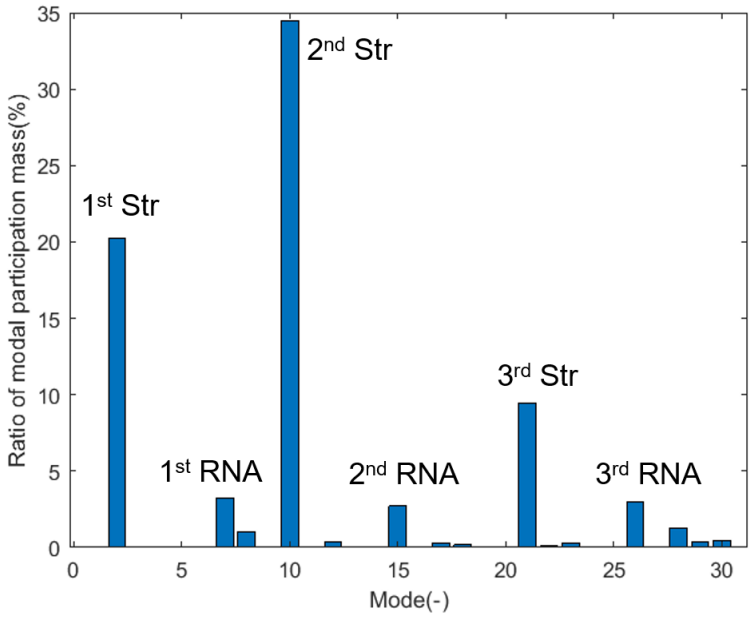

Figure 3.7: Modal participation mass for each mode

3.3.1.3 Eigen analysis on the whole structure

Then, natural frequencies and mode shapes for the whole structure is calculated and compared with the ones from BHawC, especially about the 6 principal vibration modes, such as 1st/2nd/3rd structural mode and 1st/2nd/3rd RNA mode.

Some components (i.e. stiffness around RNA and soil spring) are calibrated in order to get the agreement with BHawC based on the eigen analysis. This section shows only the final result. The details about the calibration can be found in Appendix A.

Figure 3.8 shows the mode shapes for dominant vibration modes in fore-aft direction. Figure 3.9 shows the comparison on mode shapes to BHawC for the structure part and table 3.3 shows the comparison on natural frequencies. Although the model shows slight deviations to BHawC especially for higher vibration modes, it shows good agreement both for the natural frequency and mode shape.

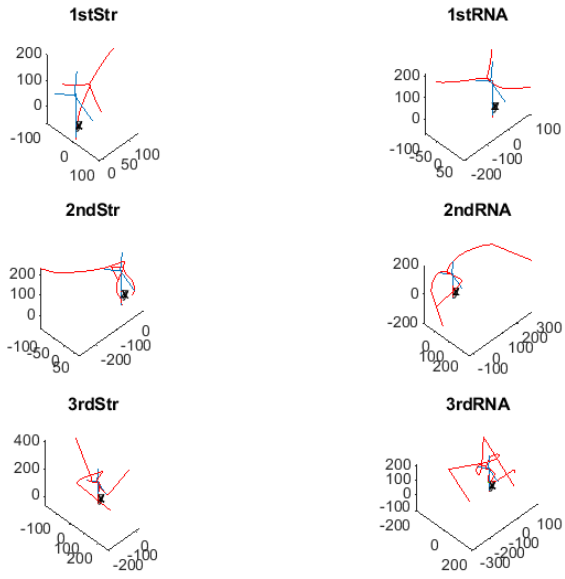

Figure 3.8: Mode shapes on the whole structure from the model

Mode	Mode No.	Natural frequency (Hz)		
		BHawC	Model	Error
1st structure	2	0.215	0.211	2%
1st RNA	7	0.661	0.665	1%
2nd structure	10	0.976	0.980	0%
2nd RNA	15	1.792	1.853	3%
3rd structure	21	2.359	2.365	0%
3rd RNA	26	4.017	3.854	4%

Table 3.3: Comparison of natural frequencies for structure

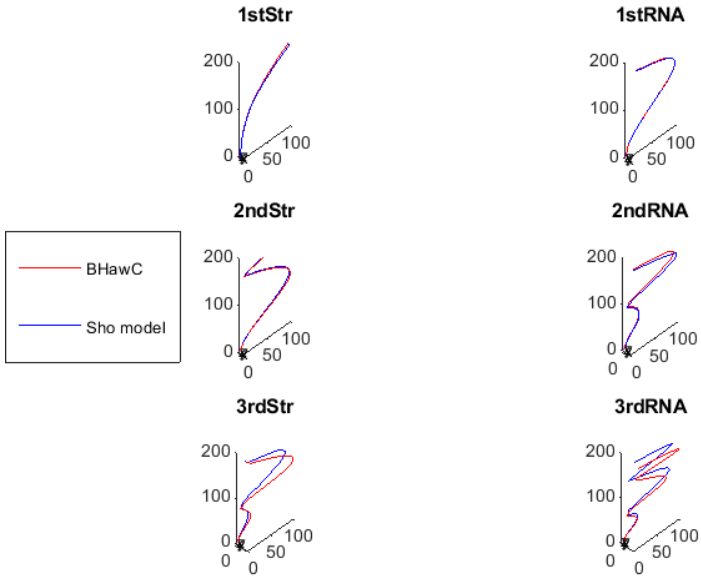

Figure 3.9: Comparison of mode shapes on the whole structure

3.3.2 Forced vibration analysis

Seismic inputs are applied to the system and the response (i.e. bending moment) is calculated by different two methods, such as the frequency domain method and the response spectrum method.

3.3.2.1 Forced vibration analysis by the frequency domain method

This section summarizes the result of the forced vibration analysis by the frequency domain method. Bending moments from tower top to mudline for all 5 seismic inputs are compared with the ones from BHawC. The most interesting parameter for the clustering is the maximum bending moments for the whole time series. Figure 3.10 shows the comparison of the maximum bending moments between the model and BHawC.

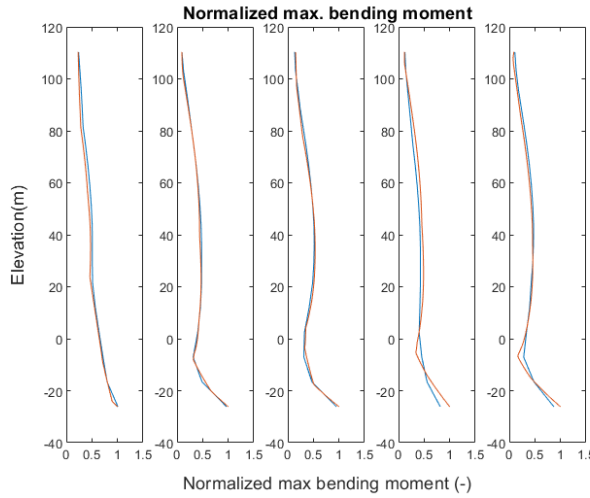

Figure 3.10: Max. bending moment, Red:BHawC & Blue:Model, Input-1 to 5 from left to right

Additionally, time histories of bending moment and spectrum in the frequency domain are compared for the confirmation as shown in the figure 3.11, 3.12, 3.13 and 3.14. As seen in the frequency spectrum, the model captures the peaks well in the dominant frequency range, such as 1st and 2nd structural modes (less than 1.5 Hz), while it shows some deviation to BHawC for the higher frequency range (i.e.

more than 1.5 Hz). But in general, it shows good agreement with BHawC on the time history of bending moment and the maximum bending moment.

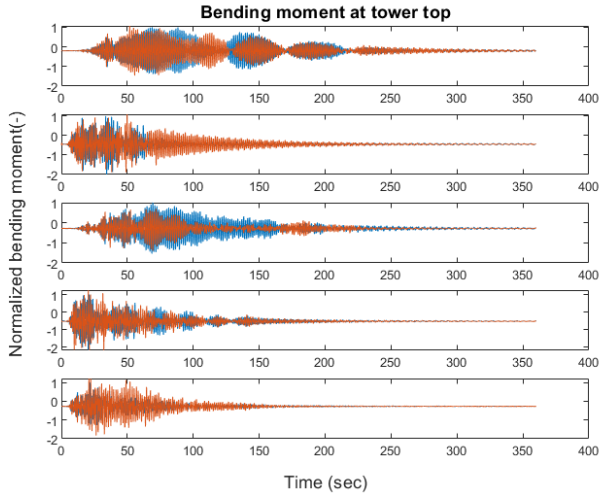

Figure 3.11: Time history at tower top (Red:BHawC & Blue:Model)

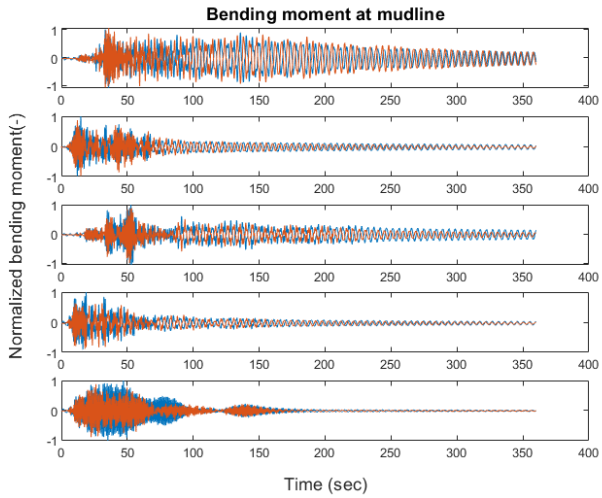

Figure 3.12: Time history at mudline (Red:BHawC & Blue:Model)

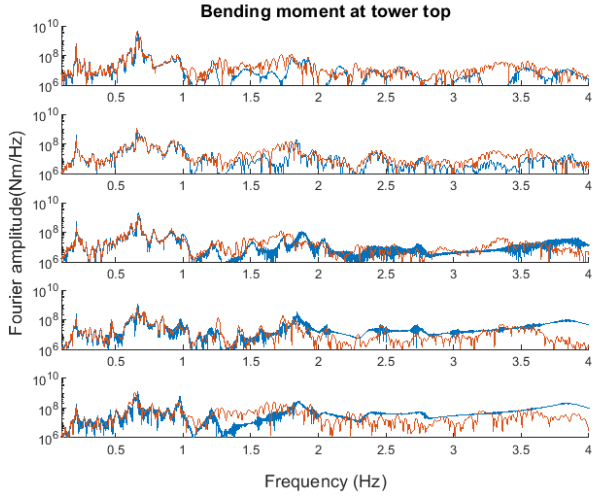

Figure 3.13: Frequency spectrum at tower top (Red:BHawC & Blue:Model)

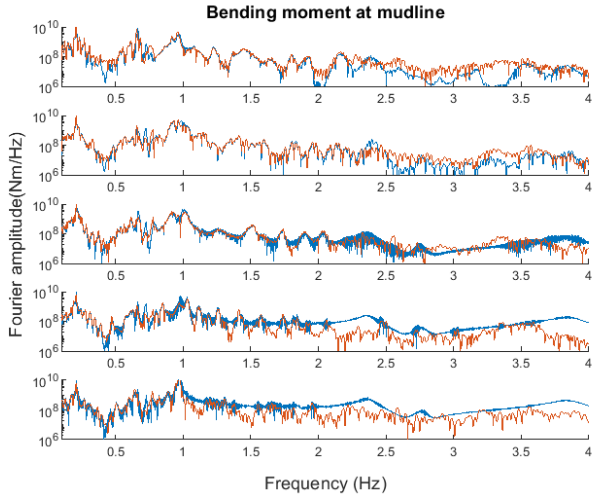

Figure 3.14: Frequency spectrum at mudline (Red:BHawC & Blue:Model)

3.3.2.2 Forced vibration analysis by the response spectrum method

In the same way, the maximum bending moments from tower top to mudline for all 5 seismic input are compared with the ones from BHawC by the response spectrum method as shown in the figure 3.15. Only the max. bending moment is calculated in this method because this method is not able to analyze the time history of the response. The result also captures the trend well while it shows a bit less accurate results compared to the frequency domain method.

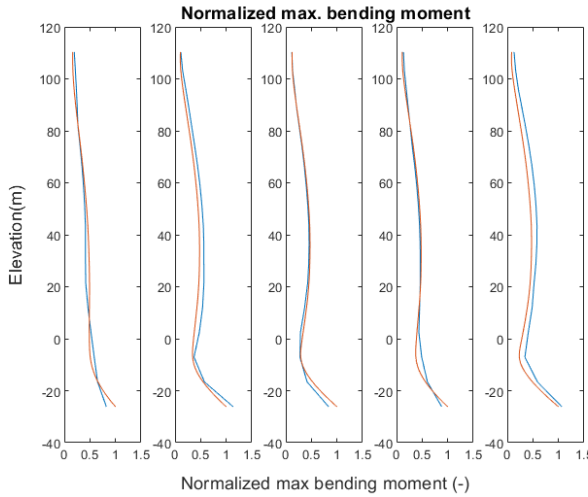

Figure 3.15: Red:BHawC & Blue:Model, Seismic input 1 to 5 from left to right

3.3.2.3 Summary of the forced vibration analysis

The errors on the maximum bending moment at the critical section for structural design, such as tower top and mudline are summarized in the table 3.4. The averaged errors on the frequency domain method are 8 to 10 % while the ones on the response spectrum analysis method are 15 to 16%.

Two types of errors are contained in these errors, such as errors from the analysis method and modeling errors. In the case of the linear system, the frequency domain method should provide almost the identical result with the time domain analysis result (although there are some causes such as the p-delta effect etc.) while the response spectrum method should have some errors since it is not able to accurately

consider the modal superposition and approximate it by using the squre-root sum (SRSS) approach. So, the difference on the error between the frequency domain method and the response spectrum method, which is around 5%, comes from the analysis method. The remaining 10% should come from the modeling error.

Although they don't show complete agreement with BHawC, the accuracy is acceptable for further study because the purpose is to check the general trend between input and output.

Input	**Freq domain**		**Response spectrum**	
	Tower top	**Mudline**	**Tower top**	**Mudline**
1	5%	0%	16%	22%
2	0%	6%	7%	12%
3	12%	6%	5%	19%
4	6%	21%	16%	13%
5	16%	15%	36%	6%
Average	**8%**	**10%**	**16%**	**15%**

Table 3.4: Summary of model errors

3.3.3 Comparison with lumped mass model

For the purpose to check the effect of the modeling approach on RNA, lumped mass model, which models RNA as a single lumped mass at the tower top, is analyzed.

The model overview is shown in the figure 3.16. The left figure shows the original model (called discretized mass model) and the right figure shows lumped mass model. As for the lumped mass model, blade masses (incl. mass moment of inertia from the blades) are added at the tower top.

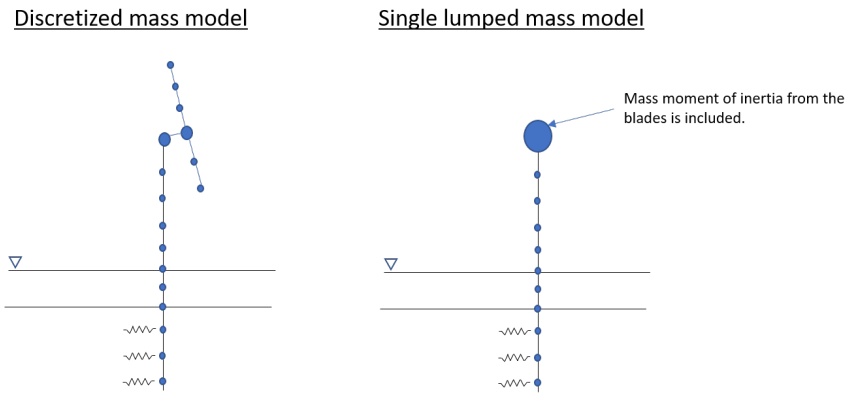

Figure 3.16: Model overview on lumped mass model

3.3.3.1 Eigen analysis on the whole structure

First, the results from eigen analysis are compared. Table 3.5 shows the comparison of natural frequencies for discretized and lumped mass models. Figure 3.17 shows the comparison with BHawC to verify the accuracy of the model for the single lumped mass case.

As for 1st structural mode, deviations on natural frequencies and mode shapes are negligibly small between discretized and lumped mass models. In the case of 2nd and 3rd structural mode, on the other hand, natural frequencies become much smaller value and the mode shape changes. This is quite a reasonable tendency because blade elements provide additional stiffness in the case of discretized mass model, which induces to increase the natural frequency of 2nd and 3rd structural mode.

Mode	BHawC		Research model			
	Discretized	Lumped	Discretized		Lumped	
	Freq(Hz)	Freq(Hz)	Freq(Hz)	Error (%)	Freq(Hz)	Error (%)
1st structure	0.215	0.215	0.211	2%	0.211	2%
2nd structure	0.976	0.901	0.981	1%	0.897	0%
3rd structure	2.359	1.753	2.365	0%	1.741	1%

Table 3.5: Comparison of natural frequencies for lumped mass model

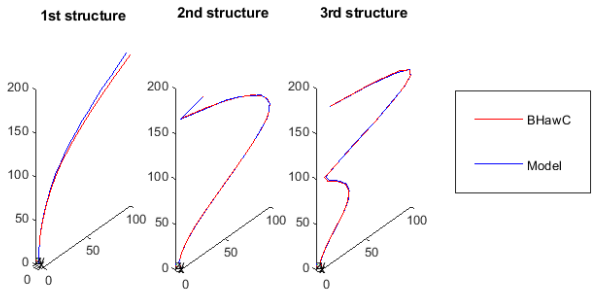

Figure 3.17: Mode shape comparison with BHawC

3.3.3.2 Forced vibration analysis by the frequency domain method

Seismic input No.2 is applied to the system and the system response is compared with discretized mass model. Figure 3.18 shows the comparison of the maximum bending moments between discretized and lumped mass model. Dot-lines (i.e. results from BHawC) clearly show that the max. bending moment becomes much larger values than the ones from discretized model since the natural frequencies are shifted to a lower frequency range, where the seismic input has a larger spectrum in the frequency domain. The solid lines (i.e. results from the model) captures the trend very well although it has a slight deviation. Hence, it is verified for the model to model the blade-tower coupling effect well.

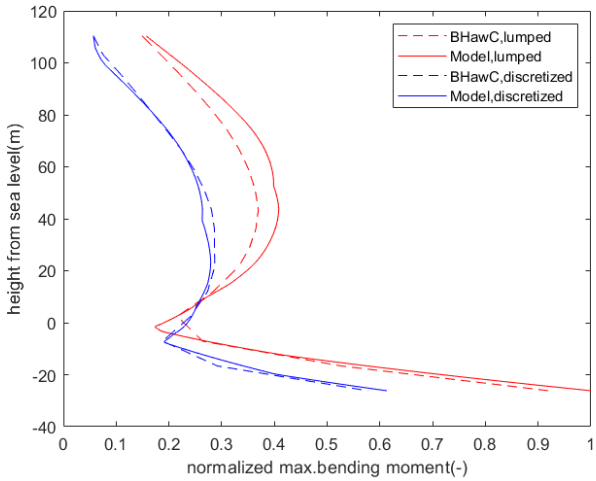

Figure 3.18: Comparision of bending moment for discretized and lumped mass model

3.4 Applicability and limitation of the calculation model

This section discusses the applicability and limitation of the calculation model.

The simplified calculation models (frequency domain method and response spectrum method) are compared with proven software, such as BHawC, and checked its accuracy and computational demand. The results are summarized in the table 3.6.

	BHawC	**Frequency domain method**	**Response spectrum method**
Accuracy	The most accurate	10% error from BHawC	15% error from BHawC
Computatioal demand	30 minutes for 1 case	2.2 minutes for 1 case	1.8 minutes for 1 case

Table 3.6: Comparison of model accuracy and computational demand

Both models generally capture the trend of the system response well, but the frequency domain method shows a bit better accuracy. Hence, this study uses the frequency domain method as a primary method to do sensitivity studies in the further chapters. Response spectrum method is used just as a reference method.

Meanwhile, it is noted that the model (i.e. frequency domain method) has limitations as follows;

- The model neglects the non-linearity of the system, such as material and soil

non-linearity.

- The model does not consider liquefaction due to seismic excitation.
- Only fore-aft direction is verified in this study since it tends to be a critical case.
- Only idling condition is considered in this study since it tends to be a critical case.
- The model contains imperfection on the full RNA model (i.e. the one used in BHawC)

Because of these limitations, the model is not durable to do detailed analysis in the real project. However, it is suitable to investigate the sensitivity from input parameters (i.e. water depth, soil condition etc.) to output (i.e. max. bending moment) for seismic excitations and to capture the trend of seismic analysis.

Chapter 4

Development of clustering strategy

This chapter describes the procedure to develop a clustering strategy for seismic analysis.

4.1 Approach to find the relationship between input and output

This section describes the way to relate the input parameters (i.e. water depth, soil condition and bedrock depth) to the output (i.e. maximum bending moment at tower top and mudline). Through the sensitivity studies, ”library” is experimentally created to store the relationship for the representative case. Extracting and processing the data from the library, the output can be estimated with a much smaller computational demand. The following sections explain the details of this procedure.

4.1.1 Approaches to estimate the maximum bending moment

The most interesting output for structural analysis is the maximum bending moment at critical locations, such as tower top for RNA and mudline for the foundation. In order to make an efficient clustering strategy, it is important to properly estimate the relationship between input parameters and the maximum bending moment.

In the case of response spectrum analysis, the maximum bending moment can be calculated with the following formula. The maximum force vector ($\boldsymbol{F}$) for each

mode can be calculated by mass matrix ($\boldsymbol{M}$), eigen vector ($\boldsymbol{\Phi}$) and acceleration response spectrum (S_a). And, the maximum bending moment for each mode ($\boldsymbol{Q}$) can be derived by multiplying the lever arm ($\boldsymbol{l}$). Then, the maximum bending moment for the whole system can be derived by taking summation over the whole modes (e.g. taking square root summation, summation of maximum values etc.).

$$\boldsymbol{F} = \boldsymbol{M} \times \boldsymbol{\Phi} \times S_a \tag{4.1}$$

$$\boldsymbol{Q} = \boldsymbol{F} \times \boldsymbol{l} = \boldsymbol{M} \times \boldsymbol{\Phi} \times S_a \times \boldsymbol{l} \tag{4.2}$$

The response spectrum analysis is relatively quick and handy approach in comparison with time history analysis, but it still takes time and does not fit clustering strategy. Hence, the following three assumptions are adopted to the formula to simplify and make it quick.

- Truncate minor vibration modes
- Assume the representative depth for the acceleration response spectrum at mudline
- Estimate the effect from $\boldsymbol{M}$,$\boldsymbol{\Phi}$ and $\boldsymbol{l}$ by implementing scaling factor

Following sections explain these assumptions one by one.

4.1.1.1 Truncate minor vibration modes

First, minor vibration modes are truncated and only principle modes, such as 1st/2nd/3rd structure and 1st/2nd/3rd RNA modes, are considered for the calculation. As shown in the figure 3.7, modal participation masses for minor modes are much smaller than the principal modes. So, they don't affect the final output so much.

4.1.1.2 Representative depth for the acceleration response spectrum

Second, the representative depth for the acceleration response spectrum is assumed at mudline. The effect of soil amplification is dependent on the depth, which means that seismic excitation is different at each depth. Hence, the representative depth on the acceleration response spectrum is not simply determined. However, mudline tends to be a good indication for the representative depth. Seismic excitation at mudline tends to have the largest impact since the restriction from the soil is generally much smaller than the other section. Additionally, the sensitivity study (which

varies the representative depth and checks the deviation on the bending moment) is carried out as shown in the Appendix C. It shows that the deviation due to the selection of the representative depth is only a few % to 10% at most. Hence, mudline is selected as a representative depth for the acceleration response spectrum for this study.

4.1.1.3 Implementation of scaling factor

Third, the effects from M,Φ and l are combined to a single parameter, such as "scaling factor". It takes time to properly calculate M and Φ since FE model and eigen analysis are required. To simplify the process, the system property for each vibration mode is estimated by the scaling factor which is derived from the maximum bending moment divided by the acceleration response spectrum for each mode as shown in the formula below. Dividing by the acceleration response spectrum, the effect from the soil amplification is standardized and the parameter represents the sensitivity to the energy intake from the seismic excitation. Calculating scaling factor for every case in the sensitivity study, the relationship between scaling factor and input parameter (i.e. water depth, soil condition and bedrock depth) is revealed.

$$\text{Scaling factor (SF)} = \frac{Q}{S_a} \tag{4.3}$$

4.1.2 Simplified method to estimate the max. bending moment

Based on these assumptions, the maximum bending moment can be estimated by the flowchart shown in the figure 4.1.

In the case of full analysis, FE model is created based on the input parameters and then eigen analysis and forced vibration analysis are carried out to derive the maximum bending moment for each position of wind turbine.

As for the simplified approach, FE modeling, eigen analysis and forced vibration analysis for each position are omitted. On behalf of them, the relationship between input parameters and the scaling factor is quantified through the sensitivity study. The relationship between input parameters and the acceleration response spectrum is also quantified in advance. These relationships are called "library" in this study. For each position of wind turbine, the scaling factor and the acceleration response spectrum are selected from the libraries, then the maximum bending moment is estimated to take summation of multiplying these two parameters on the principle vibration modes. This approach greatly shortens the computational demand while it should have some errors due to the approximations.

The challenge of this method is the development of the library for the scaling factor. It's difficult to calculate it from the theoretical approach since many parameters interact with each other. Hence, it is experimentally derived by a sensitivity study. It means that the full analysis is carried out and the scaling factor is calculated only for the representative case within the reasonable range of input parameters. Interpolating between the representative data, the scaling factor which corresponds to each position of wind turbine can be estimated from the library for the scaling factor.

The library for the acceleration response spectrum can be created by a similar manner. Based on the given inputs for the wind farm, the acceleration response spectrum for the representative case within the reasonable range of input parameters is calculated. Interpolating between the representative data, the acceleration response spectrum for each position of wind turbine can be estimated from the library.

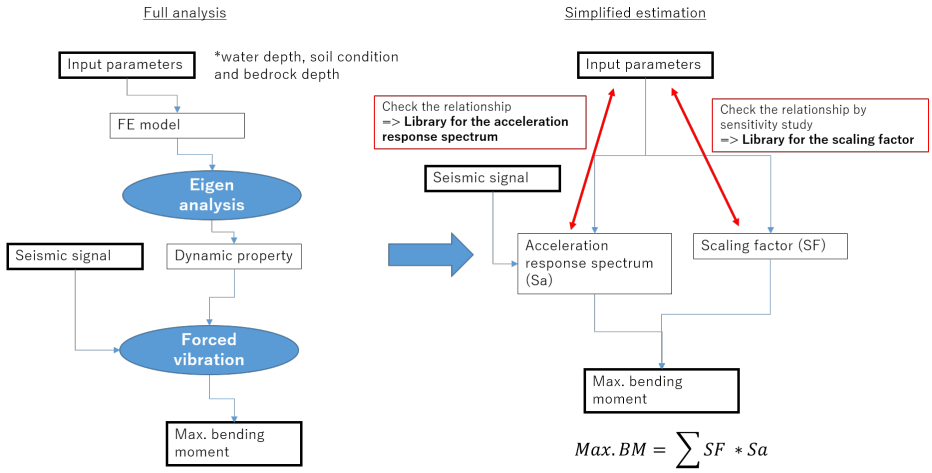

Figure 4.1: Flowchart to calculate max. bending moment (left: full analysis, right: proposed method)

4.2 Input parameters for sensitivity study

Sensitivity studies are carried out to understand the relationship between input and output for seismic analysis. This section explains which input is selected as variable

parameters for sensitivity studies and describes the reasonable range of the input parameters based on some literature studies.

4.2.1 Selection of input parameters

Three parameters are selected as dominant ones for clustering under seismic conditions, such as water depth, soil condition and bedrock depth.

Water depth and soil condition are clearly the critical parameters to determine the structural geometry, which is directly connected to the system property. The unique parameter for seismic analysis is bedrock depth. As explained in the section 2.5.1, seismic excitation is amplified due to resonance with soil. Soil condition and bedrock depth regulate the resonance frequencies and then seismic excitations applying to the system (i.e. energy intake from the seismic excitation to the system).

The range of each input parameter is determined as follows.

4.2.1.1 Water depth

Sánchez [27] summarizes the type of foundations by the range of use from 1995 to 2018 as shown in the figure 4.2. It mentions that Monopile foundation has been installed in the range from 0m to 40m water depth. Nowadays, the development of offshore wind is expanding to deeper water depth. Considering that trend, the range of water depth for the sensitivity study is set from 20m to 50m by 5m interval.

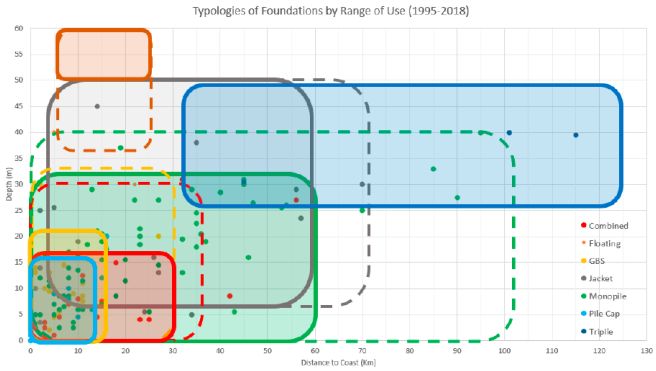

Figure 4.2: Type of foundations by depth and distance to coast (1995–2018) ([27])

4.2.1.2 Soil condition

As shown in the table 4.1, four types of soil conditions are assumed to cover a wide range of site conditions. They are extracted from the several design standards and literature, such as Eurocode [28], Japanese standard [20], Design steel structure [29], DNVGL-ST-0126 [15] and Raikar(2016) [30]. Raikar summarized the soil material damping ratio. It shows the value for sand is from 0.03 to 0.07, so 0.05 is selected for this study.

No.	1	2	3	4	Reference
Name	Hard	Medium	Soft	Very soft	
Category in Eurocode	B	C	C	D	from Eurocode
Soil type	Very dense sand	Dense sand	Medium sand	Loose sand	from Eurocode
N-value	50	30	22.5	15	from Eurocode
Internal friction (deg)	42	36	33	30	from Japanese standard
Shear wave velocity (m/s)	540	290	200	150	from Design of steel structure
Modulus of subgrade reaction,k (MN/m3)	40	25	18	10	from DNVGL-ST-0126
Density in Air (kg/m3)	2070	2000	1875	1750	from Design of steel structure
Density in water (kg/m3)	1045	975	850	725	from Design of steel structure
Material damping ratio	0.05	0.05	0.05	0.05	from Raikar (2016)

Table 4.1: List of soil condition

4.2.1.3 Bedrock depth

Shangguan [31] summarizes the depth to bedrock depth for each region in the world. As for Asia, which is one of the most booming regions for offshore wind development under seismic conditions, the mean and maximum values for bedrock depth is 10m and 65m respectively. Considering the data, this study sets the range of bedrock depth from 0m (i.e. bedrock is located at the surface) to 60m by 10m interval.

4.2.2 Seismic input

One of the most sophisticated design standards for seismic analysis is the Japanese design standard [20]. The standard requests to use the following three types of seismic inputs for seismic analysis, such as Artificial seismic waves for response spectra (Spectral matched wave), Site waves and Observed seismic waves. This study uses only the spectral matched waves because the later two types are strongly dependent on the location of the wind farm which is not suitable to capture the general trend and the spectrally matched waves tend to induce more severe results than the other two based on SGRE's past experiences.

The Japanese design standard [20] defines the target response spectrum at engineering bedrock. Seismic signals are matched to follow the target response spectrum in the frequency domain, then converted from the bedrock to the surface with consideration of soil amplification. The standard requests to use at least three seismic signals to ensure the analysis covers the most severe case.

Following this standard, these three seismic signals are prepared at engineering bedrock (which are used in a real offshore wind project in Japan) as shown in the figure 4.3. Input-1 has a long duration of excitation while input-2 and input-3 have a relatively short duration of excitation. They are spectrally matched to the target spectrum defined in [20] as shown in the figure 4.4.

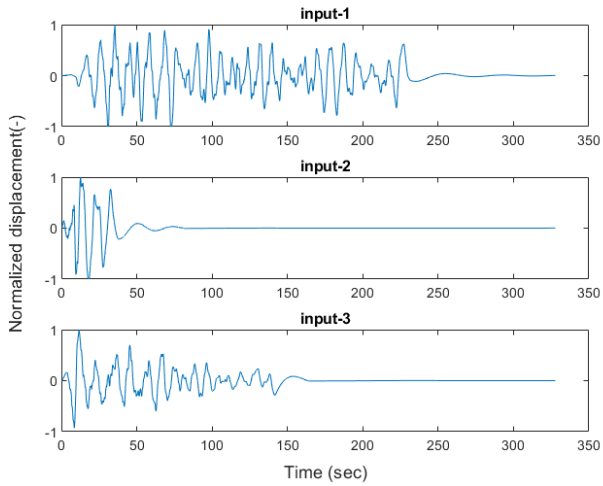

Figure 4.3: Seisimc signals to be used for sensitivity study

4.2.3 Summary of input parameters

To sum up, the following inputs are selected as variable parameters for further sensitivity studies. In total, 588 cases (=7x4x7x3) are calculated.

- Water depth: from 20m to 50m, every 5m interval [7 cases]
- Soil condition: 4 types, such as hard, medium, soft and very soft [4 cases]

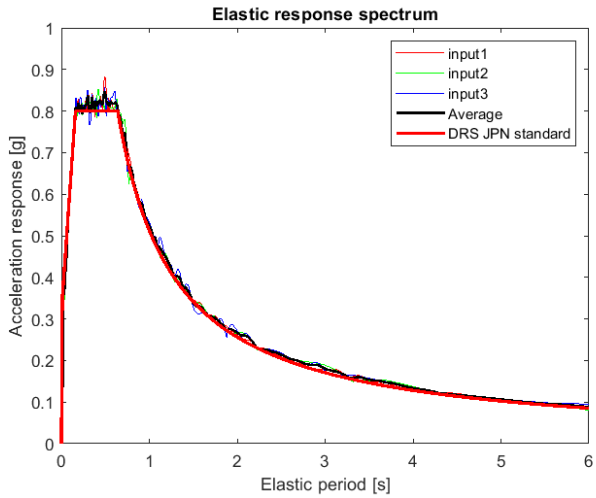

Figure 4.4: Comparison of erastic response spectrum

- Bedrock depth: from 0m to 60m, every 10m interval [7 cases]
- Seismic input: spectral matched to the Japanese design standard, 3 signals [3 cases]

4.3 Library for the scaling factor

This section describes the result of the sensitivity studies to derive a library for the scaling factor.

4.3.1 Initial geometry

Before doing structural analysis, the initial geometry of the structure shall be determined for each position to produce realistic outputs. In general, RNA and tower sections are common geometry in a wind farm, while the geometry for the foundation part (i.e. from interface level to pile tip) shall be adjusted for every position.

The structural geometry is determined by the following three components, such as outside diameter, wall thickness and pile penetration length. Arany [32] introduces the formulas which show the relationship between these three components

as follows. WT, OD, LP, E_{eq} and G represent wall thickness, outside diameter, pile penetration length, equivalent Young's modulus and modified shear modulus respectively.

$$WT = 6.35 + OD(mm)/100 \tag{4.4}$$

$$LP = max[OD * 3, OD(\frac{E_{eq}}{G})^{\frac{2}{7}}] \tag{4.5}$$

In general, 1st natural frequency of the structure should be adjusted to avoid the excitation frequency from the turbine operations. As for SG-8.0-167-DD, 1st natural frequency of the structure should be located between 0.19 Hz to 0.24 Hz. With consideration of some margin, this study limits the range from 0.2 Hz to 0.22 Hz. This criteria tends to regulate the outside diameter of the monopile.

Based on this information, the initial geometry of the structure is determined by the process shown in the figure 4.5. Once the outside diameter is set, the other two components (i.e. wall thickness and pile penetration length) are automatically determined in accordance with the formula proposed by [32]. After the 1st natural frequency is calculated, it is compared to the criteria. If it does not fit the criteria, the outside diameter is adjusted. With this iterative process, the initial geometry for each position is determined.

This procedure is applied to the input parameters explained in the section 4.2. The outside diameter and natural frequencies for each case are summarized in the figure 4.6 and 4.7.

Outside diameter shows an increasing trend in accordance with water depth and soil softness. This is a reasonable outcome because the natural frequency for the 1st structural mode tends to be a larger value in the case of larger water depth and softer soil conditions, which results in increasing the outside diameter to keep the natural frequency within the tolerance (i.e. from 0.2Hz to 0.22Hz).

Natural frequencies show a basically decreasing trend in accordance with the increase of water depth. There is a balance on the natural frequencies from the two factors. The 1st factor is the increasing trend from the increase of outside diameter (and wall thickness). The 2nd factor is the decreasing trend from the increase of geometries. Although the contribution from the 1st factor is dominant in the case of the 1st structural mode, the contribution from the 2nd factor is dominant for the other modes. Hence, the plots generally show a decreasing trend.

It should be mentioned here that the natural frequencies for 1st RNA and 2nd structure modes become quite close value (i.e. the difference is only 0.1Hz). It induces the interaction (or mixture) of these two modes, which is one of the challenges

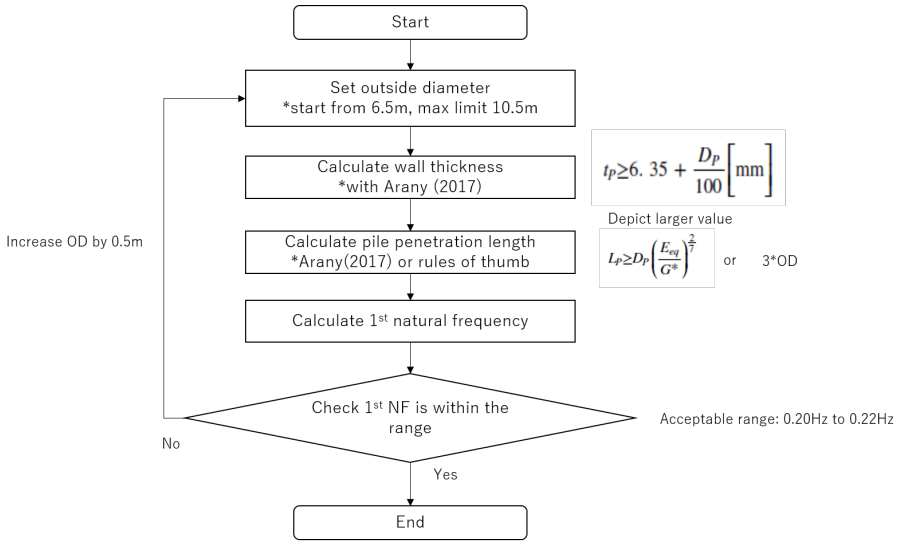

Figure 4.5: Flowchart to determine the geometry

to properly estimate the bending moment combining the effect from the principle vibration modes.

Furthermore, it should be noted that this approach has the following limitation. It can generate a valid initial design geometry, but there could be different geometries that are suitable and also it does not give (most likely) the most optimized structure.

4.3.2 Acceleration response spectrum

The acceleration response spectrum for each case is calculated since the value is required to calculate the scaling factor.

First, seismic excitation at mudline is calculated with consideration of soil amplification from the bedrock. Combining these seismic signals and the natural frequencies obtained in the previous section, the acceleration response spectrum for each mode can be derived. 5% is assumed for the damping ratio on the soil material damping.

The results are summarized in the figure 4.8. Each plot has 4 different color lines which represent different soil conditions and the hatching area represents the

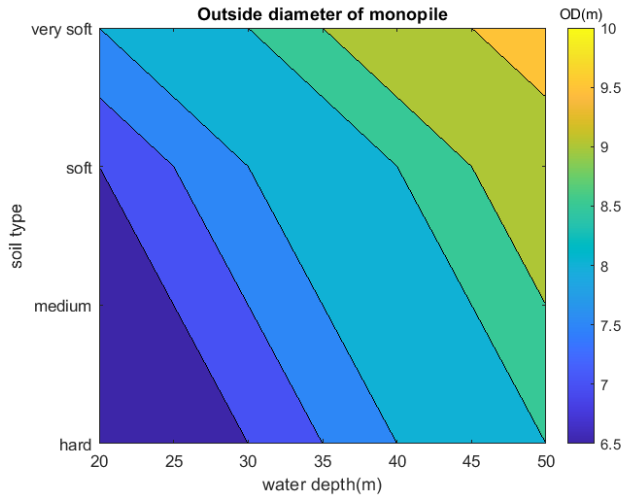

Figure 4.6: Summary of outside diameter on the sensitivity study

natural frequencies for the principle vibration modes (the natural frequencies are slightly different depending on the water depth and soil condition, so it has a range to some extent).

As clearly seen, depending on the soil condition and bedrock depth, the acceleration response spectrum shows spikes that comes from the soil amplification. In general, softer soil condition tends to induce large system responses in the seismic analysis, which corresponds to this plot since the acceleration response spectrum shows larger values in the case of softer soil condition especially for the most dominant vibration modes (i.e. 1st structure, 1st RNA and 2nd structure mode). However, it is interesting to mention that harder soil condition induces larger acceleration response spectrum in some cases. In the case of bedrock depth 60m for 2nd structural mode, for example, soft soil condition induces a larger acceleration response spectrum than the one from very soft soil condition. So, it's important to focus on not only the soil type but also the frequency of the seismic inputs when discussing the soil amplification.

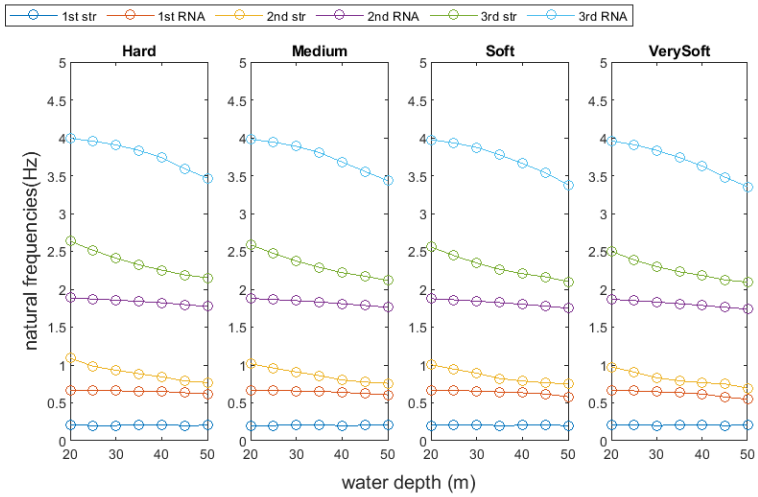

Figure 4.7: Summary of natural frequencies on the sensitivity study

4.3.3 Modal decomposition on the maximum bending moment

The simplified method to estimate the bending moment focuses on the output for each vibration mode, so it's necessary to decompose the maximum bending into the principle vibration modes.

There are two possible approaches to decompose the maximum bending moment calculated by the frequency domain method.

The most straightforward way is to decompose the bending moment when the maximum bending moment occurs in the time history. After decompose the time history of bending moment into principal modes by Fourier transformation, for each mode, the value is taken when the maximum bending moment for the whole system occurs. Figure 4.9 shows an example. In this case, the maximum bending moment occurs around 35 seconds, so the contribution from each mode is extracted at 35 seconds.

It can exactly extract the contribution ratio from each mode when the maximum bending moment occurs for the whole system. However, it may allow the abrupt change on the trend of the scaling factor since the contribution ratio can be drastically different if the maximum bending moment happens at different timing.

Another approach is to use the frequency spectrum. Applying Fourier transform

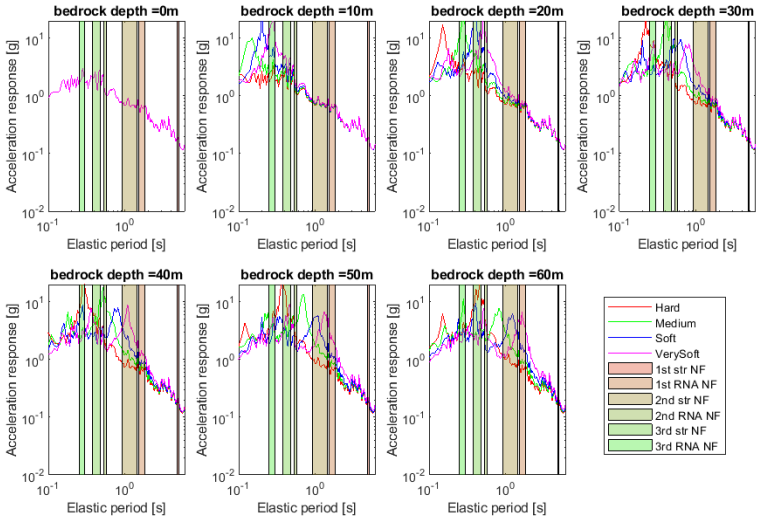

Figure 4.8: Acceleration response spectrum for each bedrock depth

to the time history of bending moment, the frequency spectrum can be derived as shown in the figure 4.10. The plot is segregated into the principal vibration modes and the contribution ratio from each mode is derived from the integrated value in each region since it represents the impact from each mode. As for the range of segregation, +/-0.05Hz is selected for this study since it shows the most reasonable result in comparison with the other options (such as +/-5%, +/-0.01Hz and +/-0.1Hz). The sensitivity study can be found in the Appendix D.

The integrated value represents the contribution ratio not for the time when the maximum bending moment occurs but for the bending moment on the whole time series, which induces some deviation to the correct result. However, there is a correlation to some extent and also it makes sure the smooth trend between input and output.

Considering the pros and cons for both approaches, the latter one (i.e. contribution ratio from the frequency spectrum) is adopted in this study since the smooth trend is expected to be stabilize the outliers on estimating the scaling factor.

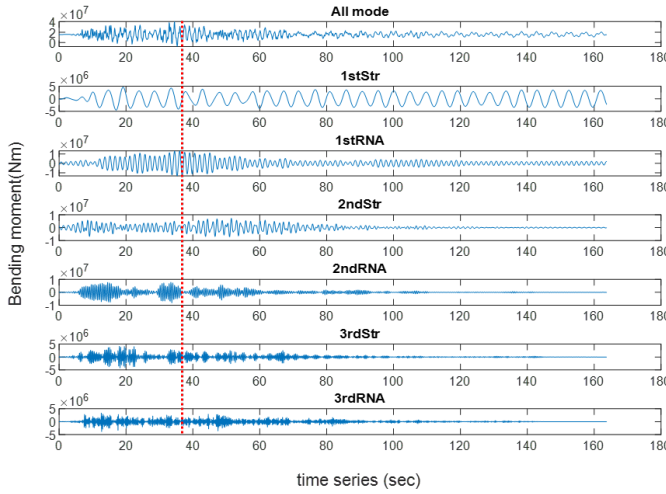

Figure 4.9: Example of modal decomposition by time history

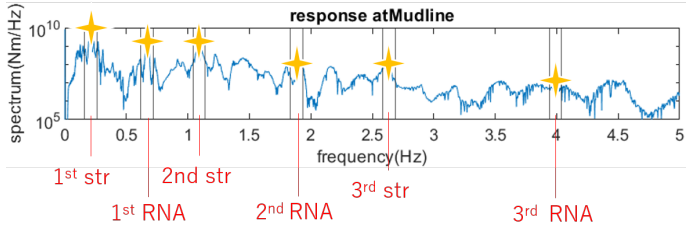

Figure 4.10: Example of modal decomposition by frequency spectrum

4.3.4 Result of sensitivity studies

The calculation model (by the frequency domain method) verified in chapter 3 is applied to all the cases. The most interesting output for RNA and foundation design is the maximum bending moment at the tower top and mudline, so they are summarized for each position. Dividing them by the acceleration response spectrum, scaling factors defined in the previous section are calculated.

4.3.4.1 Maximum bending moment

The maximum bending moment is decomposed into the principal vibration modes to see their contributing ratio. Figure 4.11 and 4.12 shows the result for bedrock depth 0m case as an example. As for tower top, 1st RNA is the most dominant mode and 2nd structure mode increases its effectiveness in accordance with a increase of water depth. As for mudline, however, 1st structural mode is clearly the most dominant mode. In the case of larger water depth, such as 45m to 50m, the effect from 1st RNA mode becomes sharply increased.

Full result can be found in Appendix F. In general, 1st structure, 1st RNA and 2nd structure modes are dominant for tower top and mudline as explained in the example. Depending on the bedrock depth, however, the contribution ratio can be changed due to soil amplification.

4.3.4.2 Scaling factor

Dividing the maximum bending moment by the acceleration response spectrum, scaling factors can be derived. Figure 4.13 shows the scaling factor for 1st RNA mode at mudline as an example.

Strong dependency can be seen on the water depth, so the data is projected to a 2D plot as a function of water depth as shown in the figure 4.14 including the other vibration modes. Focusing on the dominant vibration modes, such as 1st structure, 1st RNA and 2nd structure modes, they have different trends as a function of water depth. 1st structure mode shows an almost linear increasing trend while 1st RNA mode shows an exponential increasing trend. 2nd structure mode shows an increasing trend until the certain water depth and then changes the trend to decreasing.

A similar trend can be seen in the modal participation mass. Figure 4.15 shows the modal participation mass for each case in the sensitivity study. As for 1st structure, 1st RNA and 2nd structure, they show linear increasing, exponential increasing and increasing/decreasing trend respectively. It means that the scaling factor is

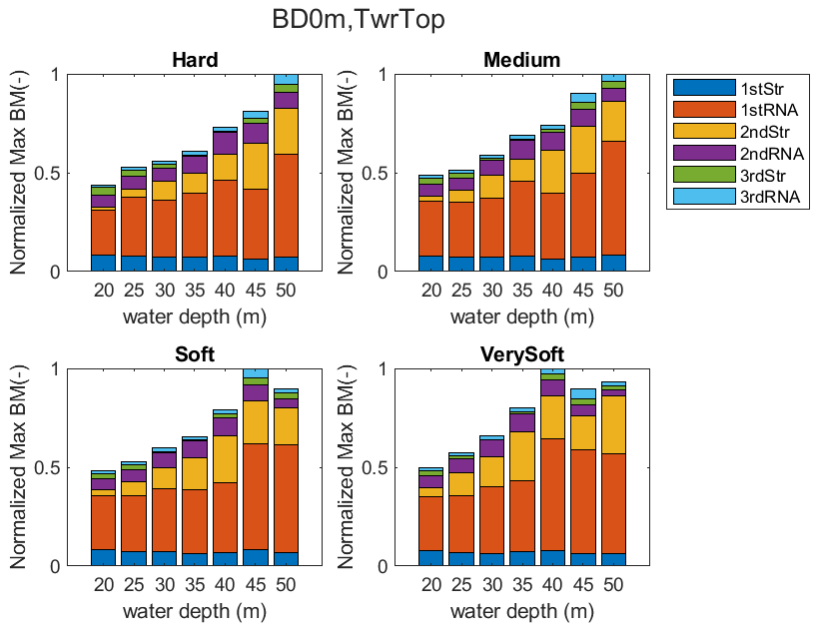

Figure 4.11: Max. bending moment (BD=0m, Tower top)

strongly affected by modal participation mass which represents the system property well as expected.

It is interesting to see the scaling factors on 1st RNA mode and 2nd structural are not linearly increasing although the water depth (i.e. structural mass) linearly increases. To figure out this phenomenon, the summation of modal participation mass for 1st RNA and 2nd structure mode is plotted as shown in the figure 4.16. It clearly shows a linearly increasing trend. It indicates that the effect from the variation of structural geometry has a linearly increasing trend, but the effect is spitted into 1st RNA and 2nd structure modes since their natural frequencies become quite close in the case of larger water depth as shown in figure 4.7.

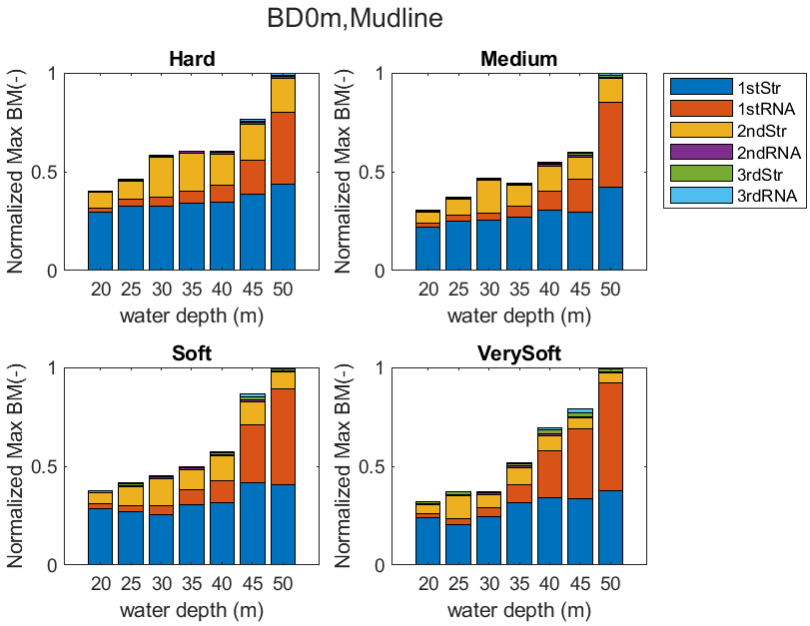

Figure 4.12: Max. bending moment (BD=0m, Mudline)

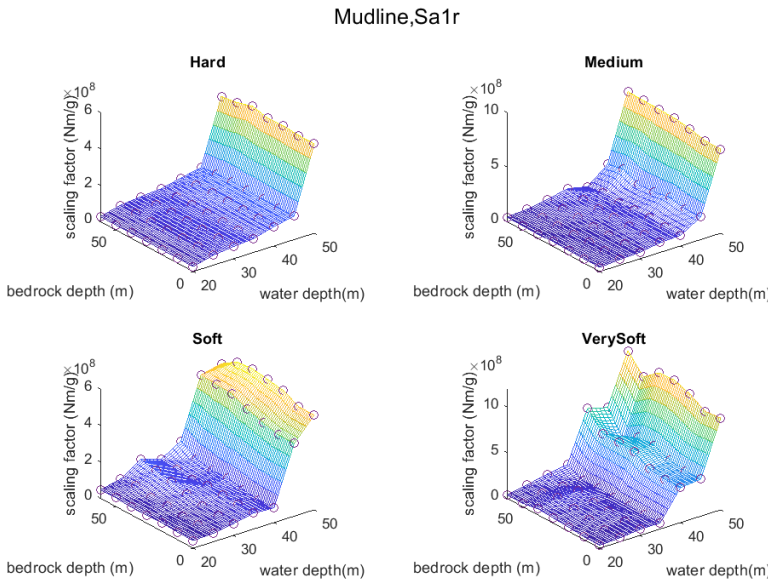

Figure 4.13: Scaling factor for 1st RNA mode at mudline

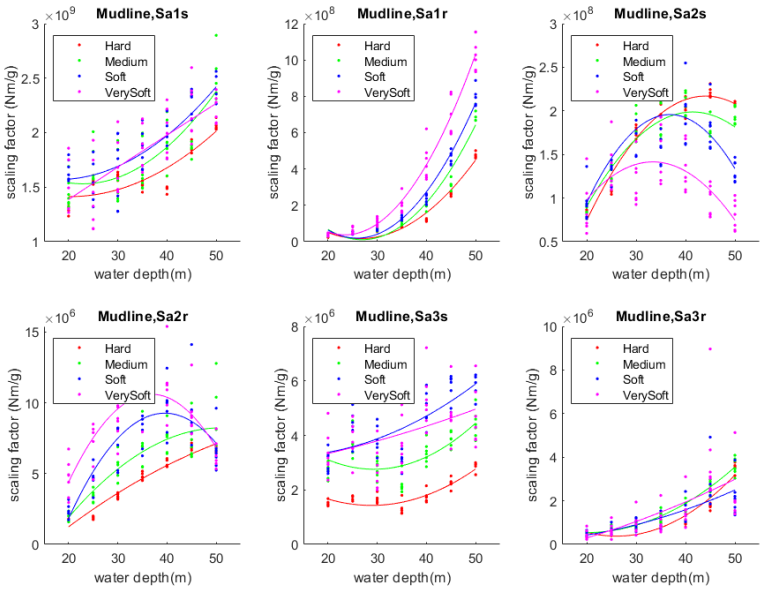

Figure 4.14: Scaling factor at mudline as a function of water depth

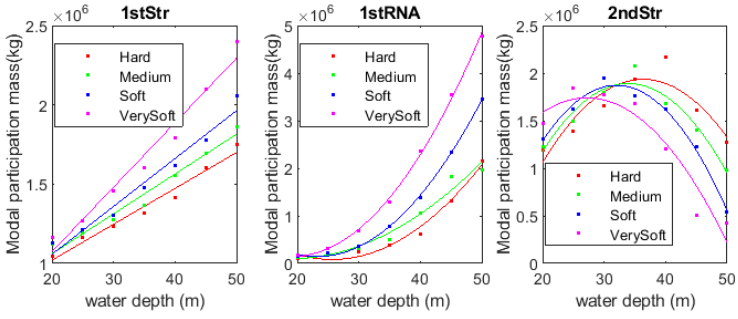

Figure 4.15: Modal participation mass for 3 modes

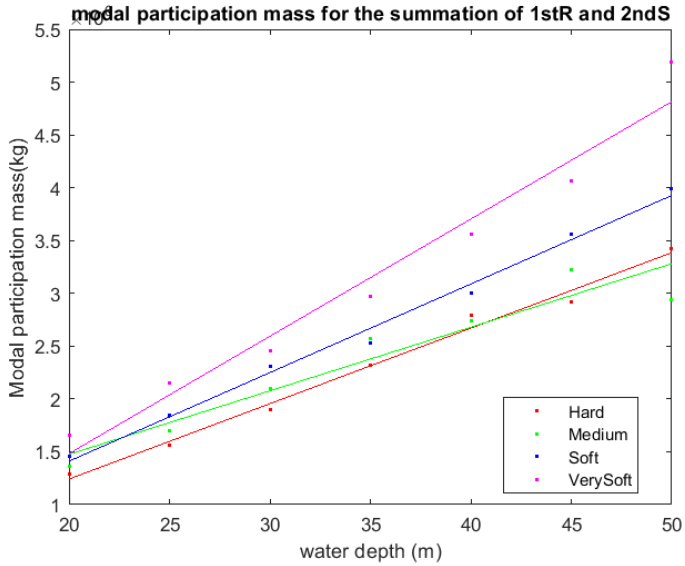

Figure 4.16: Summation of modal participation mass for 1st RNA and 2nd structure mode

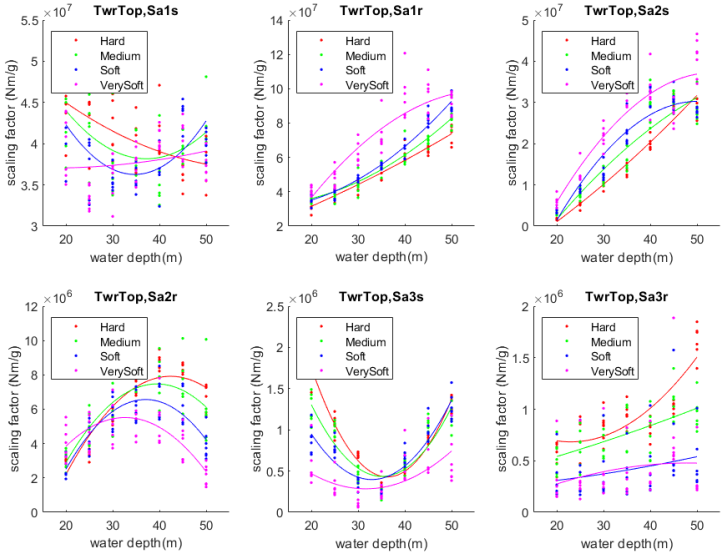

Figure 4.17: Scaling factor at the tower top as a function of water depth

Figure 4.17 summarizes the scaling factor for the tower top. It shows a different trend with mudline. As for the 1st structural mode, the scaling factor does not show linear increasing trend but shows some fluctuations. For the 1st RNA and 2nd structural modes, they show almost linear increasing trend. It means that the contribution from the 1st RNA and 2nd structural mode increase while the contribution from the 1st structural mode becomes relatively small in accordance with the increase of water depth.

4.4 Library for the acceleration response spectrum

Seismic inputs are dependent on the wind farm. Once the seismic inputs are prepared, the acceleration response spectrum for the representative case within the reasonable range of input parameters can be calculated as shown in the figure 4.8. Moreover, the natural frequencies for the representative case within the reasonable range of input parameters can be derived from the figure 4.7. Combining these two data, the relationship between the input parameters (water depth, soil condition and bedrock depth) and the acceleration response spectrum for each vibration mode is revealed as shown in the figure 4.18. This is the library for the acceleration response spectrum.

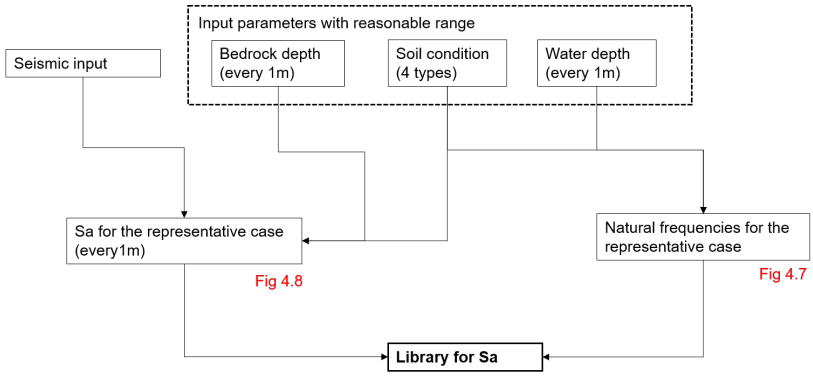

Figure 4.18: Flowchart to create a library for the accelertation response spectrum

As for creating the library, the interval of the water depth and bedrock depth is set to 1m since a parametric study proves that the interval captures the features of the soil amplification well. The details of the parametric study on the interval is summarized in Appendix E.

4.5 Summary of the strategy

The clustering strategy newly developed in this study is summarized in the figure 4.19. The followings explain the details every step by step.

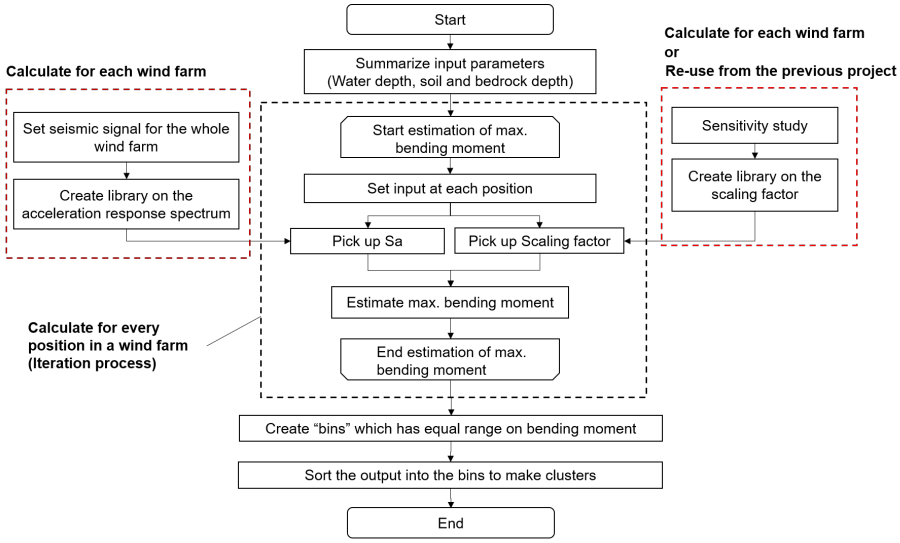

Figure 4.19: Flowchart of new clustering strategy

First, input parameters for each position in the wind farm are summarized. This strategy uses these three parameters, such as water depth, soil condition and bedrock depth as dominant input parameters.

Second, the scaling factor for each position are extracted from the library. Through the sensitivity study explained in the previous section, the scaling factor is summarized for an arbitrary position within the reasonable range of input parameters. Based on the input parameter, the suitable scaling factor is picked out from the library.

Third, the acceleration response spectrum is also extracted from the library with the similar manner as the scaling factor.

Fourth, combining the acceleration response spectrum and scaling factor extracted from the library, the maximum bending moment for the position is estimated.

Finally, ”Bins” which have a uniform range on bending moment are prepared. Then, the positions are sorted into the bins based on the estimated bending moment,

which corresponds to the clusters in the wind farm.

It is important to mention that the applicability of each library. The scaling factor represents the system property of the structure, so the scaling factor can be re-used from the different project as far as the basic system, such as turbine size and foundation type, is the same (*its limitation is explained in the later section). Meanwhile, the acceleration response spectrum can be different depending on the wind farm even if it follows the same design response spectrum at bedrock since each seismic signal has some deviations from the design one and also phase shifts. Furthermore, computational demand on the acceleration response spectrum is relatively small (i.e. it take only around 5 minutes for each wind farm). Hence, the library for the acceleration response spectrum is prepared for each wind farm.

Chapter 5

Application of the clustering strategy to virtual wind farms

This chapter describes the verification of the clustering strategy newly developed in this study by applying it to the virtual wind farm.

5.1 Virtual wind farms

The virtual wind farm should cover the possible range of input parameters shown in the section 4.2. As for soil condition and bedrock depth, they can be directly used to create the virtual wind farm since their variation is reasonable for one wind farm. With regard to water depth, however, it should be splatted into two categories since the variation (30m difference between the minimum and maximum value) is too large as one wind farm (considering reasonable project conditions). Hence, the following two wind farms (i.e. shallow and deep wind farms) are prepared for verifying the clustering strategy.

5.1.1 Wind farm 1 (deep water depth)

The range of input parameters is summarized below.

- Number of positions: 50 positions
- Water depth: from 35m to 50m

- Soil condition: 4 types, such as hard, medium, soft and very soft (same property used in the sensitivity study)
- Bedrock depth: from 0m to 60m

These parameters are randomly selected for each position and then the virtual wind farm is created as shown in the figure 5.1.

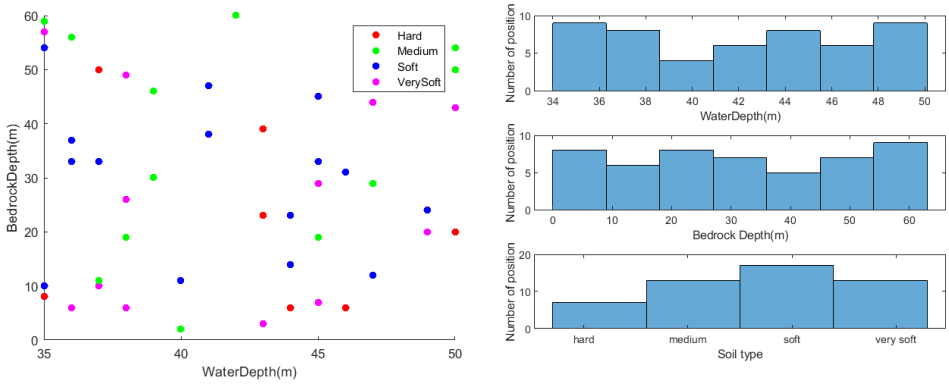

(a) Distribution on wind farm 1 **(b)** Histogram on wind farm 1

Figure 5.1: Input data on wind farm 1

5.1.2 Wind farm 2 (shallow water depth)

The range of input parameters is summarized below.

- Number of positions: 50 positions
- Water depth: from 20m to 35m
- Soil condition: 4 types, such as hard, medium, soft and very soft (same property used in the sensitivity study)
- Bedrock depth: from 0m to 60m

These parameters are randomly selected for each position and then the virtual wind farm is created as shown in the figure 5.2.

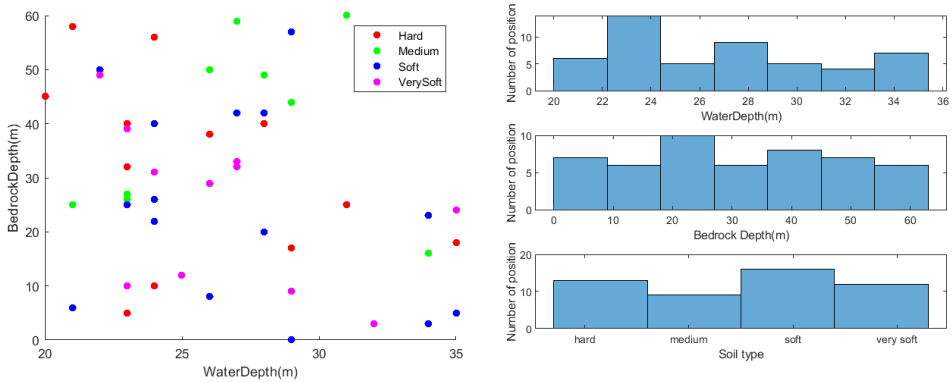

(a) Distribution on wind farm 2 **(b)** Histogram on wind farm 2

Figure 5.2: Input data on wind farm 2

5.1.3 Seismic input

Following two sets of seismic signals are applied to the virtual wind farms.

- Set-1: Seismic inputs used in sensitivity study (3 signals)
- Set-2: Seismic inputs newly created for this verification (3 signals)

The 1st set is the ones which are used to create the library through the sensitivity study in the section 4.2.2.

In addition to Set-1, the newly developed ones (i.e. Set-2) are applied as well. Set-2 also follows the target response spectrum defined by [20], but they have different duration and phase in time history. It tries to make sure if the scaling factor can be re-used as far as the turbine, foundation and the design response spectrum are the same and to check its wide applicability.

Figure 5.3 shows the time history of newly developed inputs and figure 5.4 shows the elastic response spectrum in comparison with the target response spectrum.

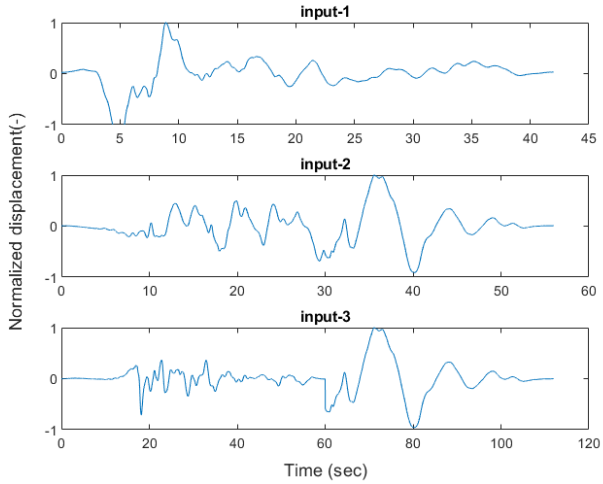

Figure 5.3: Displacement time series on Set-2 of seismic signal

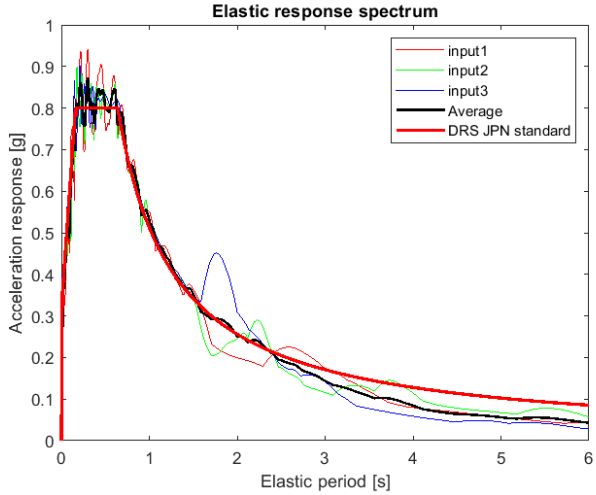

Figure 5.4: Elastic response spectrum for Set-2

5.2 Evaluation of the clustering strategy

The clustering strategy explained in chapter 4 is applied to the virtual wind farms. In parallel, the maximum bending moment is calculated by the frequency domain method and the response spectrum analysis method explained in chapter 2 as a reference to check the accuracy of the strategy. Especially, the output from the frequency domain method is dealt as a primary reference for this study since it shows better accuracy. Two sets of seismic inputs (Set-1 and Set-2) are applied to make sure the applicability of the scaling factor

5.2.1 Interesting point for RNA and foundation design

Depending on the location where the designer is interested in, the final output from the clustering is a bit different.

In the case of RNA design, the worst position (i.e. the position which shows the largest bending moment at tower top) in a wind farm should be selected. The design of RNA is independent on the position and the generic one is applied for all the positions. Hence, it is required to find the worst position (or the worst 3 positions) and check if the bending moment is an acceptable level or not.

In the case of foundation design, it is more interesting to categorize the positions which show similar loads trend especially at mudline since the foundation design is not generic for the whole wind farm but slightly adjusted to optimize material cost.

Therefore, this study verifies these two parameters in the following sections. For the purpose to compare the accuracy at each location (tower top and mudline), both results are presented.

5.2.2 Application of Set-1 seismic input

5.2.2.1 Evaluation of the worst position

In order to evaluate the accuracy of detecting the worst position(s), the worst 4 positions (i.e. positions which show the top 4 largest bending moment) are selected for each case. Figure 5.5 shows the worst 4 positions for set-1 of seismic input. Red and blue circles represent the worst 4 positions from the estimated bending moment and correct bending moment respectively. The numbers located upper and lower of the point represent the order for the estimated and correct bending moment. In all the cases, the strategy properly detects the worst 3 positions at least by extracting 4 positions.

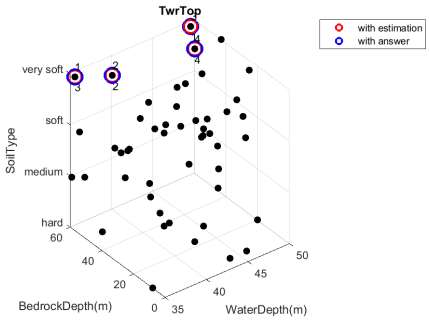

(a) At tower top for wind farm 1

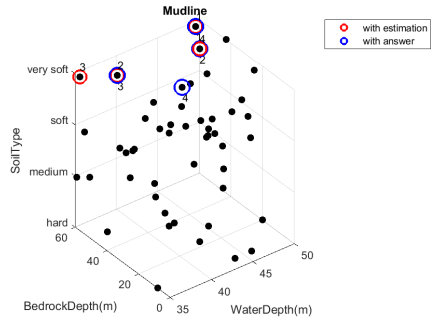

(b) At mudline for wind farm 1

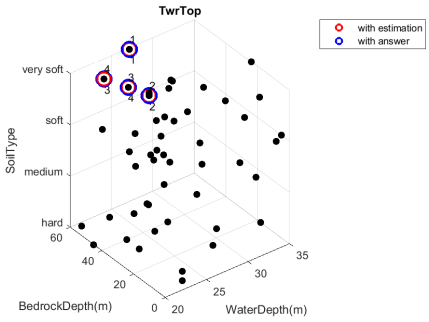

(c) At tower top for wind farm 2

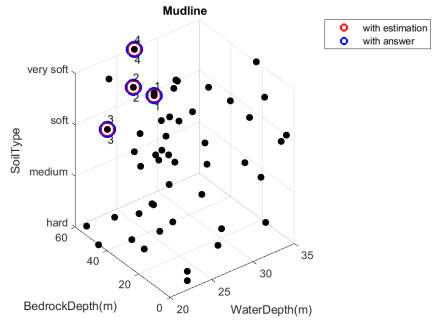

(d) At mudline for wind farm 2

Figure 5.5: The worst 4 positions in the wind farm (Set-1 seismic input)

Additionally, the absolute values of the estimated and correct maximum bending moment are compared as shown in the figure 5.6. Red and blue circles represent the estimated bending moment and correct bending moment respectively. And, table 5.1 shows the summary of errors on the maximum bending moment.

In general, the estimated bending moment captures the trend of the correct bending moment well, so the averaged errors are in the order of 10% to 20%. Focusing on the individual position, however, some positions shows relatively large errors. In the case of wind farm 1, for example, the maximum error is more than 70%. Therefore, this strategy is suitable to check the general trend and detect the worst positions, but has some limitations to directly estimate the maximum bending moment.

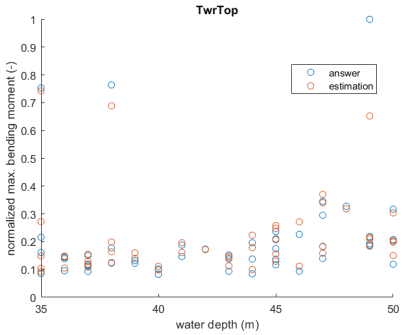

(a) At tower top for wind farm 1

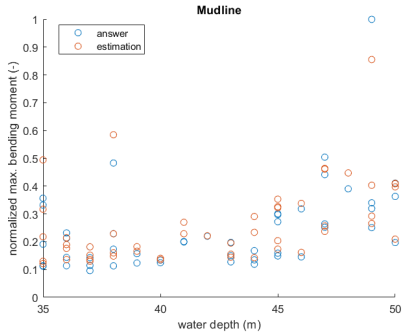

(b) At mudline for wind farm 1

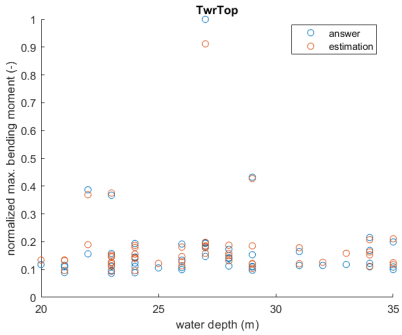

(c) At tower top for wind farm 2

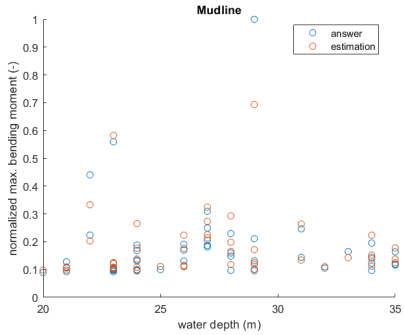

(d) At mudline for wind farm 2

Figure 5.6: Comparison of max. bending moment in the wind farm (Set-1 seismic input)

Wind Farm	Location	Ave. error for all	Max. error for all	Ave. error for top3	Max. error for top3
1	Tower top	12%	35%	16%	35%
1	Mudline	17%	74%	20%	39%
2	Tower top	12%	34%	7%	21%
2	Mudline	12%	41%	17%	31%

Table 5.1: Summary of errors on the max. bending moment (for Set-1)

5.2.2.2 Evaluation of the categorization

The positions in a wind farm are categorized into the groups which show similar load trend. It means that "Bins" which have a uniform range on bending moment are prepared. Then, the positions are sorted into the bins based on the estimated bending moment, which corresponds to the clusters in the wind farm.

In the case of efficient categorization, the load deviation in each cluster should be minimized. Based on this idea, this study uses the coefficient of variation (CV) in each cluster as a representative parameter to evaluate the efficiency of the categorization. It can represent a statistical measure of the dispersion of data points in a data series around the mean. And, it can be derived by the following formula. σ and μ represent the standard deviation and the mean value respectively.

$$CV = \frac{\sigma}{\mu} \tag{5.1}$$

The procedure to calculate CV is as follows.

1. First, the positions in a wind farm are sorted into groups based on the estimated bending moment.

2. Then, CV for each cluster is calculated with correct bending moment.

3. CV is averaged over all clusters in the wind farm. This output represents the efficiency of the strategy.

Higher CV value represents the large deviation of bending moment in the cluster and lower CV represents vice versa, so it can measure how the strategy is efficient or not.

CV for wind farm 1 and 2 are summarized in the figure 5.7. 3 types of CV are compared. The blue line represents the CV from the strategy newly developed in this study. The yellow and red lines represent the CV based on the bending moment from frequency domain method (i.e. correct values) and response spectrum method.

In general, CV decreases when increasing the number of clusters. When the number of clusters increases, the number of the position in each cluster decreases, which should decrease the deviation of bending moment in each cluster.

Depending on the line, however, the decreasing trend is different. The yellow line decreases fast and shows the smallest CV for almost all situations. This is quite natural since the line is based on the correct bending moment and represents an ideal line.

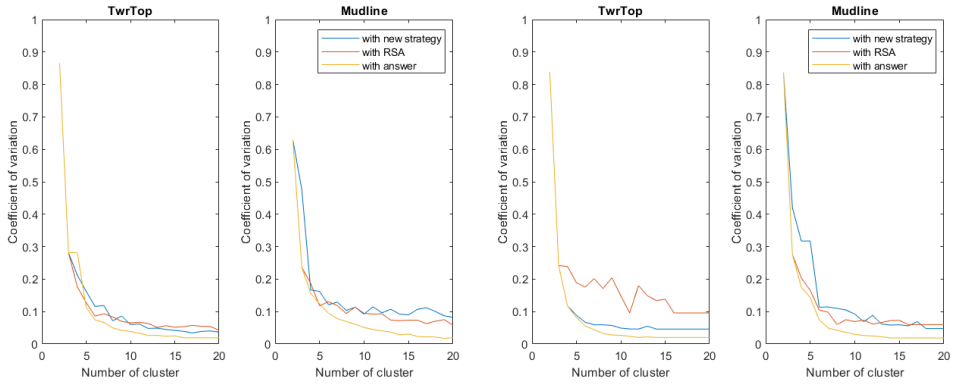

(a) CV for wind farm 1 **(b)** CV for wind farm 2

Figure 5.7: Coefficient of variation as a function of number of cluster (Set-1)

The blue line is located a bit higher position than the yellow one, but lower the red line (or almost equal to the red line). It means that the strategy shows the same order of accuracy as the response spectrum analysis method.

The number of cluster has to be specified in the real project with consideration of the acceptable range of load deviation in each cluster. Although the acceptable range is strongly dependent on the project (and project phase), these plot can be a good reference to determine it. In the case of acceptable range of load deviation is 10%, for example, the number of cluster for the tower top and mudline shall be set to 5 and 10 respectively in accordance with the figure 5.7.

5.2.2.3 Detect the worst position in each cluster

This section evaluates the ability to detect the worst position in each cluster. As a typical case, the wind farms are categorized into 5 clusters. Then, it is checked for the strategy to properly detect the worst position (i.e. max. bending moment) for each cluster. The results are summarized in the table 5.2. In parallel, the number of position is summarized in the table 5.3 for the reference.

The values in the table 5.2 represent the errors on the maximum bending moment between the real and detected worst position. 0% means that the strategy properly detects the worst position. If the value is large, the strategy is not able to detect the worst position well. Cluster-1 gathers the positions which show high maximum bending moment while Cluster-5 gathers the positions which show low

Wind farm	Location	Cluster-1 (High load)	Cluster-2	Cluster-3	Cluster-4	Cluster-5 (Low load)
1	Tower top	0%	24%	0%	9%	0%
1	Mudline	0%	0%	29%	10%	14%
2	Tower top	0%	0%	5%	7%	8%
2	Mudline	0%	0%	0%	16%	12%

Table 5.2: Errors to detect the worst position in each cluster

Wind farm	Location	Cluster-1 (High load)	Cluster-2	Cluster-3	Cluster-4	Cluster-5 (Low load)
1	Tower top	1	2	4	12	31
1	Mudline	1	1	8	21	19
2	Tower top	1	1	2	16	30
2	Mudline	1	1	6	12	30

Table 5.3: Number of positions in each cluster

maximum bending moment.

It shows that the strategy detects the worst positions within 15% errors for most of the cases. In some cases, however, it shows relatively large errors (i.e. from 20% to 30%) and it does not correctly detect the worst position. As explained in the table 5.1, the strategy shows some errors in the estimation of the maximum bending moment. It is accurate enough to detect the worst position in a wind farm, but is not accurate enough to detect the worst position in each cluster.

5.2.3 Application of Set-2 seismic input

For the purpose to check the applicability of the scaling factor, different seismic input (Set-2) is applied to the virtual wind farms. Acceleration response spectrum is calculated with Set-2 while the scaling factor is not changed (i.e. scaling factor from Set-1 is used). This study intends to prove that it is not required to re-generate the scaling factor even if the location of the wind farm is different as far as the turbine, the foundation type and the design response spectrum are identical.

The analysis condition is summarized in the table 5.4.

	Acceleration response spectrum	**Scaling factor**	**Correct bending moment from**
Original Study	Set-1	Set-1	Set-1
This study	Set-2	Set-1	Set-2

Table 5.4: Summary of analysis condition (choice of seismic input)

5.2.3.1 Evaluation of the worst position

The result for evaluating the worst position is summarized in the figure 5.8. As well as the original case, the strategy properly detects the worst 3 positions at least by extracting 4 positions for all the cases.

The absolute values of the estimated and correct maximum bending moment are compared as shown in the figure 5.9. And, table 5.5 shows the summary of errors on the maximum bending moment.

The estimated bending moment captures the trend of the correct bending moment as accurately as the original study does. Table 5.6 shows the averaged errors for all the locations (tower top and mudline) and wind farm (1 and 2) for both seismic inputs.

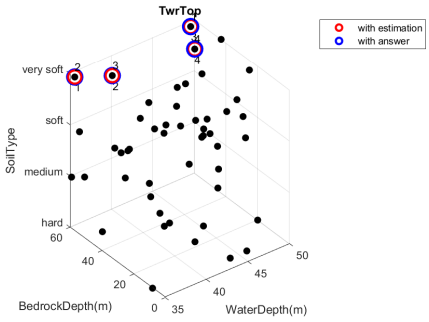

(a) At tower top for wind farm 1

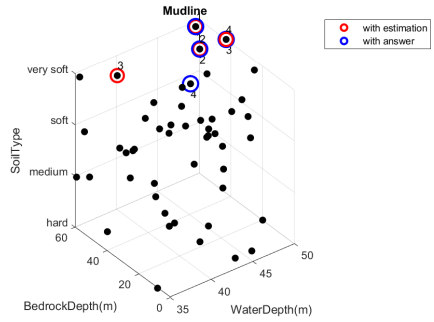

(b) At mudline for wind farm 1

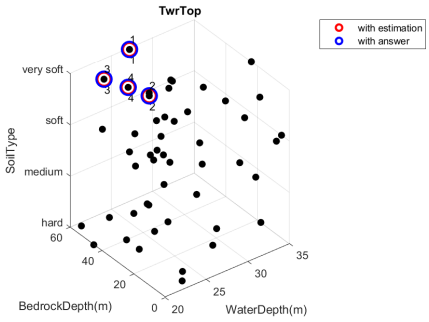

(c) At tower top for wind farm 2

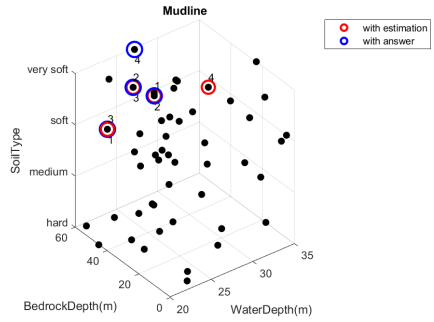

(d) At mudline for wind farm 2

Figure 5.8: The worst 4 positions in the wind farm (Set-2 seismic input)

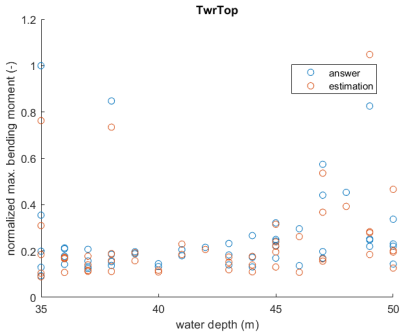

(a) At tower top for wind farm 1

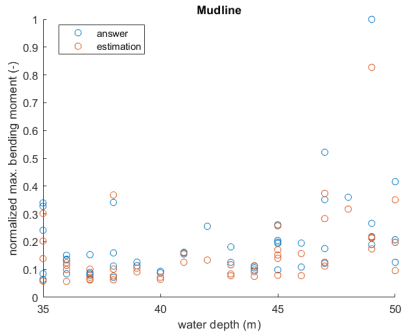

(b) At mudline for wind farm 1

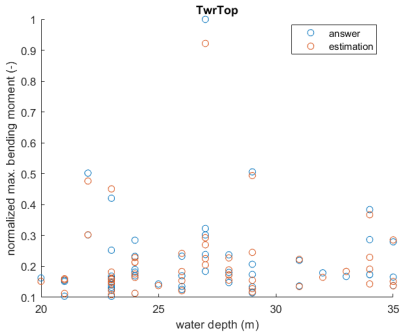

(c) At tower top for wind farm 2

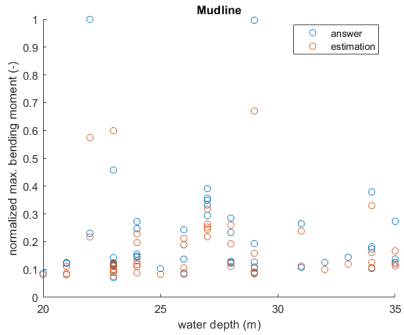

(d) At mudline for wind farm 2

Figure 5.9: Comparison of max. bending moment in the wind farm (Set-2 seismic input)

Wind Farm	Location	Ave. error for all	Max. error for all	Ave. error for top3	Max. error for top3
1	Tower top	15%	38%	23%	38%
1	Mudline	21%	48%	16%	28%
2	Tower top	8%	28%	4%	8%
2	Mudline	16%	43%	27%	43%

Table 5.5: Summary of errors on the max. bending moment (for Set-2)

	Ave. error for all	Max. error for all	Ave. error for top3	Max. error for top3
Set-1	13%	46%	15%	31%
Set-2	15%	39%	18%	29%

Table 5.6: Comparison of Set-1 and Set-2

5.2.3.2 Evaluation of the categorization

Next, the CV as a function of the number of clusters is summarized in the figure 5.10. It also shows the competitive results with the original study. It means that the strategy shows a bit worse efficiency in comparison with the correct result (i.e. yellow line), but it is as efficient as the response spectrum response analysis.

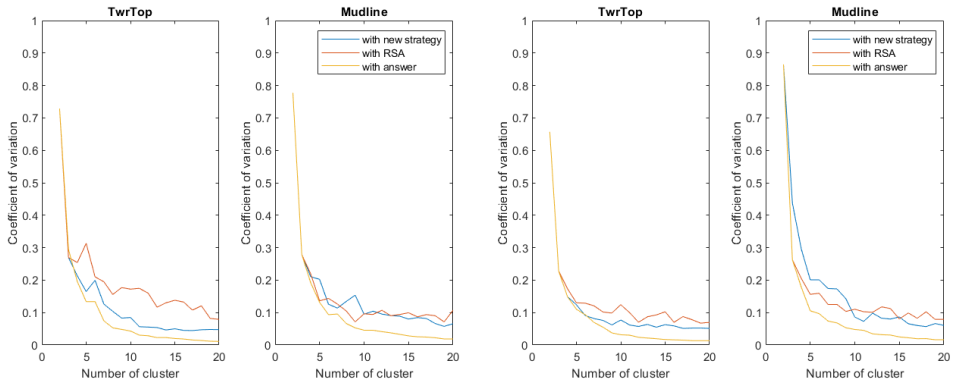

(a) CV for wind farm 1 **(b)** CV for wind farm 2

Figure 5.10: Coefficient of variation as a function of number of cluster (Set-2)

To sum up, the strategy shows reasonable applicability even if changing the seismic signals. It means that it is not required to re-generate the scaling factor even if the location of the wind farm is different as far as the turbine, the foundation type and the design response spectrum are identical.

5.3 Discussion

This section discusses the reasons for the errors, the computational demand of the strategy and the applicability of the clustering strategy.

5.3.1 Discussion about the error

5.3.1.1 General reasons for errors

The strategy generally estimates the maximum bending moment well and creates reasonable clusters by sorting them. Focusing on the maximum bending moment itself for the individual position, however, it sometimes shows considerable errors.

There are mainly these two reasons for the error. It is noted that the errors from the calculation model itself are discussed in section 3.3. This section focuses on the errors from the strategy.

- Errors from modal decomposition; as explained in 4.3.3, the maximum bending moment is decomposed into the principle vibration modes based on the frequency spectrum. It certainly grasps the general trend but does not exactly capture the contribution ratio from each mode when the maximum bending moment occurs. It could induce some discrepancy from the correct bending moment.

- Data interval for the library on the scaling factor; sensitivity study to create the library for the scaling factor is carried out for the wide range of input parameters. Considering the balance between computational demand and accuracy, every 5m and 10m interval are selected for water depth and bedrock depth respectively, and it shows reasonable accuracy for clustering as expected. If using finer mesh size, however, the accuracy could be improved.

5.3.1.2 Trend of the error on the water depth

Table 5.7 summarizes the errors on each virtual wind farm by taking the average values on the two locations(tower top and mudline) and the two sets of seismic input. Estimation for wind farm 2 shows a bit better accuracy than the one for wind farm 1. It means that the strategy works better for shallow water depth.

This difference may come from the natural frequencies for 1st RNA and 2nd structural mode. As mentioned in the section 4.3.1, the natural frequencies for these two modes become closer in accordance with the increasing of water depth. It may

induce errors in the modal decomposition since the effect of these two modes is overlapped with each other.

Wind farm	Ave. error for all	Max. error for all	Ave. error for top3	Max. error for top3
1	16%	49%	19%	35%
2	12%	36%	14%	26%

Table 5.7: Comparison of the error between wind farm 1 and 2

5.3.2 Discussion about the computational time

One of the main feature of this strategy is its small computational demand since it can directly estimate the maximum bending moment from the input parameters, such as water depth, soil condition and bedrock depth (no need to create FE model).

Table 5.8 summarizes the comparison of computational time with BHawC and response spectrum method. It assumes the computational time on the virtual wind farms (wind farm 1 and 2) introduced in 5.1. The strategy takes time (i.e. 1 day) to create a library that contains acceleration response spectrum and scaling factor as reference data, but the other computational time is almost zero. On the other hand, BHawC and response spectrum analysis take time for creating FE model and computation itself, such as 11 days and 6 days respectively.

Even assuming only these two wind farms, the strategy is the fastest way to estimate the maximum bending moment and to do clustering. It is noted that the library can be used for the other wind farms without additional computation as shown in the section 5.2.3.

Option	Time (days)			
	Create library *Sensitivity study	Create geometry and FE model	Computation	Total time
Developed Strategy	1	N/A	Almost 0	1
BHawC	N/A	5	6	11
RSA	N/A	5	0.4	5

Table 5.8: Comparison of computational time

From the accuracy point of view, BHawC should provide the most accurate result and the strategy show some errors. It means that there is a trade-off between accu-

racy and computational demand. Hence, the method should be selected depending on the project phase (i.e. required accuracy and available time).

Especially, the strategy tends to be powerful in the early project phase. The strategy requires not detailed information and FE model but only a few input parameters, such as water depth, soil condition and bedrock depth for each position. So, it can be used when very few information are available (like at the early stage of the project). This is one of the benefit of this strategy.

5.3.3 Applicability of the strategy

The strategy uses two libraries to estimate the maximum bending moment for each position in a wind farm, such as a library for the scaling factor and a library for the acceleration response spectrum. If there is sufficient time and the high accuracy is required, it is preferable to generate the library for each wind farm, but normally the design schedule is tight and the design clustering has to be done during short duration.

The computational demand for the scaling factor is relatively high (i.e. 2 minutes for 1 case) while the one for the acceleration response spectrum is low (i.e. few seconds for 1 case). Hence, it is preferable to re-use the scaling factor for the other wind as much as possible to minimize the computational demand.

The library for the scaling factor is dependent on the following three conditions, such as turbine, foundation and seismic input. Turbine and foundation may change the trend of the system property. Seismic input is also related to the scaling factor because it has some dependency on the bedrock depth even trying to exclude the effect of soil amplification in scaling factor dividing the maximum bending moment by the acceleration response spectrum. If the difference of seismic input is minor, the same scaling factor can be used since their dependency on bedrock depth should be similar. As discussed in the section 5.2.3, for example, the same scaling factor can be applied for different seismic inputs as far as they follow the same design response spectrum at bedrock.

Based on the discussion above, the applicability of the scaling factor is summarized in the flowchart 5.11. There are three checkpoints, such as turbine type, foundation type and design response spectrum. If all of them are identical to the original case, the same scaling factor can be used as verified in the case of Set-2 seismic input. If one of them is different, however, the scaling factor shall be updated.

Some examples are summarized in the table 5.9. 8MW wind turbine, monopile foundation and design response spectrum defined by Japanese design standard are used in the chapter 4, so the scaling factor for this case is available now.

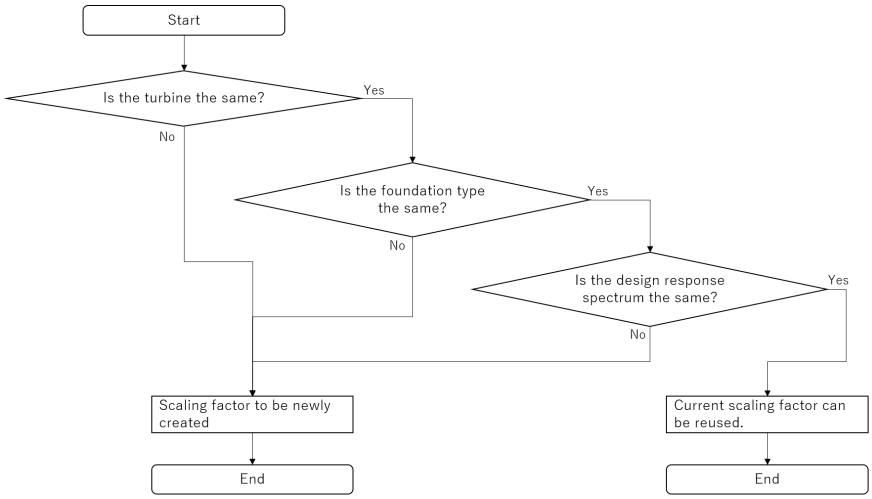

Figure 5.11: Flowchart to check the applicability of the scaling factor

Case-0 represents the original case shown in this chapter with Set-1 seismic input and Case-1 represents the one for Set-2 seismic input. In the case of Case-1, the same scaling factor with Case-0 can be used and the additional computation is not required because the trend on the system property does not change and also it follows the same design response spectrum at bedrock. Case-2 and Case-3 use different turbine or foundation types, but the seismic input is completely the same as Case-0. In this case, the scaling factor shall be updated because they induce different trends on the system property. Case-4 uses the same turbine and foundation type, but the location is not in Japan but another country. In this case, the scaling factor should be updated as well since the seismic input does not follow the same design response spectrum. If the design response spectrum is close to the Japanese one, probably the same scaling factor can be applied, but further studies shall be carried out to verify it.

Case	Turbine	Foundation	Location	Requirement of additional computation
Case-0	8MW turbine	Monopile	Japan, Location-1	-
Case-1	8MW turbine	Monopile	Japan, Location-2	No additional computation
Case-2	12MW turbine	Monopile	Japan, Location-1	Scaling factor shall be newly calculated
Case-3	8MW turbine	Jacket	Japan, Location-1	Scaling factor shall be newly calculated
Case-4	8MW turbine	Monopile	Other country	Scaling factor shall be newly calculated

Table 5.9: Applicability of the strategy for different case

5.3.4 Limitation of the strategy

The newly developed clustering strategy shows its capability to find the worst case in a wind farm with reasonable accuracy and categorize the positions into groups which show similar load trends with small computational demand.

Meanwhile, it is noted that the strategy has limitations as follows;

- The strategy shows some errors (average value is 10%-20%) to estimate the maximum bending moment. The errors are durable to detect the worst position in wind farm and the categorization, but are not suitable for the detailed structural analysis.
- The strategy is not able to properly detect the worst position in each cluster since it has a certain amount of errors to estimate the maximum bending moment.
- The scaling factor is customized to the specific wind turbine (i.e. SG-8.0-167-DD) and foundation type (i.e. Monopile). In the case of the different wind turbine or foundation type, the scaling factor has to be recalculated.
- The scaling factor is customized to the specific design response spectrum at bedrock. In the case of the different design response spectrum, the scaling factor has to be recalculated.

Chapter 6

Application of the clustering strategy to inhomogeneous soil condition

This chapter describes the application of the strategy to an inhomogeneous soil condition. One sample position is selected as an example and the maximum bending moment is estimated by the strategy. Then, the result is compared with the one from BHawC.

6.1 Procedure to apply the strategy to inhomogeneous soil condition

In the chapter 5, homogeneous soil conditions are assumed for the virtual wind farms to make the problems simple. In real projects, however, the soil condition is more complicated, such as inhomogeneous ones.

In this chapter, the strategy is applied after converting the inhomogeneous soil into the equivalent homogeneous soil condition. Then, the estimated maximum bending moment is compared with the one from BHawC to verify the strategy works well.

6.1.1 Conversion from the inhomogeneous soil to the equivalent homogeneous soil

To apply the strategy to inhomogeneous soil conditions, it is required to convert them into equivalent homogeneous soil conditions. The shear wave velocity averaged over 30m from the mudline (V_{s30}) is generally used for the soil classification in the seismic analysis. V_{s30} can be calculated with the following equation which is extracted from [33]. d_i and v_i represent the height and the shear wave velocity of the soil layer.

$$V_{s30} = \frac{30}{\sum_{i=1}^{N} \frac{d_i}{v_i}} \tag{6.1}$$

This study classifies the soil conditions into the four types based on the shear wave velocity as shown in the table 6.1. Referring to the table, the inhomogeneous soil is classified to the corresponding soil type. If V_{s30} is 160 m/s, for example, it is classified to the condition between soft and very soft soil. The weighed average value is taken for the scaling factor to estimate the maximum bending moment.

	Hard	Medium	Soft	Very soft
Shear wave velocity	540 m/s	290 m/s	200 m/s	150 m/s

Table 6.1: Soil classification based on the shear wave velocity

6.1.2 Site conditions of the example case

The site conditions of the example case are summarized below. Only one case is verified due to time constraints in this study.

- The water depth is assumed 26m.
- The structural geometry and soil stiffness for BHawC follows the ones used in the section 3.2. It is noted that this information is not necessary for the strategy since it directly estimated the maximum bending moment from the water depth, soil condition and bedrock depth.
- The soil conditions at the example case are summarized in the table 6.2. V_{s30} is around 160 m/s, which is classified to the condition between soft and very soft soil.
- The bedrock depth is assumed 60m since the shear wave velocity is more than 400 m/s after the No.8 layer.

Excluded due to confidential reason

Table 6.2: Soil condition for the example case

- The seismic signals explained in the section 4.2.2 are used for this study as well. The wave propagation from the bedrock depth to mudline is calculated by commercial software (i.e. given data in this study).

6.1.3 Preparation of libraries

Two libraries should be prepared to carry out the strategy, such as the library for the acceleration response spectrum and the scaling factor.

As for the scaling factor, the ones created in the section 4.3 can be re-used since the same turbine and foundation are used in this study. The example case is classified between soft and very soft, so the scaling factor is interpolated between these two soil conditions.

Meanwhile, the library for the acceleration response spectrum is created by using given data from the real project. Normally, the acceleration response spectrum from the bedrock to mudline is given data for structural designers. It makes easy to apply this strategy to a real project.

Three different depths, such as 0m, 5m and 10m from the mudline, are selected to check the sensitivity of the maximum bending moment to the selection of the representative depth for the acceleration response spectrum. The acceleration response spectrum is summarized in the plot 6.1. DRS represents the design response spectrum at bedrock depth. 0m, 5m and 10m represent the acceleration response spectrum at different representative depths. The hatching area represents the natural frequencies from very soft to soft soil conditions. As for the dominant vibration

modes, such as 1st structure, 1st RNA and 2nd structure modes, the acceleration response spectrum decreases in accordance with that the representative depth becomes deeper since the effect of soil amplification becomes smaller.

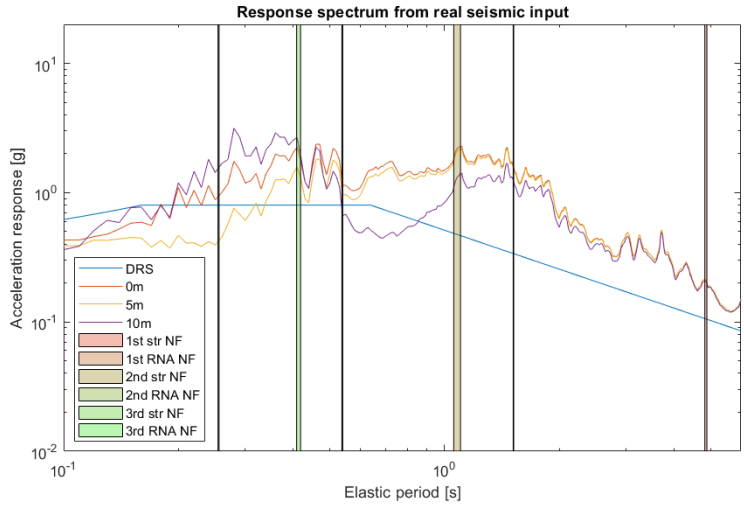

Figure 6.1

6.2 Results of the application

The maximum bending moment estimated by the strategy is compared with the ones from BHawC. The errors between these two outputs are summarized in the table 6.3. When selecting the mudline as a representative depth, the errors are relatively large (i.e. from 60% to 80%). If selecting deeper representative depth, the errors decrease.

The strategy overestimates the maximum bending moment for all the cases (position values in the errors mean the overestimation). It might come from the difference on the geometries.

The strategy is based on the structural geometries explained in the section 4.3.1 while BHawC uses the geometry from the real project. Table 6.4 summarizes the geometry both for BHawC and the strategy. The soil condition is positioned between soft and very soft soil condition, so both cases are shown in the table. The pile

Representative depth for Sa	Error on max. bending moment (%)	
	Tower top	Mudline
Mudline	77%	60%
5m below mudline	69%	54%
10m below mudline	32%	28%

Table 6.3: Summary of the errors for different representative depth

penetration length for BHawC is much longer than the strategy while the outside diameter is a bit smaller in the case of the very soft condition. It might induce the smaller bending moment in the case of BHawC since the foundation can easily get the resistance from the soil.

	Outside diameter (m)	Pile penetration (m)
BHawC	7.5	36.0
The strategy (Soft)	7.5	22.5
The strategy (Very soft)	8.5	25.5

Table 6.4: Difference of structural geometries

6.3 Discussion

6.3.1 Reasons of the errors

There are the following four reasons for the errors;

- Errors from the modeling part: As explained in the section 3.3, the calculation model has some errors (average 10%) to BHawC. The scaling factor is derived from the calculation model, so it still contains this modeling error in the case of comparing with BHawC.

- Errors from the strategy part: As explained in the section 5.2, the strategy may induce some errors (average 10% to 20%) due to the imperfection of the modal decomposition and the mesh size on the scaling factor.

- Errors from the soil classification: When extracting the scaling factor from the library, the inhomogeneous soil is converted into the equivalent homogeneous soil based on V_{s30}. It could be a source of the errors since it does not completely represent the inhomogeneous soil condition.

- Errors from the representative depth: As shown in the previous section, the errors can be largely varied depending on the representative depth for the acceleration response spectrum. Basically, the seismic excitation at mudline tends to be a valid indication to regulate the system response since the soil resistance at mudline is relatively low. In the case of inhomogeneous soil, however, the soil property can locally deviate a lot, which may induce the shift of the representative depth from the mudline to a deeper position.

- Errors from the difference of the structural geometries: As explained in the previous section, the structural geometries for BHawC and the strategy are not based on the same concept. The structural geometry is directly related to the system property, and it regulates the maximum bending moment. So, this difference may be one of the reasons of the errors.

6.3.2 Applicability and required future studies

The result shows relatively large errors (e.g. the maximum error is around 80%) to estimate the maximum bending moment. Even in the best case (i.e. 10m below mudline), the errors on the maximum bending moment is around 30%, which is not an ideal value for the clustering. Also, this study deals with only one position for verification. It is not sufficient to fully discuss if it can do clustering properly (i.e. to detect the worst position and to do categorization) and if the soil classification method and the selection of the representative depth for the acceleration response spectrum are suitable or not. So, the applicability to inhomogeneous soil is still ambiguous.

To mitigate the errors and sophisticate the strategy, the following future studies are required;

- The impact from the different structural geometries should be evaluated. And, if the impact is relatively large, they should be standardized (e.g. the concept to determine the structural geometries in the calculation of the scaling factor shall be adjusted).

- The strategy should be applied not only to one position but also to a large number of positions, such as the whole wind farm. Based on a large number

of data, the selection of the representative depth for the acceleration response spectrum and the way to classify the inhomogeneous soil condition can be calibrated accordingly.

Chapter 7

Final conclusion and recommendation

This chapter describes the final conclusions and recommendations for the future studies from this study.

7.1 Conclusion

The final conclusions are summarized below.

Calculation model

- Simplified calculation model for the structural analysis against seismic excitation is created. Applying efficient analysis methods (i.e. frequency domain method and response spectrum method) and also focusing on the dominant vibration modes, it performs the seismic analysis with reasonable accuracy and much smaller computational time in comparison with proven software.
- Dominant vibration modes are detected, such as 1st, 2nd and 3rd structure/RNA modes. Even truncating higher modes than these dominant ones, the result shows good agreement with proven software (which considers higher vibration modes in its calculation).
- Two different modeling approaches on RNA, such as Euler-Bernoulli beam with discretized masses and conventional lumped mass model, are compared. It

proves that the former approach shows good agreement with full RNA model used in the proven software and it represents the blade-tower coupling effect well.

Clustering strategy

- This study proves that maximum bending moment can be reasonably estimated by the combination of acceleration response spectrum and scaling factor with small computational demand. The approach is accurate enough to detect the worst positions in a wind farm and also categorize the positions which show similar load trends especially in the case of homogeneous soil condition.
- The estimation of the maximum bending moment works better for the positions with shallow water depth since the natural frequencies for the principle vibration modes are clearly separated from each other.
- In the case of using the same turbine, foundation type and design response spectrum, the same scaling factor can be used for clustering even if the seismic inputs have some phase shift with the original ones.

7.2 Recommendation

Recommendations from this study are summarized below.

Calculation model

- The simplified calculation model is not able to consider material/soil nonlinearity and liquefaction. The model may be improved by including these factors.
- This study considers only fore-after direction as seismic excitation since it tends to provide the dominant output. However, side-side and combination of multiple directions (depending on the design standard) are also considered in real projects. It might improve the accuracy of the strategy.
- This study considers only idling conditions for RNA operating conditions since it tends to be a driving case for the seismic analysis. In the detailed analysis in real projects, the other conditions (e.g. operating condition, emergency stop etc.) should be considered as well for further studies.

- Although this study considers only seismic excitation as an input, there are other environmental loads in reality, such as wind, current and wave loads. Including them, the result should become more accurate.

Clustering strategy

- The required number of clusters should be finalized with the acceptable load deviation in each cluster. This study reveals the relationship between the number of clusters and the load deviation in each cluster as a form of coefficient of variation, but the acceptable deviation is not determined. Hence, as a future study, the acceptable deviation shall be summarized with consideration of the trade-off between design cost (and time) and procurement cost.
- This study deals with only one type of wind turbine, such as SG-8.0-167-DD and only one type of foundation, such as monopile. New libraries shall be created when dealing with different turbine or foundation type.
- The strategy developed in this study is accurate enough to detect the worst position in a wind farm, but is not accurate enough to detect the worst position in each cluster. The accuracy may be improved by applying finer interval to the library for the scaling factor.
- P-y curve for linear regime defined in the design standard (i.e. DNVGL-ST-0126) is directly used for soil stiffness in the study for simplicity. In real projects, however, soil deformation may get into the non-linear regime, and equivalent linear stiffness is used. These phenomena should be incorporated in further studies.
- This study finds that 1m interval is suitable for the library on the acceleration response spectrum based on the parametric study. As for the scaling factor, however, the similar parametric study is not carried out. This study uses 5m and 10m interval for water depth and bedrock depth respectively when creating the library for the scaling factor and it provides acceptable results on clustering. Meanwhile, finer interval for the library could provide more accurate results while it requires longer computational time. It is recommended to carry out a parametric study on the interval to check the trade-off between accuracy and computational demand and find out the optimized interval.
- This study proves the applicability of the strategy to homogeneous soil conditions in the chapter 5, but more complicated soil conditions (i.e. inhomogeneous soil conditions) are expected in real projects. This study proposes the

method to expand the applicability to inhomogeneous soil conditions by converting them into the equivalent homogeneous soil conditions in the chapter 6, but it does not show reasonable accuracy and applicability. Further studies are expected (i.e. applying the method to a number of positions and also calibrating some parameters).

Appendix A

Calibration of calculation model

This Appendix describes how to calibrate the simplified calculation model in comparison with a proven software, such as BHawC.

A.1 Original result

Eigen analysis and forced vibration analysis are carried out with input parameters shown in 3.2.

A.1.0.1 Eigen analysis on single blade

Eigen analysis on single blade shows good agreement with BHawC without any calibration. Hence, no adjustment is applied to the blade section.

A.1.0.2 Eigen analysis on the whole structure

The restuls of eigen analysis on the whole structure are summarized in the table A.1. The natural frequencies for principal vibration modes have some deviations, such as 11% and 5% for 1st RNA and 2nd structure modes respectively.

Mode	Natural frequency (Hz)				
	BHawC	Model Bfr calibration	Error	Model Aft calibration	Error
1st structure	0.215	0.218	1%	0.211	2%
1st RNA	0.661	0.733	11%	0.665	1%
2nd structure	0.976	1.026	5%	0.980	0%
2nd RNA	1.792	1.972	10%	1.853	3%
3rd structure	2.359	2.508	6%	2.365	0%
3rd RNA	4.017	3.962	1%	3.854	4%

Table A.1: Natural frequencies before and after calibration

The mode shapes are relatively good agreement with BHawC especially for the principle vibration modes, such as 1st structure, 1st RNA and 2nd structure mode.

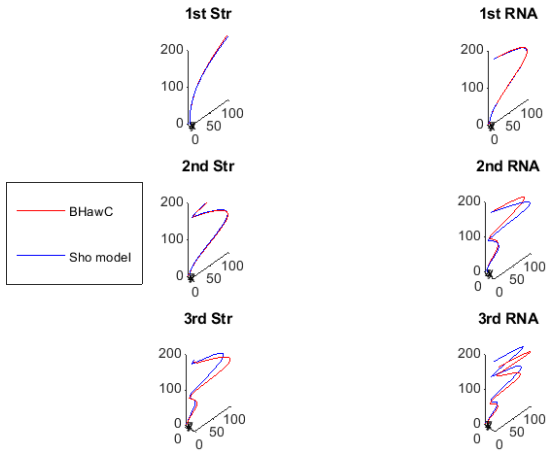

Figure A.1: Mode shape comparison

A.1.1 Forced vibration analysis

Maximum bending moments for each seismic input are compared with the ones from BHawC as shown in figure A.2 and table A.2. They clearly show large deviation from

BHawC. In the case of seismic input No.4, for example, it shows more than 100% errors at mudline.

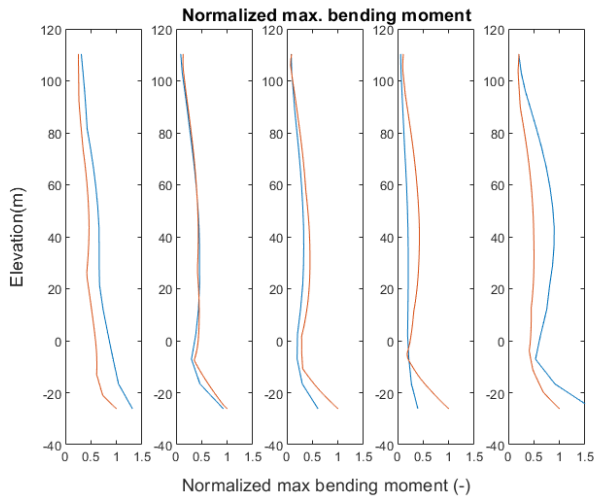

Figure A.2: Max. bending moment, Red:BHawC & Blue:Model, Input-1 to 5 from left to right

Input	Freq domain Before calibration		Freq domain After calibration	
	Tower top	Mudline	Tower top	Mudline
1	18%	24%	5%	0%
2	51%	8%	0%	6%
3	9%	64%	12%	6%
4	87%	151%	6%	21%
5	2%	39%	16%	15%
Average	**33%**	**57%**	**8%**	**10%**

Table A.2: Summary of model error (before/after calibration)

A.2 Investigation of the deviation

Based on the original results, it is founded that the difference of the natural frequencies are quite sensitive to the bending moment.

Figure A.3, A.4 and A.5 show the Fourier spectrum for 5 seismic inputs especially focusing on principle vibration modes, such as 1st/2nd structure and 1st RNA modes. Yellow dots represent the value for the model and red dots represent the value for BHawC.

Even if the difference of the natural frequencies are not so large, the spectum values can be largely different. In the case of No.3 seismic input for 2nd structural mode, for example, the spectrum for the model is around 0.3 m/Hz while the one for BHawC is less than 0.1 m/Hz while the difference of the natural frequencies is only 5%. The same trend can be seen in the case of No.4 seismic input. Due to their overestimation on the spectrum, their maximum bending moments are generally overestimated in comparison with BHawC.

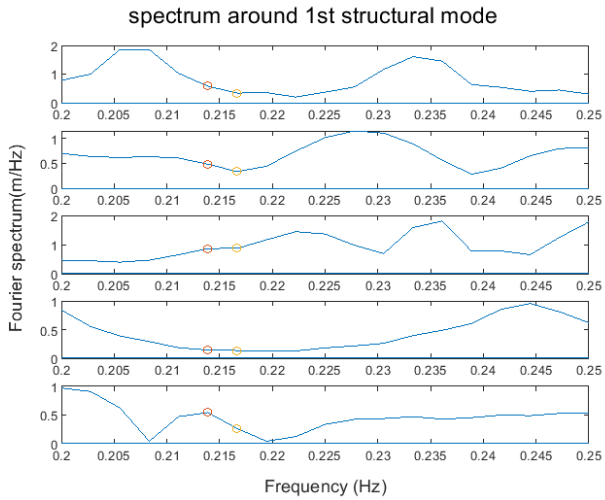

Figure A.3: Spectrum for 1st structure mode (Yellow: model, Red: BHawC)

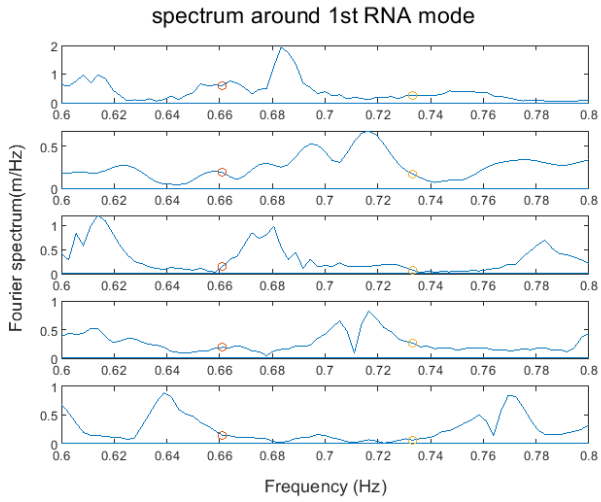

Figure A.4: Spectrum for 1st RNA mode (Yellow: model, Red: BHawC)

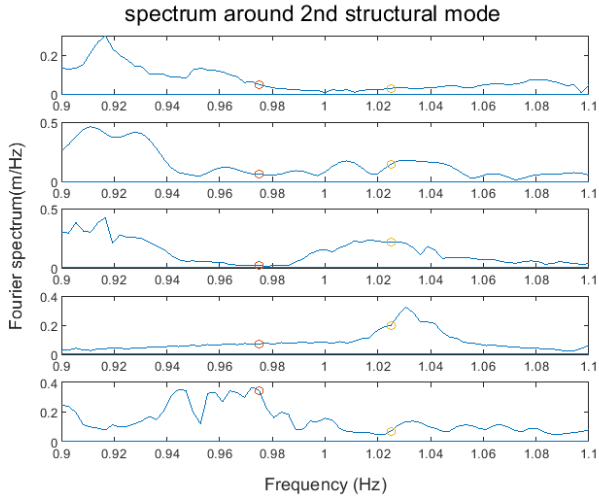

Figure A.5: Spectrum for 2nd structure mode (Yellow: model, Red: BHawC)

Hence, it's necessary to get good agreement to adjust the natural frequencies much closer to the ones from BHawC.

A.3 Calibration

In order to get good agreement with BHawC, the system property of the model is calibrated.

First, the stiffness around RNA is adjusted. The stiffness is originally set to super high value (i.e. representing rigid connection). In reality, however, it should have some flexibility. The difference may induce the error especially for RNA vibration modes. Hence, the stiffness around hub (See figure A.6) is calibrated to get the agreement with BHawC especially for 1st RNA mode.

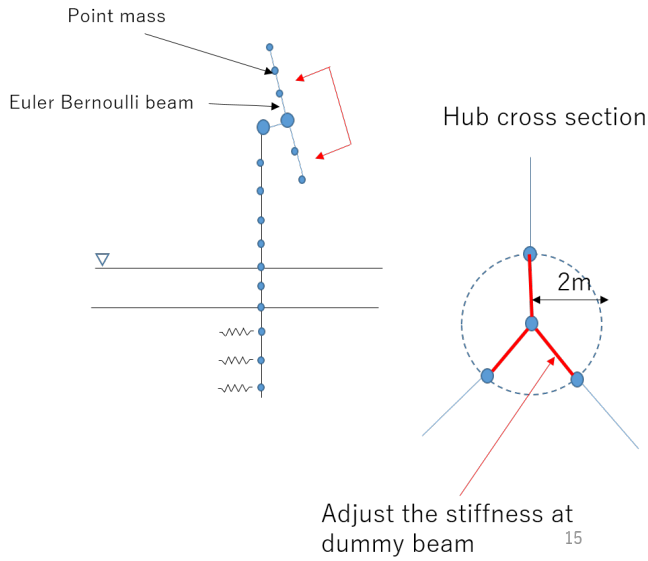

Figure A.6: Overview of adjustment on hub stiffness

Second, the mass of RNA is increased by 10% and the soil stiffness is decreased by 20%, which mainly adjust the natural frequency for 2nd structural mode.

A.4 Final result

After the calibration, eigen analysis and forced vibration analysis are carried out again. Then, the result shows much better agreement with BHawC as shown in the table A.2. The detailed results after the calibration are shown in chapter 3.

In general, the calibrated model shows good agreement with BHawC. The calibration is a bit arbitrary approach, so it is not suitable for fully accurate / detailed calculation in real projects. However, the model is suitable enough to capture the general trend in structural analysis.

Appendix B

Frequency Dependent Soil Damping

This Appendix describes the analysis which shows the impact from the frequency dependency on soil damping

B.1 Theory of the frequency dependent soil damping

Soil damping is consists of two components, such as radiation damping and material damping. Radiation damping represents energy dissipation due to waves created by pile motion. Hysterics material damping can occur as the soil is being cyclically stressed. [34] proposed the way to calculate these two components by the following equations. The first term represents radiation damping and the second one represents material damping.

$$c_s = 6a_0^{-0.25}\rho_s V_s d + 2\beta_s \frac{k_x}{\omega} \tag{B.1}$$

where $a_0 = \frac{\omega d}{V_s}$ and ρ_s, V_s, d, k_x, β_s are mass density of soil, shear wave velocity, pile diameter, soil stiffness and damping ratio. Depending on the shear-strain amplitude, damping ratio can be changed from 2% to 7%. The average value, 5%, is used in this study.

B.2 Sensitivity study

In order to evaluate the effect of frequency dependency on soil damping, both frequency dependent and independent damping are calculated.

B.2.1 Damping coefficient

First, damping coefficient (c_s) for the following cases are calculated to understand the impact depending on the soil condition and frequencies.

Soil type	1 (soft)	2 (medium)	3 (hard)	4 (bedrock)
Shear wave velocity (m/s)	131	178	250	480
Elastic stiffness (Mpa)	80	150	300	1200
Material damping ratio	5%	5%	5%	5%

Table B.1: Soil conditions for sensitivity study

7.0 m is assumed for pile diameter, 850 kg/m^3 is assumed for soil density and soil stiffness (K) is derived with the following equation. The frequency is varied from 0 Hz to 2 Hz, which covers principle vibration modes.

$$K = 1.2 * E_s \tag{B.2}$$

In case of frequency independent analysis, soil damping parameter just between 1st and 2nd structural mode (i.e. 0.6Hz) is selected as fixed value for entire frequency range.

The results are summarized in the figure B.1. Solid line represents frequency dependent soil damping and dash line represents frequency independent soil damping. As frequency increases, the fluctuation of damping coefficient becomes small. Soil condition does not show large differences on the trend.

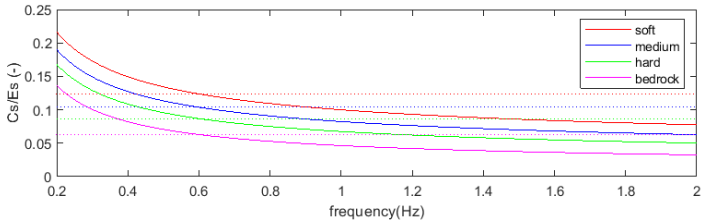

Figure B.1: Damping coefficients as a function of excitation frequency

B.2.2 Bending moment

The frequency dependent soil damping is applied to the calculation model shown in Chapter 3. 5 seismic inputs are applied and 131 m/s is assumed as shear wave velocity.

The results are summarized in figure B.2 and the table B.2. Red and blue lines represent the maximum bending moment for frequency dependent and independent soil damping respectively. It clearly shows that the deviation between these two lines are quite small. The errors at tower top and mudline are less than 3%.

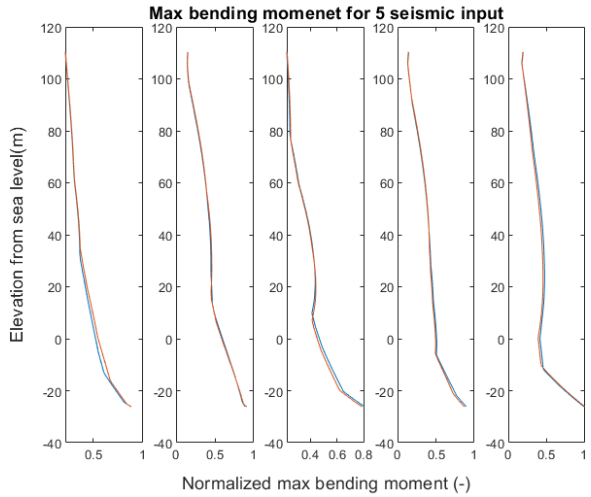

Figure B.2: Max. bending moment for 5 seismic input (red: frequency dependent, blue: frequency independent)

Seismic input	Error	
	Tower top	Mudline
1	0.5%	0.3%
2	0.9%	2.7%
3	1.0%	2.3%
4	2.9%	3.0%
5	1.8%	1.2%

Table B.2: Error on the max. bending moment

It is noted that the absolute value of the bending moment is not necessarily consistent with the one shown in Chapter 3 since the frequency dependent/independent soil damping is simply added to the Rayleigh damping considered in the main study. In practice, damping ratio on the Rayleigh damping should be reduced as a trade-off to include the frequency dependent/independent soil damping. This study does not focus on the details and just roughly checks the effect of frequency dependent soil damping.

B.3 Application to this study

In this section, the impact of frequency dependent soil damping is investigated by sensitivity studies. Although it shows certain amount of effect on the final result especially in the case of harder soil condition, in general, the impact is limited, and it does not affect so much on the general trend for clustering.

The range of dominant vibration modes is relatively small (i.e. from 0.2Hz to 1.0Hz) for the system studied in this research. If the range is much wider (e.g. seismic input with large variety of frequency component, modal participation masses are widely distributed on the large number of modes etc.), the frequency dependent soil damping could have an impact to the output.

In this study, however, frequency dependency on soil damping is neglected for simplicity since its impact is limited.

Appendix C

Representative depth on the acceleration response spectrum

This Appendix describes the sensitivity study on the acceleration response spectrum to determine its representative depth for structural analysis.

C.1 Purpose and procedure of the sensitivity study

The effect from soil amplification is dependent on the depth, which means that seismic excitation is different at each depth. Hence, the representative depth on the acceleration response spectrum is not simply determined. Hence, this chapter carries out the sensitivity studies to check the effect.

First, transfer function from the bedrock to the surface is checked. The transfer function is the ratio of seismic amplitude between at the bedrock and at the specific depth, which represents the amount of soil amplification. This study may reveal the variation of seismic excitation as a function of vertical depth.

Second, the bending moment based on the different representative depth is calculated by using response spectrum analysis method. This study can directly reveal the effect of choosing different representative depth to calculate bending moment.

C.2 Transfer function from bedrock

Transfer function is calculated for the following cases. The dominant vibration modes for the seismic analysis is 1st structure, 1st RNA and 2nd structure mode, which ranges from 0.2Hz to 1.1Hz in this study. So, the frequency is limited from 0.1Hz to 2.0Hz with some contingency.

- Bedrock depth: 0m, 20m, 40m, 60m (4 case)
- Soil condition: Hard, Medium, Soft, Very soft (4 case)
- Frequency: 0.1Hz, 0.5Hz, 1.0Hz, 2.0Hz (4 case)

Following figures show the results. It reveals the following two things. First, the larger bedrock depth induces the larger effect on the transfer function. Second, the softer soil condition induces the larger effect on the transfer function.

Even in the case of large bedrock depth and softer soil condition, however, the fluctuation of the transfer for 0.1Hz and 0.5Hz as a function of depth is not so large. In the case of bedrock depth 60m and very soft soil condition, for example, the transfer function for 0.5Hz at mudline is around 1.3 while the one at 30m depth is around 1.2. Meanwhile, the fluctuation of the transfer for 1.0Hz as a function of depth is relatively large in comparison with 0.1Hz and 0.5Hz, which may induce the differences on the bending moment.

The next section checks and confirms these findings by directly calculating the bending moment.

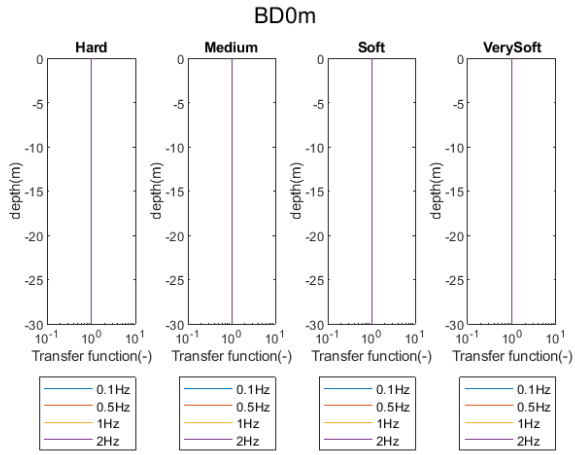

Figure C.1: Transfer function (bedrock depth 0m)

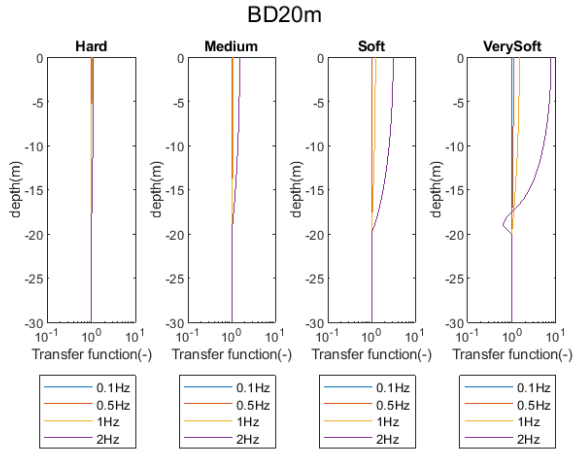

Figure C.2: Transfer function (bedrock depth 20m)

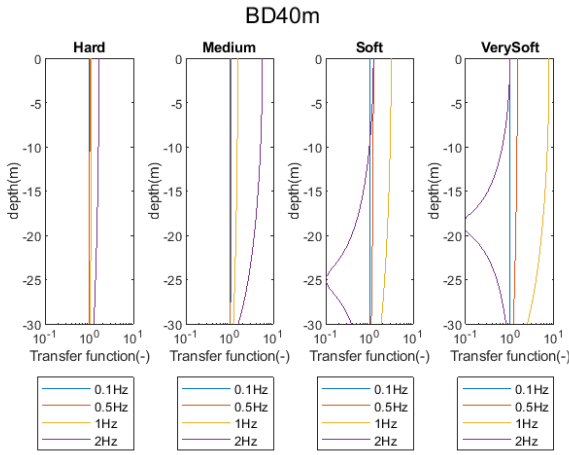

Figure C.3: Transfer function (bedrock depth 40m)

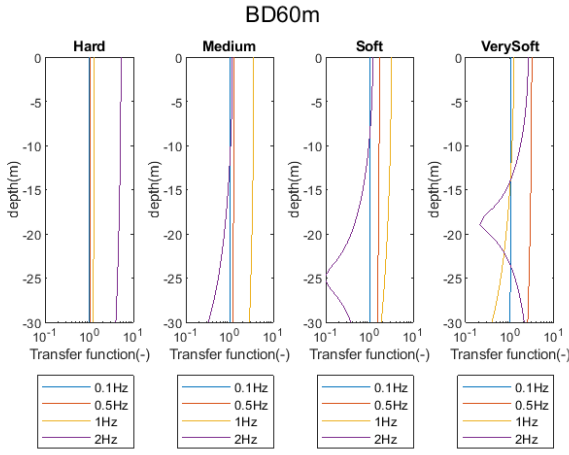

Figure C.4: Transfer function (bedrock depth 60m)

C.3 Comparison of bending moment

Maximum bending moment is calculated for the following conditions. Frequency domain method is applied to derive the correct bending moment and response spectrum analysis method is applied by changing the representative depth as sensitivity study.

- Water depth: 30m (1 case)
- Soil condition: Hard, Medium, Soft, Very soft (4 case)
- Bedrock depth: 0m, 10m, 20m, 30m, 40m, 50m, 60m (6 case)
- Representative depth for Sa: 0m, 5m, 10m, 15m, 20m (5 case)

The error to the correct bending moment is summarized in the table below. it shows that the errors are small in the case of selecting 0m (i.e. mudline) as representative depth although the difference depending on the depth is not so large as expected in the previous section. Hence, this study uses mudline as a representative depth to estimate the maximum bending moment in the strategy.

Representative Depth	Hard	Medium	Soft	Very soft
0m (Mudline)	23%	19%	17%	30%
5m	24%	20%	18%	31%
10m	24%	22%	22%	35%
15m	25%	25%	25%	39%
20m	27%	28%	29%	43%

Table C.1: Error on the max. bending moment (Tower top)

Representative Depth	Hard	Medium	Soft	Very soft
0m (Mudline)	37%	19%	16%	38%
5m	37%	19%	16%	39%
10m	38%	20%	18%	42%
15m	38%	21%	21%	45%
20m	38%	23%	25%	48%

Table C.2: Error on the max. bending moment (Mudline)

Appendix D

Sensitivity studies on modal decomposition with frequency spectrum

This Appendix explains the sensitivity studies of several approaches on modal decomposition with frequency spectrum to check which method is suitable for this research.

D.1 Options for modal decomposition with frequency spectrum

To find the most suitable range with frequency spectrum, following options are compared with each other.

The first option is 5% from the natural frequencies. It means that the range for each vibration mode varies. It represents the different damping ratio for each vibration mode. In general, higher vibration modes have a larger damping ratio. In the case of larger damping ratio, the peaks in the frequency spectrum tend to be flatten and the effect from each vibration mode is distributed to wider range of frequencies. This options tries to capture the effect.

The other three options use fixed ranges from the natural frequencies.They are not able to capture the effect explained in the first option, but the equality for every

modes is secured since the same range is used for every modes.

1. Case-1: 5% from the natural frequencies
2. Case-2: 0.01Hz from the natural frequencies
3. Case-3: 0.05Hz from the natural frequencies
4. Case-4: 0.1Hz from the natural frequencies

D.2 Results of the sensitivity study

For each case, the maximum bending moment decomposed into the principal modes are calculated. Also, the errors to estimate the maximum bending moment are evaluated in comparison with the correct bending moment.

D.2.1 Maximum bending moment decomposed into the principal vibration modes

The results for tower top, medium soil condition and 0m bedrock depth are summarized in the figure D.1. While Case-2,3,4 show relatively similar results with each other, Case-1 shows that the larger contribution from the higher vibration modes. Case-1 shows around 10% contribution from the 3rd structure and RNA modes while its contribution in Case-2,3,4 is less than 5%. Kitahara [25] and Zhao [26] mentioned that mainly 1st and 2nd modes are impactive for the seismic analysis. Case-2,3,4 are in-line with this trend.

D.2.2 Errors for the estimation of the maximum bending moment

The maximum bending moment estimated by the strategy is compared with the correct bending moment for the virtual wind farm 1 and 2 introduced in the section 5.1. The average errors for all the locations (i.e. tower top and mudline) and wind farms are summarized in the table D.1.

The difference is not so major, but Case-3 shows a bit better accuracy in comparison with Case-2 and Case-4.

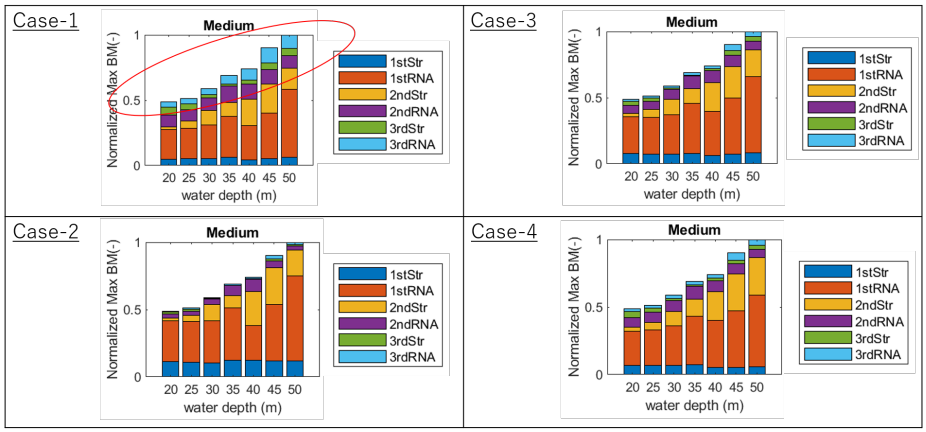

Figure D.1: Maximum bending moment (Tower top, medium soil, bedrock depth 0m)

	Ave. error for all (%)	Max. error for all (%)	Ave. error for top3 (%)	Max. error for top3 (%)
Case-1 (5%)	12%	53%	15%	30%
Case-2 (0.01Hz)	15%	48%	15%	32%
Case-3 (0.05Hz)	13%	46%	15%	31%
Case-4 (0.10Hz)	13%	47%	15%	32%

Table D.1: Errros for the estimation of maximum bending moment

D.3 Selection of the method for the modal decomposition

Based on the sensitivity study, Case-3 (0.05Hz from the natural frequencies) is selected as a range for the modal decomposition because of the following reasons.

First, fixed frequency ranges (Case-2,3,4) show more reasonable result on the maximum bending moment decomposed in the principal vibration modes. As mentioned, the contribution from 1st and 2nd structural and RNA modes should be dominant in comparison with the higher modes, especially in the case of no soil amplification (i.e. 0m bedrock depth). From this point, Case-1 shows less reasonable result in comparison with the other three options.

Second, Case-3 shows better accuracy to estimate the bending moment in com-

parison with Case-1 and Case-2. This is one of the important factor to secure the applicability of the clustering strategy.

Appendix E

Parametric study for the library of the acceleration response spectrum

This Appendix describes the parametric study to determine the interval of input parameters for the library of the acceleration response spectrum.

E.1 Procedure

To check the suitable interval for the library of the acceleration response spectrum, parametric studies are carried out for the following two cases.

	Interval for water depth	Interval for bedrock depth
Case-1	1.0m	10.0m
Case-2	1.0m	1.0m

Table E.1: Interval conditions for the parametric study

The errors on the estimation of the maximum bending moment by the strategy are compared with each other, then the suitable interval size is discussed.

E.2 Result

The errors for estimating the bending moment by the strategy are summarized in the table E.2 and E.3. The differences between Case-1 and Case-2 are summarized in the table E.4 (position values mean Case-1 shows less errors (i.e. better accuracy)). For most cases, Case-2 shows much better accuracy in comparison with Case-1.

Wind farm	**Location**	**Ave. error for all**	**Max. error for all**	**Ave. error for top3**	**Max. error for top3**
1	Tower top	15%	37%	21%	33%
1	Mudline	17%	65%	14%	25%
2	Tower top	16%	42%	16%	25%
2	Mudline	17%	78%	25%	56%

Table E.2: Errors for estimating the maximum bending moment (Case-1)

Wind farm	**Location**	**Ave. error for all**	**Max. error for all**	**Ave. error for top3**	**Max. error for top3**
1	Tower top	12%	35%	16%	35%
1	Mudline	17%	74%	20%	39%
2	Tower top	12%	34%	7%	21%
2	Mudline	12%	41%	17%	31%

Table E.3: Errors for estimating the maximum bending moment (Case-2)

Wind farm	Location	Ave. error for all	Max. error for all	Ave. error for top3	Max. error for top3
1	Tower top	-3%	-3%	-5%	2%
1	Mudline	0%	8%	6%	14%
2	Tower top	-4%	-8%	-9%	-4%
2	Mudline	-4%	-37%	-8%	-25%

Table E.4: Difference between Case-1 and Case-2

To investigate the reason of this difference, the acceleration response spectrum and the estimated bending moment for an example position is checked. Larger improvement can be seen at mudline in the wind farm2 (shallow water depth), so one of the position in the wind farm 2 is selected as an example and the values at mudline is investigated. The input parameters for the example position are below;

- water depth: 29m
- soil condition: soft soil
- bedrock depth: 57m

Figure E.1 shows the maximum bending moment at mudline for the soft soil and 60m bedrock depth case, which is similar case with the example position. As highlighted by a red circle, the 2nd structural mode is a dominant vibration mode for this position. So, the acceleration response spectrum for the 2nd structural mode for this position is checked.

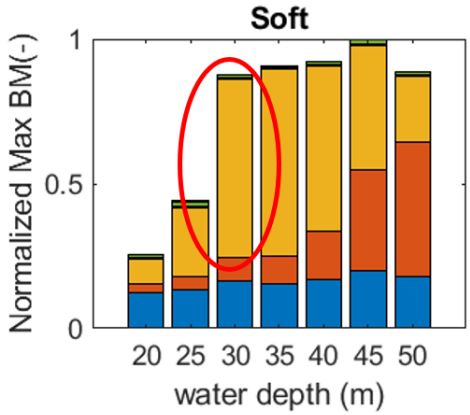

Figure E.1: Maximum bending moment for soft soil and 60m bedrock depth

The natural frequency for the 2nd structural mode for this position is around 1.12Hz. The acceleration response spectrum for Case-1 and 2 is summarized in the figure E.2. The red, orange and blue lines represent the acceleration response spectrum for each seismic input (3 signals to be applied to the system) and the purple line represents the design response spectrum.

In Case-1, the acceleration response spectrum for the example position is linearly interpolated between two data, such as the acceleration response spectrum for 50m and 60m bedrock depth. The value is around 6.3g. In case-2, the acceleration response spectrum for the example position can be directly derived since the interval of data is 1m. The value is around 11.4g. It clearly shows large deviation since Case-1 misses out the resonance of soil column.

The maximum bending moment estimated by Case-1 and 2 is summarized in the table E.5. The maximum bending moment in Case-2 is much larger than Case-1 and close to the correct bending moment because Case-2 captures the resonance of the soil column and detects the proper acceleration response spectrum for the dominant vibration mode (i.e. 2nd structural mode).

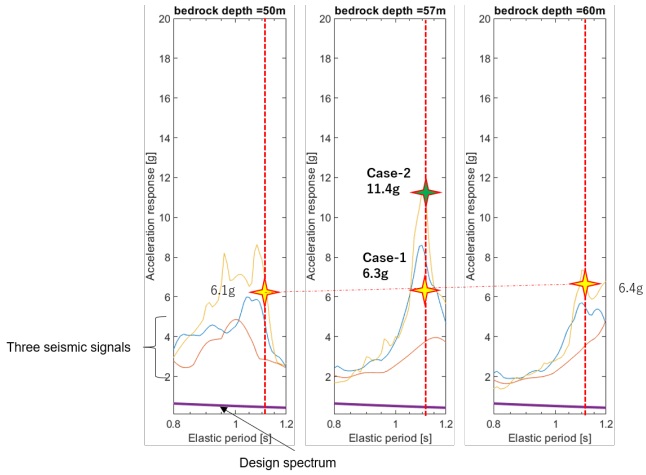

Figure E.2: Comparison of the acceleration response spectrum for 2nd sturctural mode

	The acceleration response spectrum for the 2nd structural mode (g)	Estimated max. bending moment (Nm)	Errors to correct bending moment
Case-1	6.3	2.3E+09	56%
Case-2	11.4	3.6E+09	31%

Table E.5: Comparison between Case 1 and 2 for the example position

E.3 Application to the study

As shown in the previous section, it is important to capture the resonance of the soil column for the acceleration response spectrum. It largely affect the accuracy of the strategy. 10m interval (i.e. Case-1) for the acceleration response spectrum is not fine enough to capture the resonance, so 1m interval (i.e. Case-2) is used for this study.

Appendix F

Result of sensitivity studies

This Appendix summarizes all the results (i.e. max. bending moment and scaling factor) from the sensitivity study done in the section 4.3.

F.1 Maximum bending moment

Maximum bending moment are summarized below.

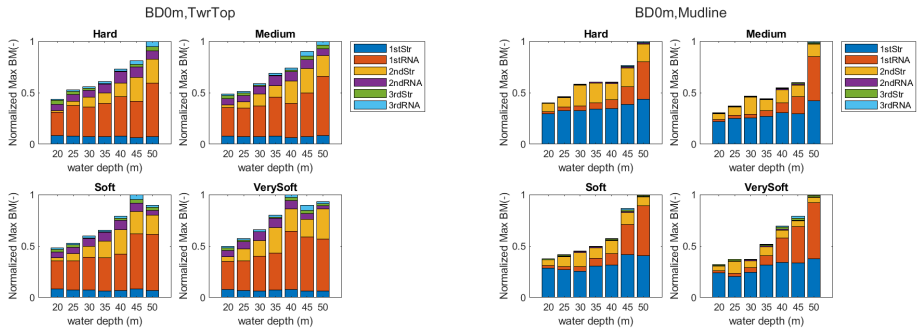

(a) BD=0m, Tower top

(b) BD=0m, Mudline

Figure F.1: Max. bending moment (BD = 0m)

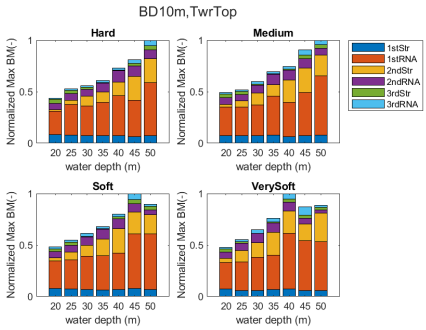

(a) BD=10m, Tower top

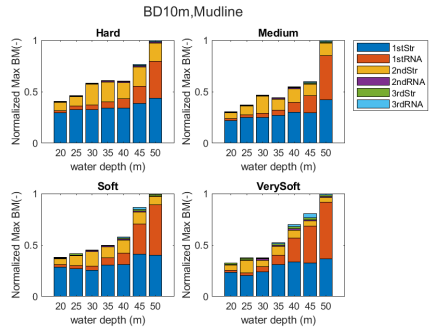

(b) BD=10m, Mudline

Figure F.2: Max. bending moment (BD = 10m)

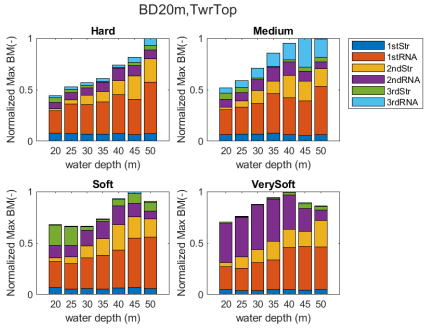

(a) BD=20m, Tower top

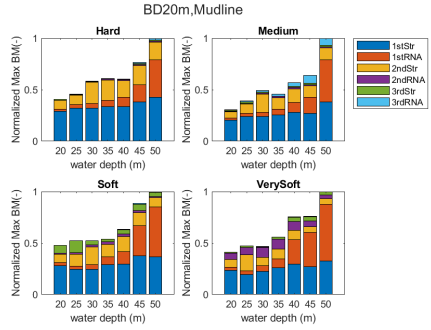

(b) BD=20m, Mudline

Figure F.3: Max. bending moment (BD = 20m)

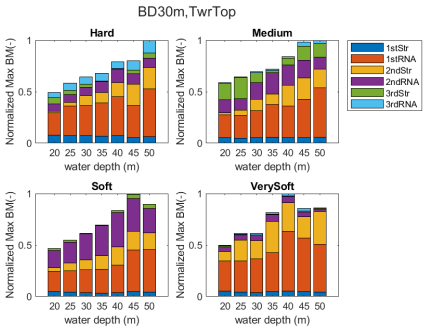

(a) BD=30m, Tower top

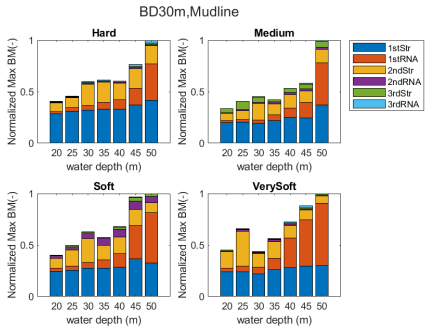

(b) BD=30m, Mudline

Figure F.4: Max. bending moment (BD = 30m)

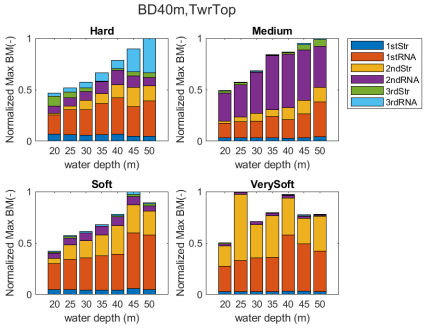

(a) BD=40m, Tower top

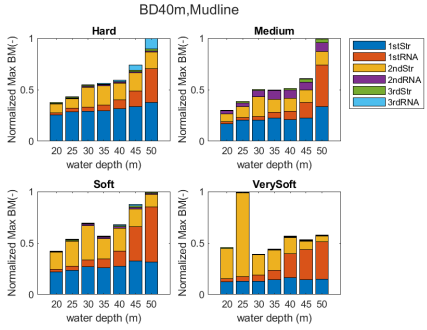

(b) BD=40m, Mudline

Figure F.5: Max. bending moment (BD = 40m)

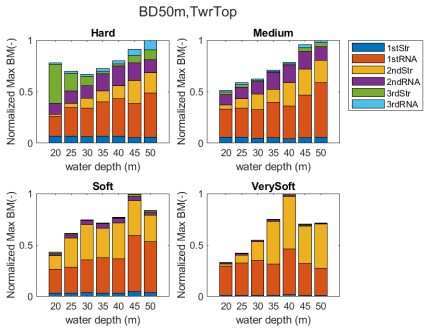

(a) BD=50m, Tower top

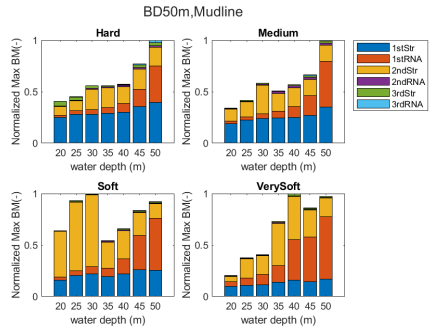

(b) BD=50m, Mudline

Figure F.6: Max. bending moment (BD = 50m)

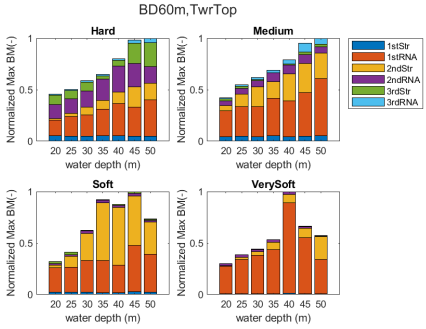

(a) BD=60m, Tower top

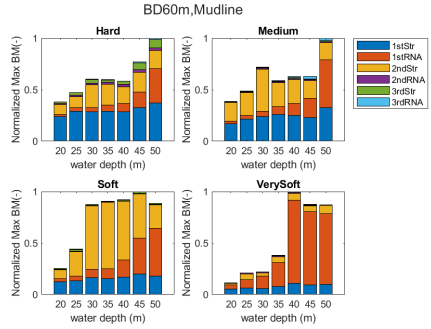

(b) BD=60m, Mudline

Figure F.7: Max. bending moment (BD = 60m)

F.2 Scaling factor

Scaling factors are summarized below.

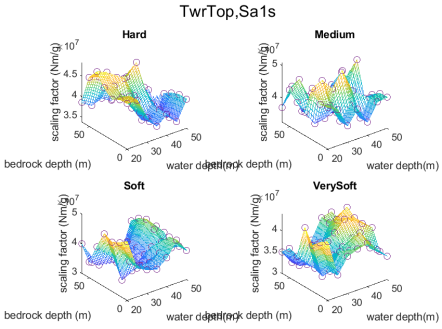

(a) 1st structure, Tower top

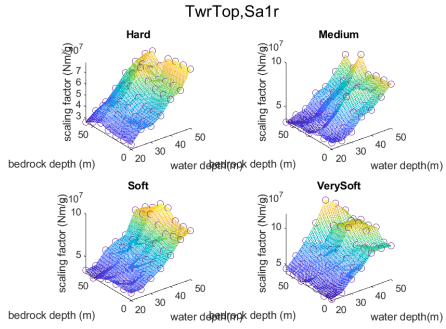

(b) 1st RNA, Tower top

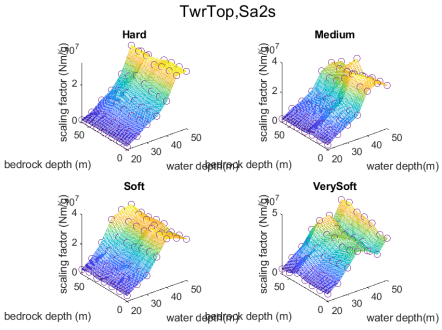

(c) 2nd structure, Tower top

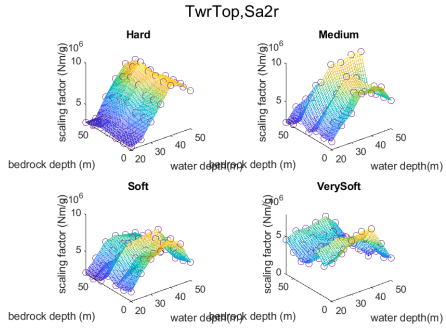

(d) 2nd RNA, Tower top

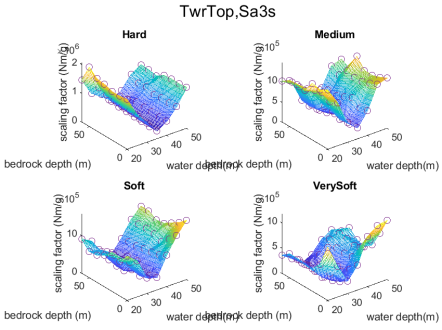

(e) 3rd structure, Tower top

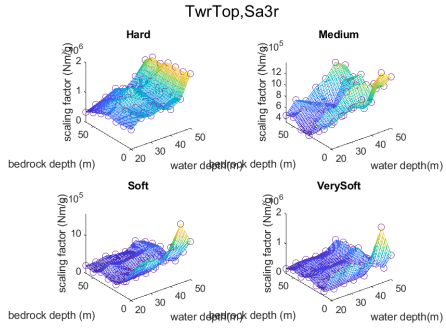

(f) 3rd RNA, Tower top

Figure F.8: Scaling factor for tower top

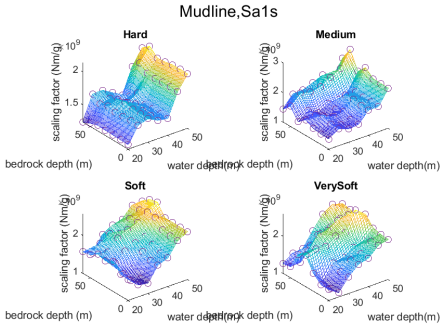

(a) 1st structure, Mudline

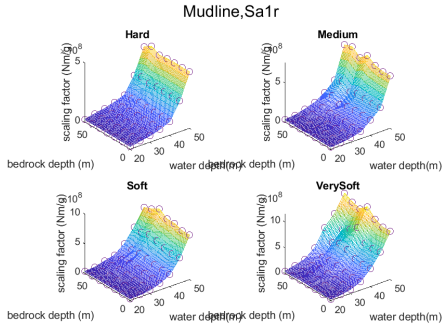

(b) 1st RNA, Mudline

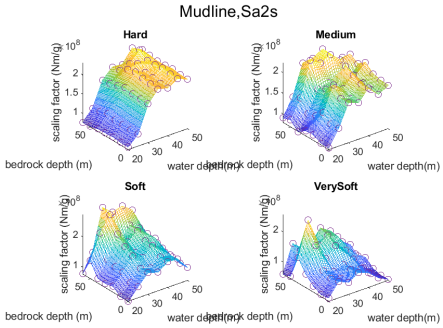

(c) 2nd structure, Mudline

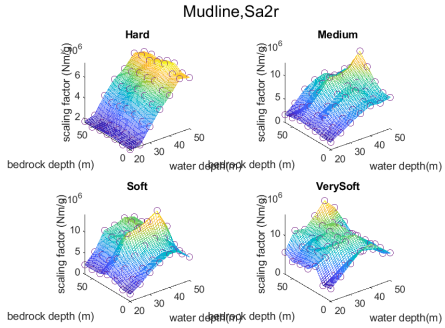

(d) 2nd RNA, Mudline

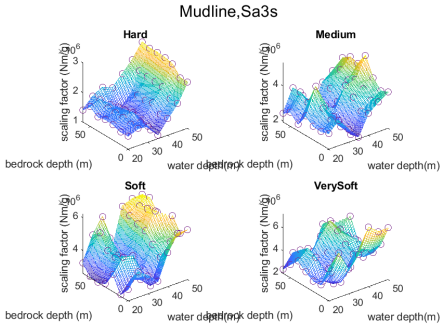

(e) 3rd structure, Mudline

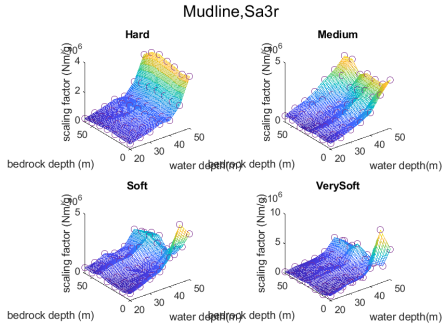

(f) 3rd RNA, Mudline

Figure F.9: Scaling factor for mudline

Bibliography

[1] IRENA. Future of wind. 2019.

[2] Raffaele De Risi, Subhamoy Bhattacharya, and Katsuichiro Goda. Seismic performance assessment of monopile-supported offshore wind turbines using unscaled natural earthquake records. *Soil Dynamics and Earthquake Engineering*, 109:154 – 172, 2018.

[3] Lisa Ziegler, Sven Voormeeren, Sebastian Schafhirt, and Michael Muskulus. Sensitivity of wave fatigue loads on offshore wind turbines under varying site conditions. *Energy Procedia*, 80:193 – 200, 2015.

[4] Fabian Vorpahl, Holger Schwarze, Tim Fischer, Marc Seidel, and Jason Jonkman. Offshore wind turbine environment, loads, simulation, and design. *WIREs Energy Environ*, 2:548 – 570, 2013.

[5] Lisa Ziegler, Sven Voormeeren, Sebastian Schafhirt, and Michael Muskulus. Design clustering of offshore wind turbines using probabilistic fatigue load estimation. *Renewable Energy*, 91:425 – 433, 2016.

[6] Marc Seidel. Wave induced fatigue loads on monopiles - new approahces for lumping of scatter tables and specific interpolation of fatigue loads. *IWEC*, 2014.

[7] Maria Luisa Rosales Gonzalez. Seismic analysis on monopile based offshore wind turbines including aero-elasticity and soil-structure interaction, July 2016.

[8] Ahmer Ali, Raffaele De Risi, and Anastasios Sextos. Finite element modeling optimization of wind turbine blades from an earthquake engineering perspective. *Engineering Structures*, 222(111105), 2020.

[9] Renjie Mo, Haigui Kang, Miao Li, and Xuanlie Zhao. Seismic fragility analysis of monopile offshore wind turbines under different operational conditions. *MDPI Energies*, 10(1037), 2017.

[10] Namcheol Kang, Sung Chul Park, Junhong Park, and Satya N Atluri. Dynamics of flexible tower-blade and rigid nacelle system: dynamic instability due to their interactions in wind turbine. *Journal of Vibration and Control*, 22(3):826 – 836, 2014.

[11] Guanzhong LIU, Xingming GUO, and Li ZHU2. Dynamic analysis of wind turbine tower structures in complex ocean environment. *Applied Mathematics and Mechanics*, 41(7):999 – 1010, 2020.

[12] Yoshihisa Iida and Takeshi Ishihara. Numerical study of combined aerodynamic and seismic loadings on wind turbine support structures. *Japan Society of Civil Engineers, 2020 Annual Meeting, 75th Academic Presentation*, 2020.

[13] Seyhan Firat, Nihat S. Isik, Hasan Arman, Mesut Demir, and Isa Vural. Investigation of the soil amplification factor in the adapazari region. *Bulletin of Engineering Geology and the Environment*, 2015.

[14] A.Tsouvalas. *Structural Response to Earthquakes*. TU Delft, 2020.

[15] Dnvgl-st-0126 support structures for wind turbines, 2016.

[16] WindEurope. Windeurope annual offshore statistics 2019. 2019.

[17] B.K.Gupta and D.Basu. Applicability of timoshenko and euler–bernoulli and rigid beam theories in analysis of laterally loaded monopiles and piles. *Géotechnique*, 68(9):772 – 785, 2018.

[18] Heiko Panzer, Jorg Hubele, Rudy Eid, and Boris Lohmann. Generating a parametric finite element model of a 3d cantilever timoshenko beam using matlab. *Technical Reports on Automatic Control*, TRAC-4, 2009.

[19] Dnvgl-st-0437 loads and site conditions for wind turbines, 2016.

[20] Takeshi Ishihara. Guideline for design of wind turbine support structures and foundations, 2010.

[21] Steven Lawrence Kramer. *Geotechnical earthquake engineering*. Prentice-Hall international series in civil engineering and engineering mechanics. Prentice Hall.

[22] Chao Chen and Philippe Duffour. Modelling damping sources in monopile-supported offshore wind turbines. *Wind Energy*, 21:1121 – 1140, 2018.

[23] Siemens Gamesa Renewayble Energy. siemens gamesa offshore wind turbine brochure sg-8.0-167-dd.

[24] G. M. Calvi M. J. N. Priestley, F. Seible. *Seismic Design and Retrofit of Bridges*. John Wiley and Sons, 1996.

[25] Masaru Kitahara and Takeshi Ishihara. Prediction of seismic loadings on wind turbine support structures by response spectrum method considering equivalent modal damping of support structures and reliability level. *Wind Energy*, 1:1 – 22, 2020.

[26] Mi Zhao, Zhidong Gao Risi, and Piguang Wang. Response spectrum method for seismic analysis of monopile offshore wind turbine. *Soil Dynamics and Earthquake Engineering*, 136(116212), 2020.

[27] Sergio Sánchez, José-Santos López-Gutiérrez, Vicente Negro, and M. Dolores Esteban. Foundations in offshore wind farms: Evolution,characteristics and range of use. analysis of main dimensional parameters in monopile foundations. *Journal of Marine Science and Engineering*, 2019.

[28] European Committee for Standardization. Eurocode-8: Design of structures for earthquake resistance, 2004.

[29] N. Subramanian. *Design of Steel Structures*. Oxford University Press, 2016.

[30] Priyanka Raikar. Modelling soil damping for suction pile foundations, September 2016.

[31] Wei Shangguan, Tomislav Hengl, Jorge Mendes de Jesus, Hua Yuan, and Yongjiu Dai. Mapping the global depth to bedrock for land surface modeling. *Journal of Advances in Modeling Earth Systems*, 2016.

[32] Laszlo Aranya, S.Bhattacharyab, John Macdonalda, and S.J. Hogana. Design of monopiles for offshore wind turbines in 10 steps. *Soil Dynamics and Earthquake Engineering*, 92:126 – 152, 2017.

[33] P. Anbazhagan and T.G. Sitharam. Site characterization and wite response studies using shear wave velocity. *Japanese Society for Engineering Education*, 10:53 – 67, 2008.

[34] N.Makris and G.Gazetas. Dynamic pile-soil-pile interaction, part 2 lateral and seismic response. *Earthquake engineering and structural dynamics*, 21:145 – 162, 1992.